Faculty of Engineering of the University of Porto

Mechanical Engineering Department

A study on finite element modelling of roll levelling as a roll forming pre-process

Author:
Rui Pedro Pimenta Ribeiro

Supervisors:
Dr. Thomas Dietl
Prof. Dr. Abel D. Santos

Co-Supervisors:
ir. André Abee
Dipl.-Ing. Johann Harraßer
M.Sc. Miguel Pereira

This dissertation was submitted for the degree of

M.Sc. in Mechanical Engineering to the

Faculty of Engineering, University of Porto

Porto, September 2019

A study on finite element modelling of roll levelling as a roll forming pre-process

Rui Pedro Pimenta Ribeiro

Dissertation submitted for the degree of

M.Sc. in Mechanical Engineering

Faculty of Engineering of the University of Porto

September 2019

Abstract

Due to the high requirement for CO_2 emissions reduction, a huge effort has been made in order to develop lightweight materials for structural applications. However, such progress represents new manufacturing challenges and drives the progress of industrial processes. Particularly for sheet metal forming, additional pre-processes have been implemented to control sheet properties and understanding how the full process chain affects the final products became a priority.

As a consequence of the higher industrial demand, some CAE software companies, namely data M Sheet Metal Solutions GmbH, look forward to study the feasibility of integrating a wider spectrum of the process chain in their products in order to improve their quality. COPRA® RF and COPRA® FEA RF software, which are widely used in industry to design roll forming lines and further analyse the process, reflect this tendency. Therefore, comprehending how roll forming FEA benefits from roll levelling pre-processing and how can the finite element analysis of both processes be integrated, are main investigation topics.

In this work, an in depth study is proceeded in order to understand an appropriate way to model the roll levelling process in COPRA® FEA RF software. Process variables (machine layout, machine deformation, material constitutive models and initial shape defects) and simulation related parameters (analysis dimension (2D *vs* 3D), discretisation strategy, contact modelling and element type) are investigated through multiple finite element analyses. This study is cumulative, as each individual evaluation leads to conclusions that are carried on to the following evaluation. Once a proper roll levelling finite element model is developed, it is integrated as a pre-process in a simple roll forming FEA and the impact of roll levelling on the final product is assessed.

From the roll levelling analysis and corresponding results, it is concluded that highly cyclic loads are associated with the process and, therefore, the material should be characterised by Chaboche-Lemaitre combined hardening model. It is also concluded that rolls' deflection is neglectable, considering that its modelling is associated with a severe penalty on the computation time and has a minor impact on the roll levelled strip. Finally, when a combined roll levelling and roll forming model is developed and performed, the pre-process reveals to have a significant impact in the finite element analysis of roll forming, namely in the geometrical properties of the roll formed profile. Nevertheless, a severe penalty on the computation time is associated to a 3D roll levelling and roll forming analysis. Alternatively to the exclusively 3D analysis, a 2D-to-3D mapping approach is suggested as a good compromise solution, where the pre-process is studied in 2D and its results assigned to a the workpiece of a standard 3D roll forming FEA. With this last approach, the computation time of the integrated analysis is expected to reduce significantly, while the positive impact of considering the roll levelling pre-process in roll forming simulations is still observable.

Resumo

Devido aos elevados requisitos para a redução de emissões de CO_2, um grande investimento tem sido aplicado no desenvolvimento de materiais leves para aplicações estruturais. No entanto, tal progresso implica novos desafios produtivos e deste modo também se estimula a evolução dos processos de fabrico. Particularmente na conformação plástica de chapa metálica, pré-processos adicionais têm sido implementados para melhor controlar as propriedades da chapa, pelo que compreender o impacto da cadeia produtiva no produto final se tornou uma prioridade.

Como consequência de uma maior exigência industrial, algumas empresas de software CAE, nomeadamente a data M Sheet Metal Solutions GmbH, procuram estudar a viabilidade de integrar um maior espetro da cadeia produtiva nos seus produtos de modo a melhorar a sua qualidade. Os softwares COPRA® RF e COPRA® FEA RF, amplamente utilizados na indústria para projetar linhas de perfilagem (*roll forming*) e realizar uma subsequente análise do processo, são exemplo desta tendência. Entender como a simulação de *roll forming* beneficia do pré-processo de *roll levelling* e como pode a simulação por elementos finitos de ambos os processos ser integrada são importantes tópicos de investigação.

Neste trabalho é realizado um estudo aprofundado de modo a encontrar uma forma apropriada para modelar o processo de *roll levelling* no software COPRA® FEA RF. Variáveis do processo (configuração e deformação da maquina, modelos de encruamento e rigidez do material, e defeitos geométricos iniciais) e parâmetros de simulação (dimensão da análise (2D *vs* 3D), estratégia de discretização, modelo de contacto, e tipo de elemento) são investigados através de múltiplas análises por elementos finitos. Este estudo é cumulativo, uma vez que as conclusões de cada análise individual são tidas em conta no desenrolar do trabalho. Quando um modelo adequado para o processo de *roll levelling* é alcançado, este é integrado como um pré-processo numa simulação simples de *roll forming* e o impacto do *roll levelling* no produto final é avaliado.

A partir do estudo de *roll levelling* e respetivos resultados, conclui-se que pronunciadas solicitações cíclicas estão associadas ao processo e, por consequência, que o encruamento do material deve ser caracterizado pelo modelo misto de Chaboche-Lemaitre. Conclui-se ainda que a deflexão dos rolos é desprezável, uma vez que a modelação da mesma está associada a uma severa penalização no tempo de computação e o impacto nas propriedades da chapa nivelada é reduzido. Por fim, quando um modelo combinado de *roll levelling* e *roll forming* é desenvolvido e analisado, o pré-processo revela ter um impacto significativo na análise por elementos finitos do processo de *roll forming*, nomeadamente nas propriedades geométricas do perfil conformado. Não obstante, uma grande penalização no tempo de computação é observada quando uma análise de *roll levelling* e *roll forming* é realizada em 3D. Em alternativa à análise exclusivamente 3D, uma estratégia de mapeamento 2D-para-3D é sugerida como uma boa solução compromisso, na qual o pré-processo é estudado em 2D e os respetivos resultados atribuídos à chapa de uma simulação convencional de *roll forming* em 3D. Através desta estratégia, estima-se que o tempo de computação da análise combinada reduza significativamente, ao mesmo tempo que o impacto positivo de considerar o pré-processo de *roll levelling* nas simulações de *roll forming* permanece observável.

Acknowledgements

During the last five months I had the opportunity to fulfil my expectations regarding this master's dissertation project, namely developing an exciting topic and working in an international business environment. Therefore, I would like to express my gratitude to every person, institution and company which made this experience possible and contributed to its success.

To data M Sheet Metal Solutions GmbH and Dipl.-Ing. Albert Sedlmaier, for the opportunity to develop this master's dissertation project at data M's facilities in Munich, Germany.

To my supervisor at University of Porto, Prof. Dr. Abel Santos, for his support, encouragement and guidance not only during the progress of this dissertation but also throughout my studies.

To my supervisor at data M, Dr. Thomas Dietl, for his support and guidance defining all the work and help driving it in the right track. To my co-supervisors at data M, ir. André Abee, Dipl.-Ing. Johann Harraßer and M.Sc. Miguel Pereira, for all the advices, help and teaching regarding finite element modelling and analysis. To all of them, for the long discussions, valuable critics and friendliness.

To my friends, with whom I have shared this journey, for all their support and friendship. Their presence inspired five enjoyable and rewarding years.

To my family and girlfriend, for their ever-present support, encouragement and love, not only during this last semester but also all over my academic path and life in general. Thank you for everything.

Contents

List of Figures

List of Tables

Abbreviations and symbols

2D	Two dimensions
3D	Three dimensions
AHSS	Advanced high strength steel
CPU	Central processing unit
DP	Dual-phase steel
FEA	Finite element analysis
IU	International Unit
N2S	Node-to-segment contact algorithm
NU	Non-uniform discretisation
PR	Plastic rate
RF	Roll forming
RL	Roll levelling
S2S	Segment-to-segment contact algorithm
U	Uniform discretisation
UHSS	Ultra high strength steel

A	Section's area
α	Kinematic factor
b	Chaboche-Lemaitre's isotropic hardening parameter
C	Chaboche-Lemaitre's kinematic hardening parameter
d	Distance between two consecutive working rolls
D_i	Diameter of the intermediate rolls
D_w	Diameter of the working rolls
e	Plastic rate uncertainty
e_{max}	Maximum plastic rate uncertainty
e_{min}	Minimum plastic rate uncertainty
E	Young's modulus
E_o	Young's modulus with no pre-strain
E_a	Young's modulus at an infinitely large pre-strain
E_{eq}	Equivalent Young's modulus
ε	Strain
ε_o	Pre-strain
ε^p	Plastic strain
ε_o^p	Plastic pre-strain
$\overline{\varepsilon^p}$	Accumulated plastic strain
$\boldsymbol{\varepsilon^p}$	Plastic strain tensor
ε_y	Yield strain
$\varepsilon_{y,init}$	Initial yield strain

f	Locally variation of working rolls' radius
F	Force
g	Gravity acceleration
g_{in}	Entry gap
g_{out}	Exit gap
γ	Chaboche-Lemaitre's kinematic hardening parameter
h_{wave}	Wave height
I	Inercia moment
J_2	Second main tensor invariant
K	Swift law's strength coefficient
K_{eq}	Equivalent stiffness
L	Length
l_{wave}	Wave length
μ	Friction coefficient
n	Swift law's hardening exponent
ν	Poisson's coefficient
Φ	Von Mises yield domain
Q	Chaboche-Lemaitre's isotropic hardening limit
R	Chaboche-Lemaitre's isotropic hardening component
ρ	Density
σ	Stress
$\boldsymbol{\sigma}$	Stress tensor
σ_y	Yield stress
$\sigma_{y,0}$	Initial yield stress
t	Thickness
t_e	Thickness which has not plastified
t_p	Thickness which has plastified
θ	Angle between the upper and lower set of working rolls
w	Width
X	Virtual load
$\boldsymbol{X}$	Chaboche-Lemaitre's deviatoric backstress tensor
ξ	Chord modulus parameter

Chapter 1

Introduction

Within the scope of the Integrated Master of Mechanical Engineering, from the Faculty of Engineering of the University of Porto (Porto, Portugal), an individual project comprising the knowledge acquired during the degree is developed. Problems in the area of production, product development and manufacturing should be approached and solved.

This dissertation is part of an investigation project from data M Sheet Metal Solutions GmbH (Munich, Germany) and FLATBEND European Project and was developed during a 5-month internship within data M's roll forming finite element analysis R&D department. It consists on the study of roll levelling technologies, finite element modelling of the sheet levelling pre-process, integration in a standard roll forming FEA and evaluation of the effect on the final roll formed product.

In this chapter, the project background and motivation are presented, as well as the company, dissertation objectives, planning and strategy followed in the research in addition to the structure of this report.

1.1 Background and motivation

Due to the up-going consequences of global heating, governments have been pushing the industry to reduce greenhouse gas emissions. A clear example of the sensibility and awareness for this topic is the United Nations Framework Convention on Climate Change (UNFCCC), an international environmental treaty established in 1992, where 192 countries agreed on the need to control the greenhouse gas concentration in order to prevent interferences with the climate system. Since then, Kyoto Protocol (1997) and Paris Agreement (2016) provided an actualization of the commitment on the nearly universal membership (Paas, 2016).

As a consequence of the international agreement, the European Commission confirmed the responsibility of reducing 20-30% in greenhouse gas emissions by 2020. Due to the fact that, by 2005, about 14% of EU's CO_2 emissions were released by light duty vehicles, a future regulation to limit new cars' CO_2 emissions was announced in 2007. In response, car manufacturers were led to improve the efficiency of their products. Taking into consideration that, in average, reducing 1% on the weight of a car implies saving of 0.8% on gas emissions (Kelly et al., 2015), new materials, manufacturing processes and analysis tools have been developed and implemented (Dings, 2007).

Roll forming is a continuous sheet metal forming process with high production rates and it is widely used in several industries, including the automotive one. Despite showing great improvements in the mechanical properties, the most recent materials, such as Advanced High Strength Steels (AHSS) or Ultra High Strength Steels (UHSS), represent an extra challenge to the inherent particularities of sheet metal forming processes, including roll forming. Therefore, product defects induced during the full production cycle, such as in sheet manufacturing processes, transport (coiling and uncoiling) and forming processes, have been studied. Industry concluded that such defects should be contained and pre-processes (e.g. roll levelling, which aim to reduce shape defects and homogenise residual stresses in the sheet) have been introduced upstream the main forming processes.

1.2 data M Sheet Metal Solutions GmbH

Located in Oberlaindern, approximately 40km south of Munich (Germany), data M Sheet Metal Solutions GmbH was first established in June 1987 by Albert Sedlmaier and Stefan Freitag, two research engineers from Technical University of Munich (data M SMS, 2012).

Figure 1.1 – Logo of data M Sheet Metal Solutions GmbH.

Throughout the years, the company developed several tools to design and simulate sheet metal forming processes, having specialised in roll forming. In 1989, the first version of COPRA® RF was developed, a design software for roll forming tools which was based on HP-UX ME10 and AutoCAD®. Due to an effort to provide a process simulation solution, COPRA® FEA RF was released in 2002. This software was developed using MSC Marc/Mentat software, having been established an OEM partnership between data M and MSC (data M SMS, 2012; Ferreira, 2016).

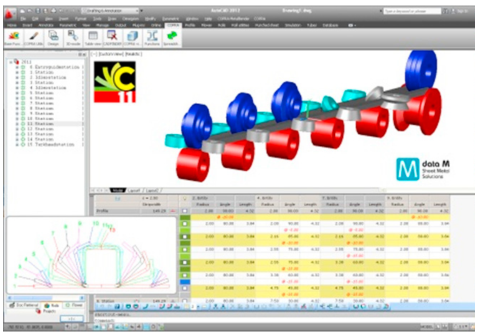

Figure 1.2 – COPRA® RF (Sedlmaier et al., 2018).

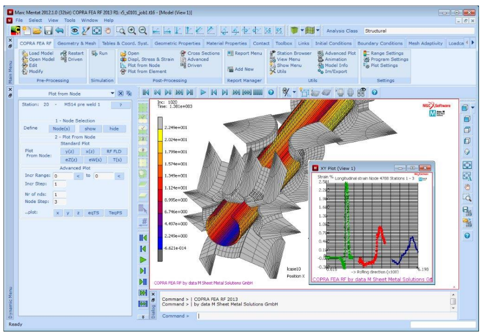

Figure 1.3 – COPRA® FEA RF (data M SMS, 2013).

Other products have also been developed in order to extend the product range for roll forming industry, such as COPRA® RollScanner (1993), COPRA® ProfileScan Desktop (2015) and COPRA® ProfileScan In-line (2018), automatic inspection machines for roll forming tools and profiles, respectively. Nowadays, data M's mission is to grow their COPRA® EcoSystem, starting by acquiring knowledge in all areas of roll forming technology, from process design and development, conception of roll forming lines and prototyping, to process control, defect analysis and troubleshooting. There is also focus on the development of new roll forming applications, namely flexible roll forming (e.g. 3D RollForming Center®) (Sedlmaier et al., 2018; data M SMS, 2019a; Ferreira, 2016).

Figure 1.4 – COPRA® ProfileScan Desktop (data M SMS, 2019b).

Figure 1.5 – 3D RollForming Center® (data M SMS, 2019a).

Due to the industrial progress, data M Sheet Metal Solutions GmbH is involved in FLATBEND project, an European project aiming to study the effect of roll levelling pre-process in cutting and bending lines. Despite being used in the industry, no sheet metal forming FEA software provides the integration of roll levelling pre-processing. For that reason, data M looks forward to evaluate the feasibility of complementing roll forming finite element analysis with previous roll levelling FEA.

1.3 Objectives of the dissertation

The ultimate objective of this dissertation is to integrate roll levelling and roll forming processes in a single finite element model and compare it with a standard roll forming FEM.

In order to accomplish the main goal, several minor objectives are accomplished. Initially, an extensive research on roll levelling finite element modelling is executed. Later, a practical research on roll levelling modelling is performed. Considering the computational effort required, most of the study is performed in 2D, where sensible topics such as material modelling are studied. Due to the fact that some research topics are not easily analysed in 2D (e.g. rolls' deflection), a three dimensional FEM is developed. The limitations of both 2D and 3D models are analysed and an adequate roll levelling finite element modelling strategy is suggested, taking into account the ultimate objective. Finally, a roll levelling and roll forming model is developed and analysed. The results are compared with those from a standard roll forming simulation and final remarks are also considered.

1.4 Planning and methodology

During the dissertation period of time, the tasks are executed according to the Gantt chart presented in Figure 1.6.

In a first stage, the literature review is accomplished, in order to acquire knowledge in topics such as shape control technologies and sheet metal process chain. Once comfortable with these topics, a research on roll levelling modelling is performed and a hypothesis about the feasibility of this pre-process FEA is established. In order to validate the hypothesis, several finite element analyses of roll levelling and a parametric study are performed. Also, roll levelling FEA results are integrated in a simple roll forming simulation.

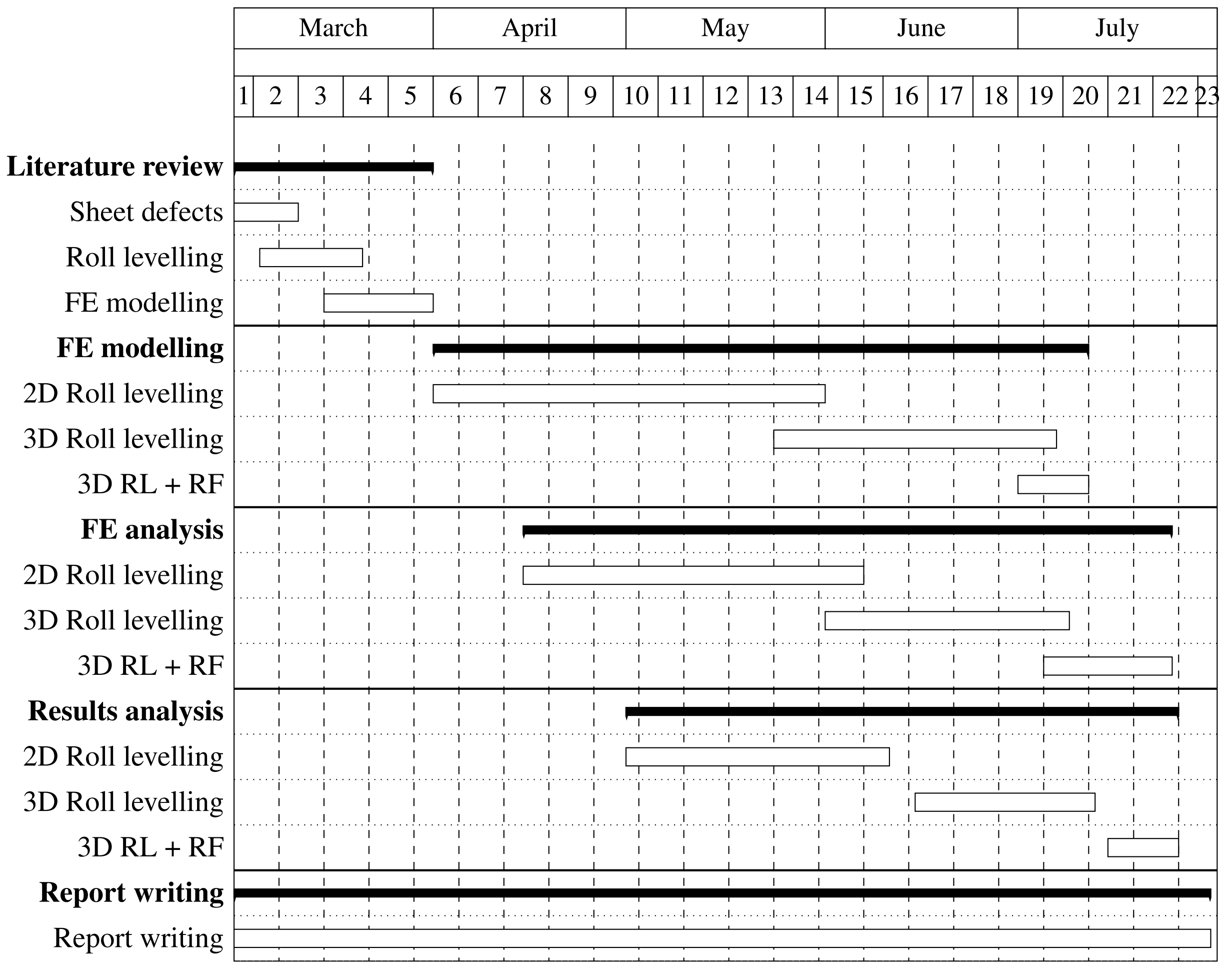

Figure 1.6 – Gantt chart.

1.5 Dissertation structure

This dissertation is organised in seven chapters, from which the first is the introduction (current chapter). The remaining chapters are enumerated and briefly described bellow:

Chapter 2 - Roll levelling review
In this chapter the literature review is performed. Topics such as sheet defects, shape control technologies, roll levelling process and finite element modelling are studied.

Chapter 3 - Modelling of roll levelling process
This is a very important part of the report, since it contains a detailed description of the roll levelling finite element models analysed in the two following chapters.

Chapter 4 - 2D model analysis
In this chapter multiple two dimensional roll levelling finite element models are developed and analysed, in order to study diverse process and modelling parameters. Most of the modelling research is performed in this chapter, considering that three dimensional simulations require a higher computation effort.

Chapter 5 - 3D model analysis
In order to complement the work developed in the previous 2D analysis, three dimensional roll levelling finite element models are developed and, particularly, working rolls' deflection is studied.

Chapter 6 - Integration with roll forming FEA
This is the chapter where the ultimate goal is accomplished. Considering the conclusions from Chapters 4 and 5, a combined 3D roll levelling and roll forming finite element model is developed and an assessment on the impact of roll levelling pre-process on a standard roll forming FEA is executed.

Chapter 7 - Conclusions and discussion
In the final chapter, the observations drawn throughout the work are summarised and discussed, some final remarks are made and future developments are suggested.

Chapter 2

Roll levelling review

In this second chapter, a literature review on the current roll levelling technologies and strategies is executed, as well as a review on sheet defects. As mentioned before, despite being widely used in industry, roll levelling process is still under progress and research work on this topic is still active. This initial approach aims to gather knowledge and sensibility on the essential topics related with the dissertation theme.

Not only in roll forming processes but also in stamping, bending and other sheet forming processes, the unprocessed material is supplied in sheet format, which means that the material has a very small thickness, when compared to the other two dimensions.

Sheet forming processes often face problems related with geometry, usually due to a poor process design but also associated with pre-existent conditions in the unprocessed material, such as stresses, strains and other defects. In order to better understand the need for roll levelling, one needs to comprehend the common post processing defects and the conditions that lead to them.

2.1 Processing defects

As mentioned before, diverse shape defects are associated with forming processes. Particularly in roll forming, defects are a daily issue, as this process submits the material to complex plastic deformations. The most important and indispensable plastic deformations are those from the transversal bending, which are induced as a main objective.

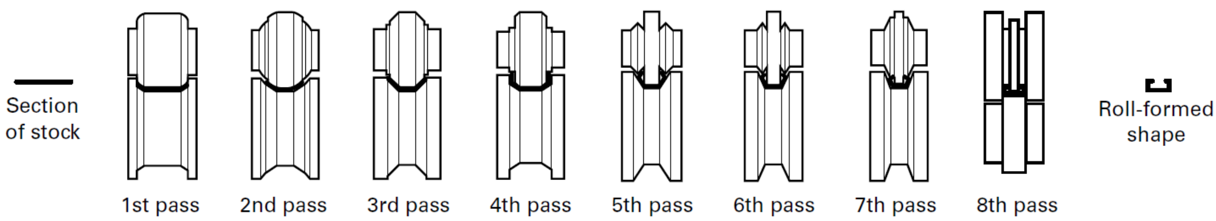

Figure 2.1 – Example of a roll forming sequence (Black et al., 2012).

Deformations of this kind are responsible for continuous change on the cross section until a desired geometry is achieved. The transversal bending is better observed through a *flower* graphic (Figure 2.2), which is when multiple cross sections (usually at the stands) are projected in the flow direction.

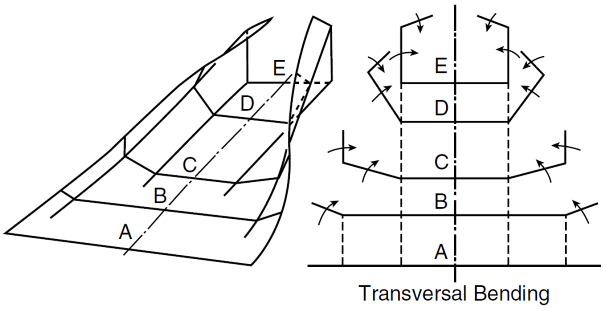

Figure 2.2 – *Flower* illustration as a sequence of roll forming processing (Halmos, 2005).

However, as the forming process occurs in three dimensions and one can not ignore the strains and stresses in the flow direction, there are other deformations that should be considered. Those are the additive redundant deformations, which are illustrated in Figure 2.3.

- Longitudinal elongation and/or shrinkage (a, a', a'');
- Transversal elongation and/or shrinkage (b, b');
- Longitudinal bending and bending back (c, c');
- Shear in the metal's plane;
- Shear in the direction of the metal's thickness;
- Various combinations of the above.

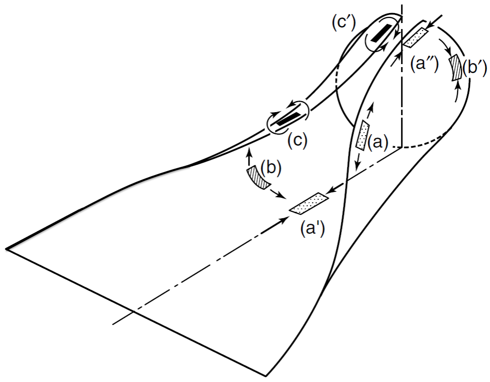

Figure 2.3 – Representation of the additive redundant deformation on a metal sheet during roll forming. Adapted from Halmos (2005).

These undesired redundant deformations have a big impact in the final product, influencing the transversal bending required to achieve the desired profile geometry. For instance, undesired deformations can induce stresses and strains in the material, increase the final springback and degrade the residual stress distribution through the strip/blank.

As a result, commonly known defects appear (Figure 2.4), such as longitudinal bow, twisting, buckling (at the edges and/or corners), cracking and end flare after cutting. Actions such as re-design of the number of stands, stand-to-stand distance and flower evolution, straightening and levelling pre-processes enable the reduction of redundant deformations and consequent defects (Halmos, 2005).

Despite part of the defects may be induced during the forming process, the unprocessed material also has a strong influence in the quality of the final roll formed product, since from two coils of the same material one can present an almost perfectly homogenous residual stress distribution and high geometrical tolerance and the other a non-homogenous residual stress distribution and poor geometrical

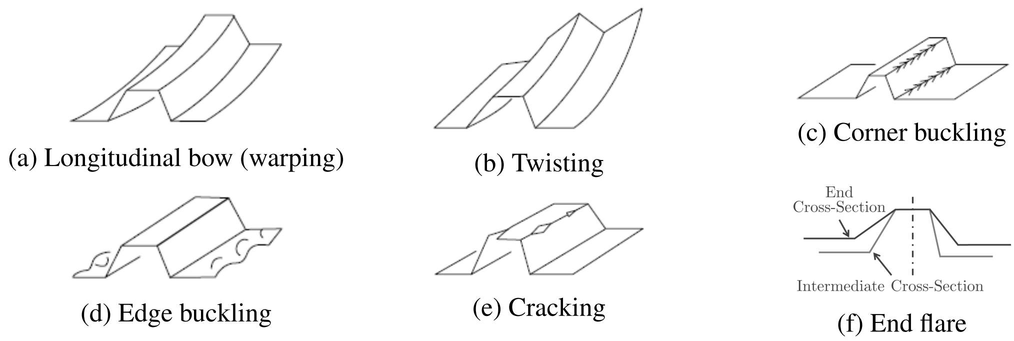

(a) Longitudinal bow (warping) (b) Twisting (c) Corner buckling

(d) Edge buckling (e) Cracking (f) End flare

Figure 2.4 – Example of defects induced due to residual stress (Halmos, 2005).

tolerances. These two coils would represent different challenges to produce an acceptable roll formed product, being the latest the most challenging.

During the production of a steel sheet, several common defects are likely to occur. The different defects can be resumed in two types: casting defects and rolling defects, which are induced in different production stages. Casting defects occur during the first phase of the process chain (hot phase) and usually imply the rejection of the strip. They are motivated by factors related with the material, casting parameters, phase transformations, mechanical and thermal stresses and others. (Satyendra, 2016).

On the other hand, rolling defects are often accepted in the metal sheet. These type of defects is induced during the cold phase of the process chain (cold phase). Some of the most relevant rolling defects are mentioned and explained bellow (Black et al., 2012; Satyendra, 2016; Soszyński et al., 2012; Ginzburg, 2009):

1. **Crown and wedge**. Being crown the difference between the thickness in the centre of the strip and the average thickness in the edges, this value is desired to be small but higher than zero, so that the strip is pulled from the middle of the width. Wedge is the difference between the average thickness of both edges, which means that the desired value is zero. Having high crowns and wedges is considered a non-acceptable defect.

2. **Mill spring**. As the mill structure and rolls suffer elastic deformation during the process, deflection is expected to reproduce a higher and uneven thickness across the width. Improving the design of the machine, particularly rolls' inertia, will help reducing this defect. Another solution is to add backup rolls, design crowned mill rolls (Figure 2.5), pre-apply a positive bending momentum in the rolls, cross pairs of rolls or use a continuously varying crown (CVC).

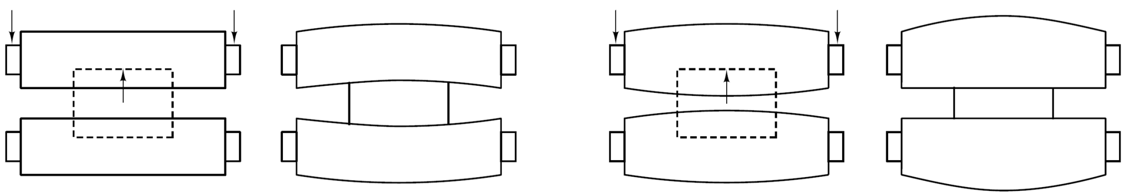

(a) Cylindrical mill roll (b) Crowned mill roll

Figure 2.5 – Deflection of different types of milling rolls. Adapted from Black et al. (2012).

3. **Flatness**. This characteristic describes the geometrical deviation of the final strip from the reference plane and represents the most interesting defect for the scope of this dissertation. Most flatness deviations are wave geometries, which can be bounded either by straight lines or curved lines.

   The waviness that is bounded by straight lines (Figure 2.6) results from a combination of tensile and compressive strains across the thickness of the strip, in the rolling direction. This leads to stresses in the top and bottom part of the strip, which are contrary to one another. Waviness across the width (cross bow) is rare, as the magnitude of stresses in the referred direction uses to be neglectable.

   The deflection of mill rolls leads to thinner and longer edges, when compared to the centre of the strip, which justify the appearance of edge waves. If a corrective measure, such as crowned mill rolls, is applied excessively, the opposite effect can happen and edge cracks or centre buckling might occur. These waviness defects are bounded by curved lines (Figure 2.7) and are divided into the following categories:

   (a) Symmetrical edge wave. Mill rolls' deflection leads to relatively longer edges and waves appear in the edges.

   (b) Asymmetrical edge wave. If rolls deflection is not symmetric, one edge will present a higher wave amplitude.

   (c) Centre buckling. When mill rolls are overcrowned, the strip becomes thinner in the centre and a wavy effect is expected.

   (d) Edge cracking. An extreme scenario under the same circumstances as the centre buckling defect.

   (e) Quarter buckling. The least common defect, is developed when a high positive bending momentum is applied in the roll in order to reduce the buckling. As the momentum might not be enough to compensate the deflection across all the width, it is halfway from the edges to the centre where the wave will appear.

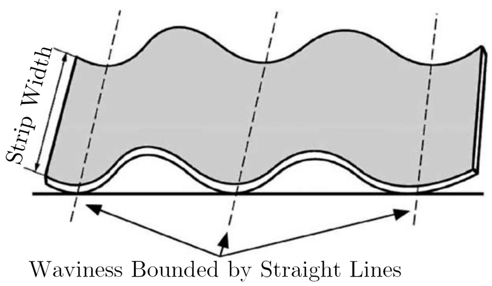

Figure 2.6 – Flatness strip defects bounded by straight lines. Adapted from Ginzburg (2009).

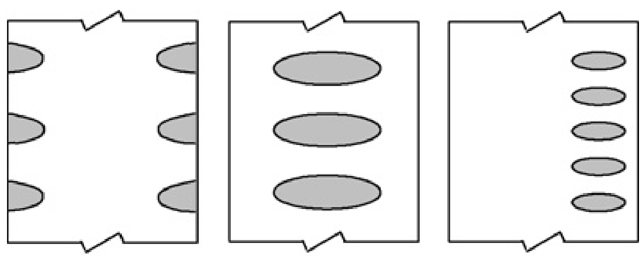

(a) Edge wave (b) Centre buckling (c) Quarter buckling

Figure 2.7 – Flatness strip defects bounded by curved lines. Adapted from Malik et al. (2008).

All the previously mentioned defects have a negative impact in the quality of the final product, after a sheet metal forming process. The presence of such defects in the sheet justifies the need for a levelling stage between the end of sheet metal processing and before the main forming process. For this reason, steel manufacturers have post-processing stages of straightening or levelling.

Despite not mentioned before, flatness defects are far more complex than just geometrical deviations and manufacturers grow in awareness and sensibility to non-geometrical flatness defects. Poor residual stress distribution is considered a major trouble because, even if the strip is geometrically perfect after levelling, future geometrical deviations are likely to occur when further processing takes place (such as roll forming, bending, cutting, etc). Therefore, Park et al. (2002) and Grüber et al. (2015) suggest that another important flatness parameter to be taken into account is the post-levelling stress distribution. In addition to correct the waviness of the strip, roll levelling stages aim to reduce and homogenise the residual stress through thickness in the final rolled metal strip.

Due to the high demand of the industry, also sheet metal forming companies have levelling and straightening pre-processes, in order to better control the flatness and residual stress of their raw materials.

2.2 Flatness quantification

In order to quantify the flatness of the steel strip, several methods and standards can be used. ISO 9445 standard, which superposed EN 10258 and EN 10259 standards, establishes tolerances for cold rolled strips (both narrow and wide). Tolerance ranges for thickness, width, length, edge camber, out of squareness, flatness and edge waviness are specified in the before mentioned standard, being the last two parameters the most important for this dissertation (BSSA, 2019).

In Table 2.1, the ISO 9445 standard is applied to a metal strip of 6000×1350×1.5 mm (length, width and thickness), as an example.

Table 2.1 – Example of ISO 9445 standard tolerances. Adapted from BSSA (2019).

Type	**Specified dimensions** t (mm)	w (mm)	L (mm)	**Tolerance** (mm)	**Observation**
Thickness (t)	$[1.50;2.00[$	$[1300;2100[$	-	± 0.10	Measured at any point located more than 20mm or 30mm from the slit or mill edges, respectively.
Width (w)	-	$[1000;+\infty[$	-	+30/-0	Strip with mill edges.
	$[1.50;2.50[$	$[1000;2100[$	-	+2.5/-0	Strip with slit edges.
Length (L)	-	$[2000;+\infty[$	-	$f(L)$/-0	$f(L) = +0.0025 \cdot L$
Edge camber	-	$[600;2100[$	$[1000;+\infty[$	1	Measured in a length of 1000mm.
	-	$[600;2100[$	$[2000;+\infty[$	2	Measured in a length of 2000mm.
Squareness	-	-	$[6000;+\infty[$	6	Difference between diagonal lengths.
Flatness	-	-	$[3000;+\infty[$	12	Maximum distance between the strip and a flat surface, when it lays under its own weight.
Waviness	-	-	-	0.03	Ratio between the wave height (h_{wave}) and wave length (l_{wave}). It is unitless.

In addition to the flatness and waviness tolerance described in standard ISO 9445 (Table 2.1), ASTM A1030 standard enables the quantification of flatness. Also, this standard introduces two other flatness parameters: the “Stepness Index” and “International Unit” (ASTM A1030, 2011).

The Stepness Index (S) is the percentage ratio between wave height and length (h_{wave} and l_{wave}, respectively).

$$S(\%) = \left(\frac{h_{wave}}{l_{wave}}\right) \cdot 100 \tag{2.1}$$

The International Unit (IU) defines a relation between the longitudinal fibres length. If one consider the difference between longest and shortest fibres, ΔL_{fibre}, and the mean length of the fibres, L_{fibre}, Equation 2.2 is achieved. Particularly when the waves are considered perfectly sinusoidal, it is possibly to quantify flatness in function of wave parameters (Figure 2.8) (ASTM A1030, 2011; Mathieu et al., 2013).

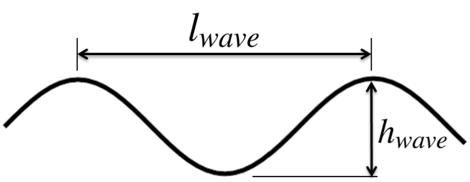

Figure 2.8 – Strip wave parameters.

$$IU = \frac{\Delta L_{fibre}}{L_{fibre}} \cdot 10^5 = \left(\frac{\pi}{2} \cdot \frac{h_{wave}}{l_{wave}}\right)^2 \cdot 10^5 \tag{2.2}$$

From Equation 2.2, one can understand that, in order to have 0 IU, all fibres should have the same length. This means that a maximum elongation of 1% is required to completely level a strip with 1000 IU.

However, defining the flatness tolerance limit through a maximum acceptable IU value is not as straight forward as measuring the flatness level. The maximum acceptable IU of a strip depends on the desired final quality and manufacturing process. Typically, strip's IU-value is 15 after cold rolling, 10 after hot rolling and 5 after levelling. With a fine levelling process, it is possible to achieve strips with less than 1 IU flatness (Theis, 2001).

Evaluating the final residual stress distribution is only feasible for academic purposes. For other purposes, an appropriate option to assess this defect is through a numerical approach. Some developments regarding this subject have been made by Park et al. (2002), Quach et al. (2004) and Grüber et al. (2015).

Finally, even though there are multiple standards and approaches to evaluate the levelling process, a feasible way to assess it in a finite element analysis is through the amount of plastic deformation induced in the strip. This measurement, which is further explained in Section 2.4 and defined in Equation 2.3, is called plastic rate (PR) and is achieved by a ratio between the total thickness of the strip and the thickness which has been plasticised.

2.3 Shape control technologies

Shape control equipments are constituted by a set of rolls which remove the undesirable flatness defects due to tension (stretcher), bending (straightener and roll leveller) or a combination of both (tension leveller). As mentioned before, the aim is always to reduce, or eliminate, flatness deviations and improve the residual stress distribution in a metal strip (Mathieu et al., 2013).

2.3.1 Straightener

Also known as flattener, the most basic levelling technology consists in a set of five to nine high diameter working rolls, when compared to other shape control technologies. These rolls are placed in two different levels (two-high equipment) with a large gap between consecutive rolls and are only supported by their own end bearings, as the equipment has no backup rolls. Typically, the rolls are non-driven and it stands out as the most affordable option (Theis, 2002b).

As expected, several disadvantages are associated to this technology. The most critical is the low maximum load (and plastic rate), since the number of rolls is very limited and there uses to be no backup structure to reduce buckling effect. This justifies that straighteners are only used to remove coil set and, therefore, found in production lines after uncoiling and before a stamping, cutting or bending process. Theis (2002b) suggests that a flatness of 5-10 IU is possible to achieve with straightening.

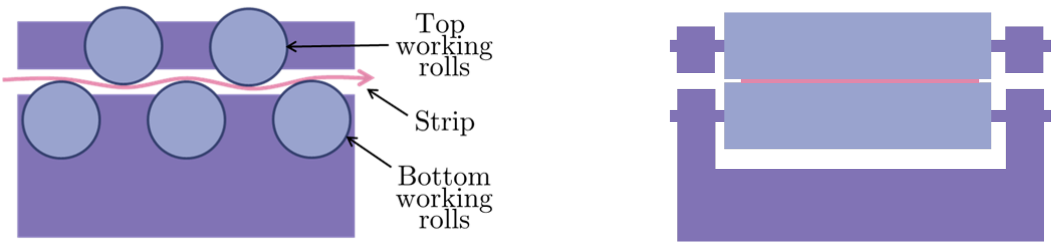

(a) Side view (b) Front view

Figure 2.9 – Straightening equipment illustration. Adapted from Theis (2002b).

2.3.2 Precision straightener

Similar to a straightener, the precision straightener is chosen either for high strength materials or when the precision required is not achievable with a normal straightening equipment.

This technology uses between 9 to 21 smaller and driven rolls and distinguishes itself by the addition of centred and vertically adjustable backup rolls, which can be used to induce a pre-deflection in the rolls. Having backup structure, it allows a better performance under high loads (less buckling) and enables not only longitudinal but also transverse curvature control. Therefore, both coil defects, cross bow and twists can be controlled (Becker, 2007; Theis, 2002b).

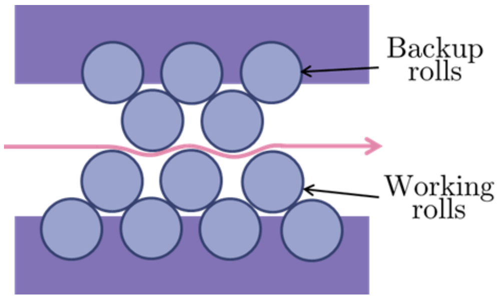

(a) Side view

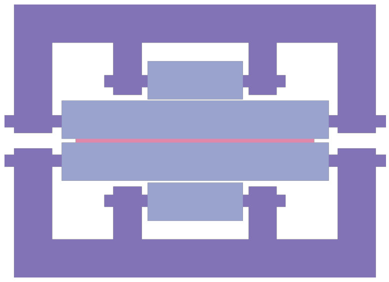

(b) Front view

Figure 2.10 – Precision straightening equipment illustration. Adapted from Theis (2002b).

2.3.3 Stretch leveller

Such as all the other shape control technologies, stretch levelling drives the material beyond its yield point. On the contrary of straightening and roll levelling, the material is not bent but stretched. For this to happen, two hydraulic clamps mechanically grip and stretch the strip (Black et al., 2012). Alternatively to the clamps, there are solutions which use sets of bridle rolls in a similar layout as in Figure 2.12, with no levelling rolls (Ginzburg, 2009).

In theory, by stretching the material in the longitudinal direction, the stress profile will be constant throughout thickness (t). This means that the material will plastically deform homogeneously, avoiding therefore inner fibres in the elastic range. Achieving a 100% plastic rate ensures a better flatness control and residual stress distribution, making this a promising technology (Leveltek Processing, 2016). According to Theis (2002b), a flatness of 0-5 IU is achievable through stretching levelling.

The downside of this technology is that it requires a finite length of metal to be stretched at a time and, consequently, leads to a low productivity rate. Geometrical changes are observed on the strip, such as length increase (the initial length, l_i, is smaller than the final length, l_f) and width reduction, and cracks are also likely to happen.

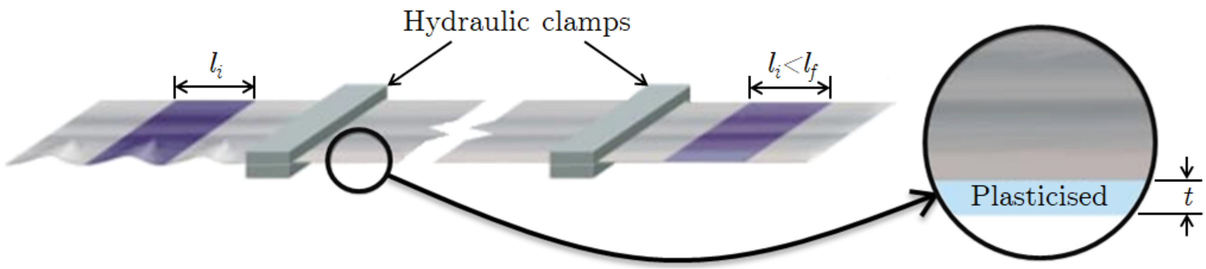

Figure 2.11 – Stretch levelling illustration. Adapted from Leveltek Processing (2016).

2.3.4 Tension leveller

A combination of two technologies: straightener and stretch leveller, it is a tension-assisted levelling method. Tension levelling has as main components two sets of large-diameter bridle rolls and a set of levelling rolls.

While the first set of bridle rolls has the function of restraining strip's flow, the second set forces the flow. This induces a significant longitudinal tension in the strip, however in a smaller magnitude then in stretch levelling. The levelling rolls promote successive reverse bending, which adds the extra 30-50% tension needed to overcome the yield limit. By superimposing longitudinal tension and bending loads, the desired levelling is achieved (Ginzburg, 2009).

When designed correctly, a tension levelling process can also induce a 100% plastic rate. It means that this technology can provide a perfectly flat strip with a quasi-homogeneous stress distribution and, on contrary to stretch levelling, it is a continuous process with reduced risks of strip cracking (Ginzburg, 2009). Theis (2002b) states that a flatness inferior to 5 IU is achievable through tension levelling.

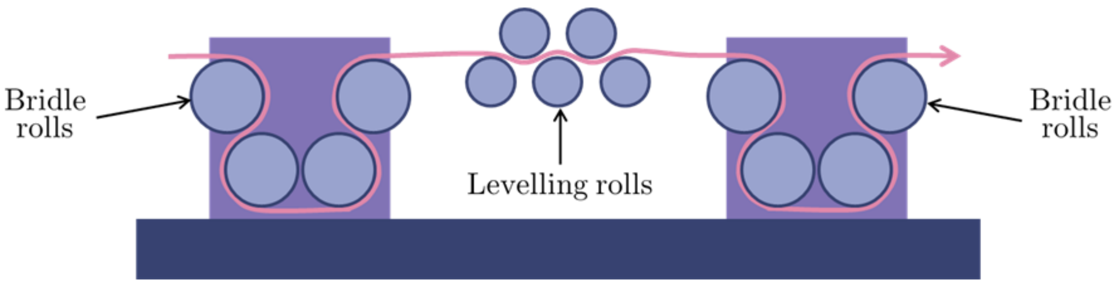

Figure 2.12 – Tension levelling illustration. Adapted from Theis (2002c).

2.3.5 Roll leveller

Typically employed to remove coil set and eliminate existing defects, this equipment is usually located after a roll mill, or before any kind of forming processing. As in most of the previous technologies, strips are bent in a cycle of reverse bendings, leading the material to cyclic tension-compression loads with the aim of equalizing fibres length and homogenise residual stress distribution, both through thickness and width (Galdos, Argandoña, et al., 2017)

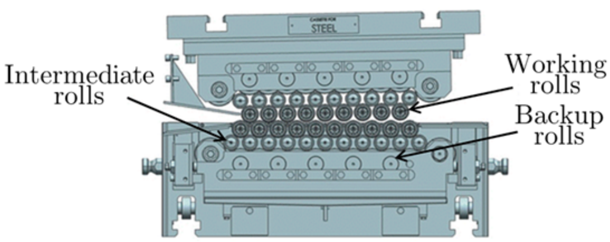

(a) Front view.

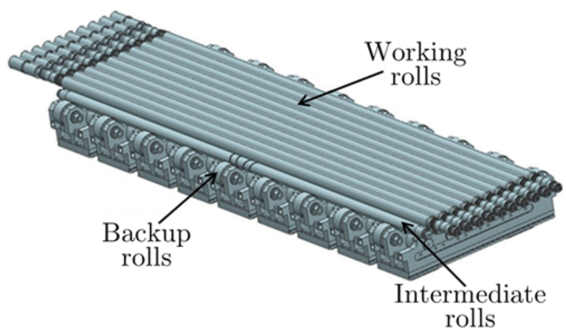

(b) Arrangement of backup rolls.

Figure 2.13 – Roll levelling equipment illustration. Adapted from Galdos and Silvestre (2018).

Although some may associate precision roll straightening and roll levelling as synonyms, these are different technologies. Despite having a similar amount of small-diameter working rolls (11 to 19), roll levellers use to have up to six-highs (e.g. Figure 2.15b) and multiple large-diameter backup rolls, both along machine length and width, as can be seen in Figure 2.13. The main advantage of this equipment is the fact that it enables the control of backup rolls' vertical position and, therefore, have more flexibility in working rolls' initial vertical position and width deflection (Theis, 2002b).

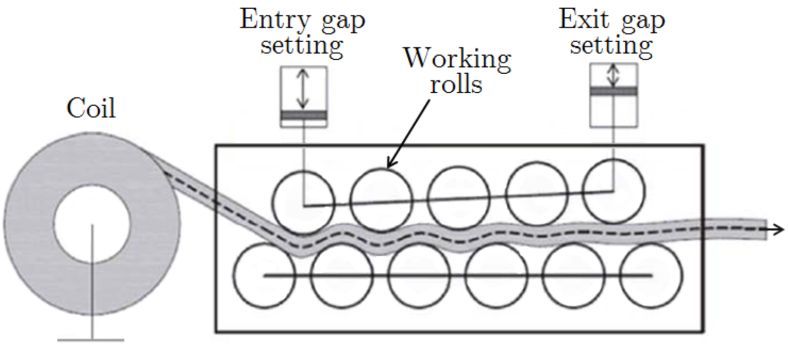

Figure 2.14 – Simplified representation of roll levelling gap setting. Adapted from Galdos, Argandoña, et al. (2017).

By fixing the lower set of rolls and varying the position of the upper set of rolls, it is possible to establish the entry and exit gaps (Figure 2.14). Usually, the upper rolls are fixed in the upper set and their vertical position is controlled by the upper set angle. The goal is to have a negative entry gap, which extent will dictate the plastic rate, and an exit gap close to strip's thickness.

Figure 2.15 illustrates two different roll levelling equipments. The four-high equipment is the most flexible option regarding shape control, since only the working rolls are continuous through width and oppose to backup rolls' induced deflection. However, when compared to a six-high solution, it is more likely that the backup rolls will mark the working rolls and, as a consequence, strip's surface. On the contrary, a six-high equipment ensures a better surface quality but is more limited when it comes to edge-to-egde shape control (Theis, 2002b). Theis (2002b) also points that a flatness of 5 IU is achievable through roll levelling.

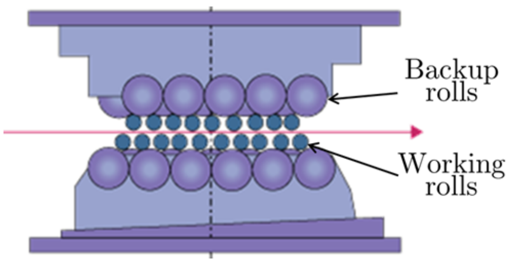

(a) Four-high

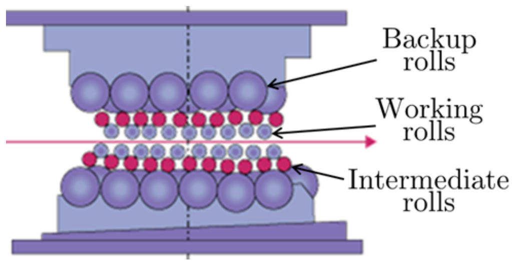

(b) Six-high

Figure 2.15 – Illustration of roll levelling equipments with different configurations. Adapted from Theis (2002b).

2.4 Process

As mentioned before, roll levelling is a pre-process that submits the strip of material to consecutive reverse bends. The material follows a waving path, according to the distance between consecutive levelling rolls, that is designed in order to force a large bend at the entry and gradually decrease to a small (or even null) bend at the exit, as illustrated in Figure 2.16 (Black et al., 2012).

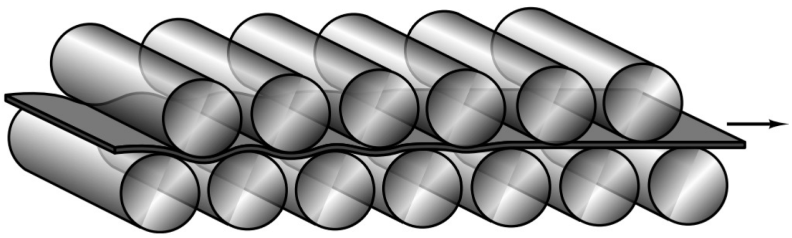

Figure 2.16 – Simplified roll levelling illustration (Black et al., 2012).

The goal of this process is to induce a tension-compression cycle in the strip, entering the plastic range and, therefore, removing any pre-existing set or defect and homogenising the residual stress distribution (Galdos, Argandoña, et al., 2017).

The amount of deformation induced in the strip is usually measured as the percentage of thickness which has entered the plastic range (in other words, the relative thickness that has non-null accumulated plastic strain), hereinafter referred as plastic rate (PR). It is defined by Equation 2.3, where t is the thickness of the strip and t_p the minimum distance between strip's surface and the fibre in the yield stress.

$$PR(\%) = \frac{2 \cdot t_p}{t} \cdot 100 \tag{2.3}$$

If one consider a strip divided into multiple layers, or fibres, across the thickness, it is easy to visualize the stresses distribution during bending. The stress levels should be positive in the outer layers (under traction) and negative in the inner layers (under compression). The stress distribution through thickness should be linear in the elastic range, which means that there is a neutral fibre (null stress) near the middle of the thickness, as Figure 2.17 illustrates. Also it should be linear in the plastic range, if no work hardening is considered.

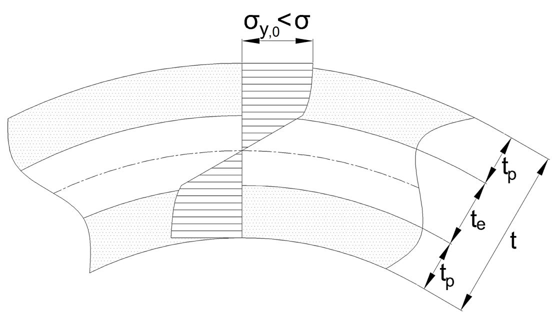

Figure 2.17 – Illustration of elastic-plastic stress profiles through thickness, considering the hardening effect.

When the stress magnitude reaches the initial yield stress (elastic limit, $\sigma_{y,0}$) the material enters into plastic range, which means that plastic deformation occur between the layers in the elastic limit and the outer/inner layer (at a distance of t_p). The layers that have not reached the elastic limit are in the elastic range and, therefore, have suffered no plastic deformation. The previously mentioned layers are in the middle part of the strip and occupy a thickness of t_e. Figure 2.17 elucidates the described concept. If work hardening effect is taken into account, material resistance increases with deformation, which justifies a stress profile similar to the one illustrated.

Being a continuous process with cyclic bending loads, roll levelling leads to a strain path also cyclic. According to Silvestre, Argandoña, et al. (2014), the strain magnitude reaches a maximum value in the third roll and then decreases from roll to roll, with the first five rolls having the most critical role. During the first five rolls, the high strain leads to the homogenisation of fibres length, which justifies the removal of geometrical deviations. The following rolls have the most influence on residual stress control. Figure 2.18 describes the previously mentioned phenomena, where each local maximum/minimum corresponds to the strain of a surface fibre in the position of a working roll.

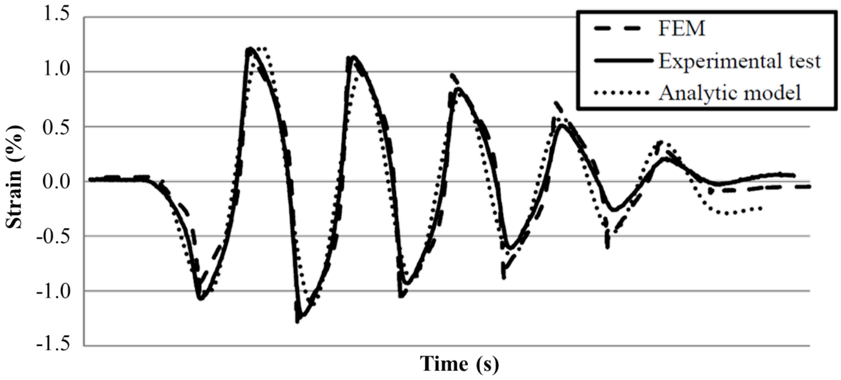

Figure 2.18 – Example of strain path during a roll levelling process, measured in a surface fibre and obtained through different methods by Silvestre, Argandoña, et al. (2014).

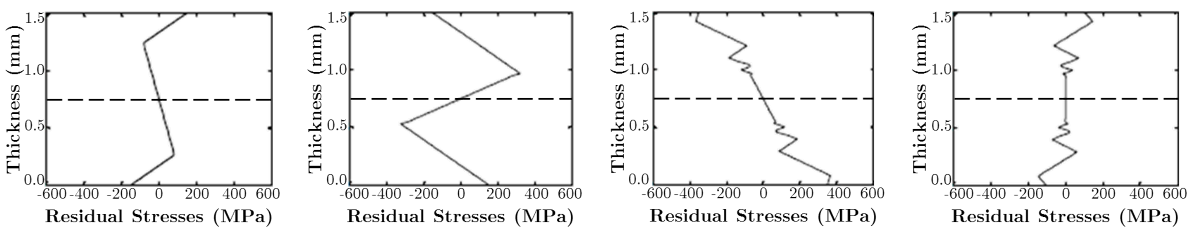

(a) Before levelling. (b) 3rd first roll. (c) 3rd last roll (d) After levelling.

Figure 2.19 – Example of longitudinal residual stress distribution through thickness in several stages of a roll levelling process. Adapted from Silvestre, Garcia, et al. (2016).

During the process, as plastic deformation occurs, a redistribution of residual stress is expected. Silvestre, Garcia, et al. (2016) generically indicate how longitudinal residual stress evolve in a simple roll levelling process to remove coil set (Figure 2.19). As one can observe, during the first five rolls, the undesired initial distribution of residual stress is overlapped by stresses of higher magnitude and poor distribution through thickness, in order to remove geometrical deviations, as mentioned before. In the following rolls a better distribution of residual stress is achieved, as smaller strain magnitudes are induced by reverse bendings. As a consequence, the stress state changes from compression to tension (or *vice versa*) and its magnitude is reduced. The goal is to, by proceeding multiple reverse bendings with a decreasing strain magnitude, achieve a final residual stress distribution through thickness with the lowest stress magnitude possible, in order to minimise unexpected shape defects after forming due to a poor consistency in the incoming material.

2.5 Limitations

Despite being widely used (Galdos and Silvestre, 2018), roll levelling has limitations which can either be geometrical, structural, material related or power limitations.

As a geometrical limitation, strip width and thickness must be within machine's range. There are different types of roll levellers, which can vary in width according to the standard strip width. When it comes to thickness it is more complicated, as the machine's gap setting range may not reach the required gap values to level both thick and thin strips (Theis, 2002a).

If the material has a very high strength, it may be impossible to level. The limitation can either be due to insufficient working rolls' inertia, inadequate number of backup rolls or over-expected machine deformation (Theis, 2002a).

Since steel is a commonly levelled material, machine suppliers provide specifications for this application. However, when different materials are levelled, a different behaviour is expected. For low Young's modulus materials, such as aluminium, a larger strain (ε) is needed to achieve the same stress level as with another material with a higher Young's modulus, such as steel, as illustrated in Figure 2.20. Therefore, a higher penetration is required to level an aluminium alloy, when compared to a steel with the same yield stress (σ_y). Also, with the increase of strain, more power is required. Thus, the same machine may not be able to level different materials due to limited gap setting range and power (Theis, 2002a).

2.6 Control parameters

Machine configuration, such as roll diameter and spacing, and settings, such as entry and exit gaps, are the most common control parameters that ensure the desired plastic rate. In order to control longitudinal shape defects, one should take into consideration the parameters illustrated in Figure 2.21: entry gap (g_{in}) and exit gap (g_{out}), which are controlled by the exit gap and angle of the upper set of rolls (θ). Although the value of g_{in} uses to be negative (overlap of rolls), g_{out} value is positive and close to the thickness.

While longitudinal shape defects are controlled by the gap evolution from entry to exit of the machine, transverse shape defects are controlled by the edge-to-edge gap evolution (across the width). Due to the flexibility of roll levelling equipments (mainly four-high roll levellers), it is possible to adjust the

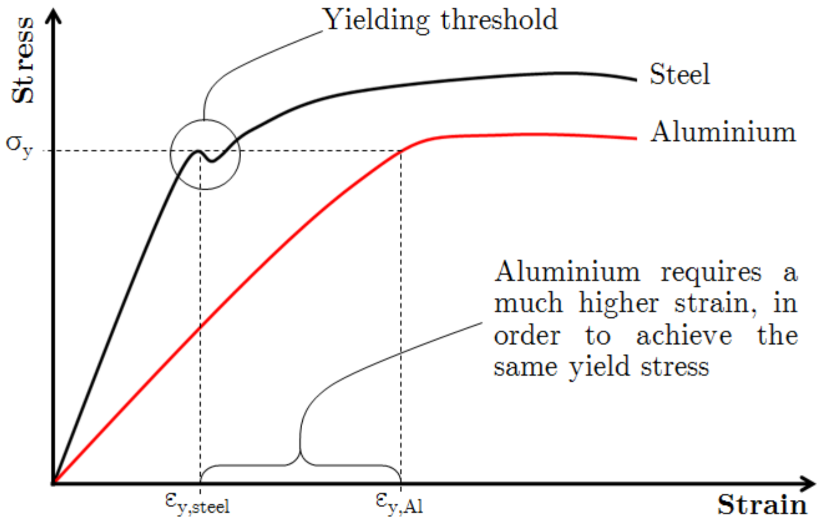

Figure 2.20 – Levelling behaviour of different materials. Adapted from A.P. Design (2009).

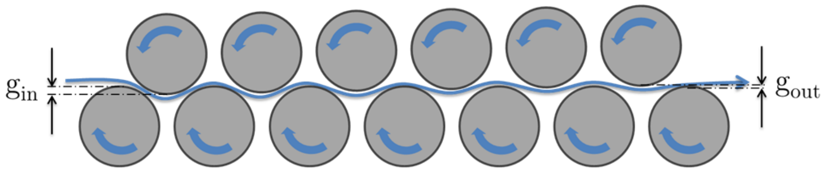

(a) Entry and exit gaps (g_{in} and g_{out}, respectively).

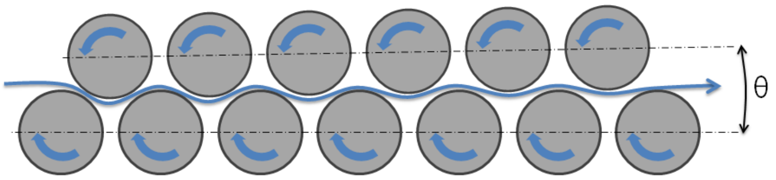

(b) Angle between the upper and lower set of working rolls (θ).

Figure 2.21 – Roll levelling settings for longitudinal shape control (only working rolls are displayed).

vertical position of each individual backup roll, which enables a highly customized pre-deflection of each working roll (Theis, 2002b). In the neutral setting of the roll leveller, both working and backup rolls are straight and parallel. This setting is used to correct coil set and waviness bounded by straight lines. If waviness defects bounded by curved lines are found, the settings suggested in Figure 2.22 should be followed. By squeezing the edges on a metal strip, one will stretch the edge fibres to a length close to those of the centre fibres and, therefore, correcting centre buckling defects. If edge waves are present in the metal strip, the opposite procedure is recommended: squeezing the centre part (Theis, 2002b).

2.7 Finite element modelling

As mentioned before, the levelling process resembles with multiple reverse bending operations, which characteristics are determined by the configuration, diameter and spacing of rolls. Therefore,

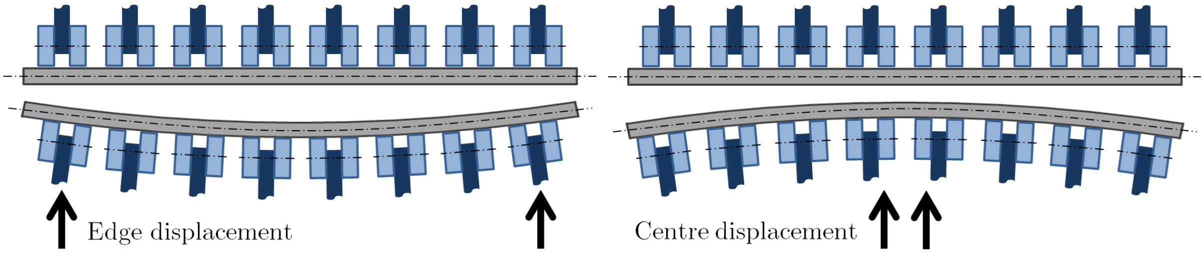

(a) Centre buckling correction. (b) Edge wave correction.

Figure 2.22 – Roll levelling setup for transverse shape control (both working and backup rolls are displayed).

in order to have a successful process, a correct setup design is required. In the recent years, many people have been researching this topic and several articles were published in this regard, but one thing has not changed: roll levelling is still a process which success is highly dependent on operator's experience and know-how.

As consequence of the already developed research, there are different ways to approach roll levelling design, which are covered in the following sections. In this section, the emphasis is given to the developments done in finite element modelling of roll levelling processes.

Despite being a time-consuming way to design a roll levelling process, finite element approach is the most flexible and reliable one, as it enables a detailed levelling design and the study of most kinds of shape defect (Silvestre, Argandoña, et al., 2014). A review on the latest developments on this topic is proceeded in detail.

2.7.1 Objective

During roll levelling processes, the objective is to achieve a metal strip with controlled flatness and residual stresses. The flatness control is done in the production line, however, controlling the residual stresses is a different challenge.

Therefore, researchers have proceeded several experiments with the general goal of finding the right roll levelling design. Those designs are not only intended to control flatness, but also to achieve a homogeneous residual stress distribution, with the least magnitude possible. In addition, some researchers have investigated the effect of material properties, constitutive models and initial defects on the levelled metal strip.

2.7.2 Dimension

During an extensive literature review, several roll levelling finite element models are analysed. All the models are two dimensional and a plane strain condition is considered for all of them.

Despite the considerable number of two dimensional approaches reviewed, no three dimensional modelling was found. This clearly states the need for an unprecedented 3D roll levelling model, in which no plane strain condition is considered and deformable rolls can be modelled.

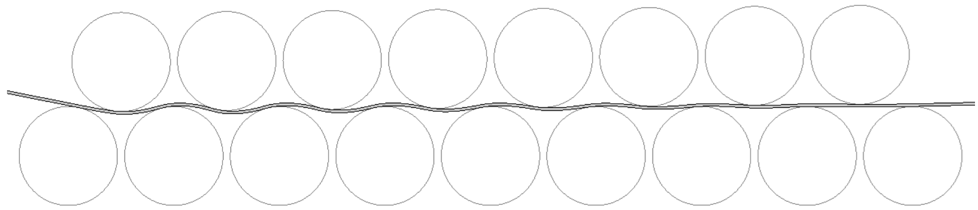

Figure 2.23 – Example of a two dimensional roll levelling finite element model (rigid working rolls).

2.7.3 Workpiece

Regarding the workpiece (metal strip) modelling, an emphasis is given to material modelling and different meshes are used to proceed multiple finite element simulations.

Since only 2D finite element models were found during this review, no reference to three dimensional elements used for roll levelling FEA is found. In two dimensional models, several authors have considered a plane strain condition and use quadrangular elements to model the workpiece for finite element simulations.

2.7.3.1 Material

Since roll levelling is a process which submits the material to high strains, there is the need to find the appropriate models and criteria for material properties. This need increases with the demand for high strength materials, such as AHSS. Several studies have been performed, mainly focusing on the material hardening characterization and some studied the Young's modulus degradation with plastic strain (illustrated in Figure 2.24 and 2.25, respectively).

Regarding material hardening characterization, a group of researchers related with Mondragon University, Spain, have done many developments on this topic. Silvestre, Galdos, et al. (2014) have analysed both isotropic, kinematic and isotropic-kinematic hardening rules and their fitting in a wide range of materials. They have observed that materials with high yield stress display a pronounced Bauschinger effect, which leads to early plastic behaviour under compression loading, and reduced work hardening. As an example, the dual-phase steel DP1000 exhibits a very high Bauschinger effect, leading to a highly kinematic hardening. Also, in this material, Young's modulus degradation is significant.

A combined hardening model, Chaboche-Lemaitre, is suggested multiple times as the adequate approach for this type of material due to its good prediction of Bauschinger effect, which is particularly important under cyclic deformations, e.g. in a roll levelling process (Silvestre, Mendiguren, Argandoña, et al., 2012; Silvestre, Argandoña, et al., 2015). In order to understand the ideal number of cycles to model the material hardening by Chaboche-Lemaitre model, Silvestre, Mendiguren, Argandoña, et al. (2013) and Silvestre, Mendiguren, Galdos, et al. (2013) performed several experiments and concluded that one cycle should be enough. The von Mises yield criteria is suggested in the previously mentioned works. Grüber et al. (2015) also proceeded a roll levelling simulation considering the same combined isotropic-kinematic hardening model.

Other researchers have chosen different material hardening models. Grüber et al. (2018) studied the impact of material yield stress on the final distribution of residual stresses and strains, assuming the Chaboche-Lemaitre hardening model simplified to pure kinematic, in order to simulate material behaviour on a roll levelling process.

Quach et al. (2004) studied the coiling/uncoiling residual stresses after levelling, Govik et al. (2014) the unloading behaviour of DP600 and Seo et al. (2016) the effectiveness of different machine configurations in levelling a defected strip. All of them followed an isotropic hardening law (Swift law) and considered the von Mises yield criteria.

With particular interest for this work, Silvestre, Mendiguren, Galdos, et al. (2015) and Gil et al. (2014) stated that the combined isotropic-kinematic hardening model is the one that predicts more accurately the material behaviour of steel DP1000.

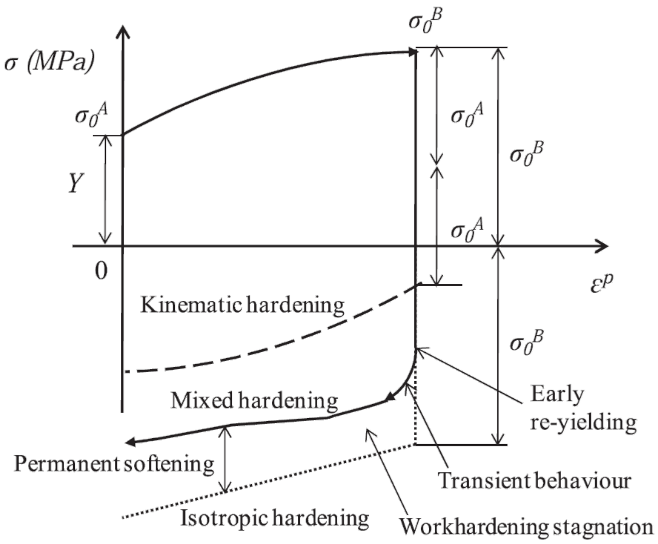

Figure 2.24 – Loading-unloading behaviour modelled by different hardening rules (Silvestre, Galdos, et al., 2014).

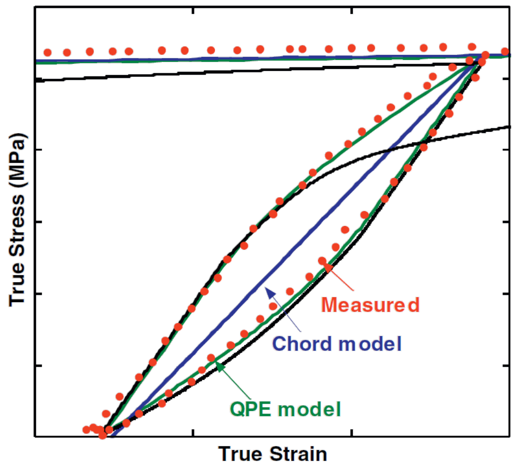

Figure 2.25 – Different Young's modulus degradation models fitting during a loading/unloading cycle of a AHSS. Adapted from Sun et al. (2011).

Regarding Young's modulus degradation with plastic strain, Yoshida et al. (2002) studied the elastic-plastic behaviour of a dual-phase steel under in-plane cyclic tension-compression large strains, which are conditions that fit the roll levelling process. During that research, it was concluded that the instantaneous Young' modulus is highly dependent on the pre-strain and a parameter average value - also known as apparent Young's modulus, or chord modulus - is suggested to be calculated in function of pre-strain.

Mendiguren et al. (2015) proceeded the experimental characterization of a TRIP700 steel and were able to fit the chord modulus model to this material. They observed a Young's modulus decrease of about 15-20% at 12% pre-strain. This Young's modulus degradation model is used in finite element analysis by Liu et al. (2017), to predict the springback of a DP980 steel after roll forming. The numerical results led to a similar conclusion, that at 10% pre-strain the Young's modulus decreases approximately 27%.

Sun et al. (2011) developed an innovative but complex Quasi-Plastic-Elastic (QPE) model and compared the unloading behaviour of a DP980 steel prediction of the QPE and chord modulus model. It was concluded that the non-linear QPE model would improve the springback prediction error of chord modulus model by a factor of two, however, the computation time increases by a factor of five. The QPE Young's modulus degradation model is applied in FEA by Jung et al. (2017).

Taking into account the developments done in the material characterization of AHSS and their application to FEA, it is possible to conclude that the combined isotropic-kinematic hardening model, developed by Chaboche and Lemaitre, is the most consensual approach to predict high-strength steels hardening and it is available in most finite element codes. When it comes to Young's modulus degradation, a conclusion is not straight-forward. Better results are expected be achieved with the QPE model, but chord modulus enable a much faster analysis. For both options, there is still the need of further research on different materials characterization, parameter databases and implementation in finite element analysis.

2.7.3.2 Mesh sensitivity

From the work developed in FEA of roll levelling processes, there is no clear focus in studying the mesh sensitivity. However, it is possible to extrapolate some conclusions from the literature review.

Grüber et al. (2015) proceeded an evaluation of the effect of initial shape defects (longitudinal curvature) on the final geometry. The analysis was carried with 5 elements across thickness and, due to the reduced number of elements, the final longitudinal residual stresses and strains across thickness were not evaluated. Other studies (Grüber et al., 2018; Grüber et al., 2017) considered 6 elements across thickness and were able to have an overview on the final residual stresses and strains distribution. Quach et al. (2004) went further in this regard, having executed a simulation with 24 elements across thickness.

In order to better represent the longitudinal residual stresses and strains thickness distribution, more elements across thickness are required. However, increasing the number of elements implies an increase of computation time. Therefore, multiple authors have chosen to have a locally refined mesh. This means that there is a longitudinal transition from a coarse mesh to a fine mesh and *vice versa*.

Silvestre, Mendiguren, Galdos, et al. (2013) and Silvestre, Argandoña, et al. (2015) have proven that this strategy works and proceeded multiple finite element simulations with a transition of 2-to-16 elements across thickness. A similar approach was done by Silvestre, Mendiguren, Argandoña, et al. (2012), but this time the transition was from 4-to-16 elements.

It is possible to conclude that, with a reduced number of elements across thickness, it is possible to proceed a roll levelling simulation and to analyse the final geometry of the strip. However, no significant representation of residual stresses and strains is possible. Therefore, a good compromise between resolution and computation time is the use of a locally refined mesh.

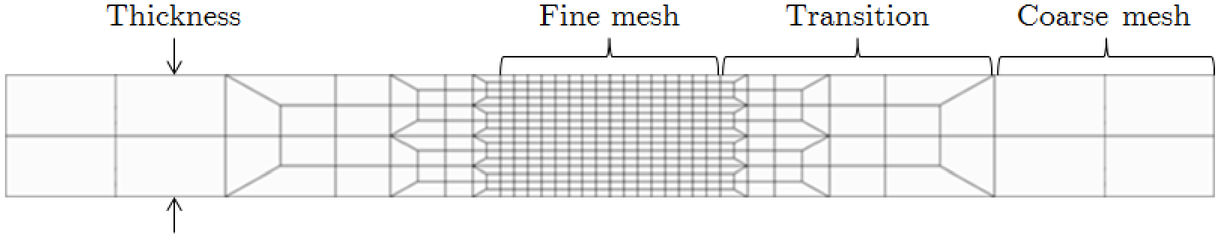

Figure 2.26 – Example of a 2D locally refined mesh with transition from 2-to-16 elements. Adapted from Silvestre, Mendiguren, Galdos, et al. (2013).

2.7.4 Tooling

Despite no report of 3D finite element modelling of roll levelling was found in the extent of this review, there have been several attempts to improve the feasibility of 2D simulations by increasing the model resemblance with the real machine.

2.7.4.1 Deformable rolls

As a limitation of the 2D simulation, it is not possible to take into account working rolls' deflection across the width of the strip and, therefore, the rolls are commonly modelled as rigid bodies with a controlled position and backup rolls are ignored. This is verified in most of the previously mentioned finite element simulations and, therefore, rigid-deformable contact is considered between working rolls and strip surface.

Some improvements in this regard are introduced by Grüber et al. (2017) and Grüber et al. (2018), who assessed machine's deflection and modelled it by linking the working rolls to the ground by means of a spring with the equivalent rigidity of the machine.

As one can easily comprehend, there is a large space for improvement in this regard. However, a detailed evaluation on the effect of deformable working rolls implies using a three dimensional model.

2.7.4.2 Friction

As in real-life roll levellers are roll-driven, it is important to establish an accurate contact between working rolls and metal strip. The most important parameter is the coefficient of friction and it depends on the material and surface quality of both working rolls and metal strip.

As a general rule, constant values of the dynamic coefficient of friction are used to model the roll levelling process, using a Coulomb friction model. For steel strip roll levelling, different dynamic coefficient of friction (μ) are found in the literature:

- $\mu = 0.05$, used by Silvestre, Mendiguren, Argandoña, et al. (2012) and Silvestre, Mendiguren, Galdos, et al. (2013);
- $\mu = 0.10$, used by Seo et al. (2016);
- $\mu = 0.14$, used by Galdos, Argandoña, et al. (2017);
- $\mu = 0.25$, used by Silvestre, Argandoña, et al. (2014).

However, assuming a constant coefficient of friction is not the most accurate approach. The variable is highly influenced by parameters such as contact pressure, sliding velocity and temperature (Ulibarri et al., 2016). At University of Mondragon, a new friction characterization method was developed by Ulibarri et al. (2016), in order to analyse the variable in roll levelling conditions and at a certain plastic rate. Several experiments were carried out to characterise TRIP700 steel's coefficient of friction at 80% plastic rate and the average dynamic coefficient of friction was found to be $\mu = 0.069 \pm 0.007$.

It is noticeable how ambiguous this topic is. As μ may change from application to application, ideally a contact characterization should be done for each application. Taking into account that such measure is not practical, a more generalized value should be used.

2.7.5 Initial defects

Ideally, one should avoid undesired plastic deformation, which leads to unnecessary hardening and Young's modulus degradation of the material. Therefore, it is important to know what is the minimum plastic rate required to level a certain initial deformation. Besides theoretical approaches to determine the plastic rate needed to remove coil set, some finite element models have been developed for different initial shape defects.

Quach et al. (2004) analysed the effect of different coil sets, by previously bending the to-be-levelled strip to the coil curvature radius. The bending was done by fixing one tip of the strip and applying a load in the other, so that the desired curvature radius is achieved. It was concluded that the higher the yield stress of the material the less plastic deformation is required and that there is a maximum radius from which no coil set is observed.

A similar procedure was done by Grüber et al. (2015) and Seo et al. (2016), this time by previously bending the strip in a three-point bending. The first one induced curvature radius in the order of coil set ones and used the resulting residual stresses and strains distribution, across thickness, to characterise the original state of the metal strip. The second has studied the levelling effectiveness when a tail-up defect, induced by a small-diameter bending, is present in the strip.

It is, therefore, possible to induce simple shape defects in strips that are later levelled. However, this may not be necessary if one considers that there is no disadvantage in overestimating the required plastic rate to level a certain metal strip.

2.7.6 Results evaluation

As mentioned before, the overall objective of all roll levelling simulations reviewed is to evaluate the final geometry (Seo et al., 2016) and distribution across thickness of residual stresses and strains (Quach et al., 2004; Silvestre, Mendiguren, Argandoña, et al., 2012; Grüber et al., 2015; Grüber et al., 2017; Grüber et al., 2018).

Some authors investigated the strain path of a superficial node during the levelling process (Silvestre, Argandoña, et al., 2014; Galdos, Argandoña, et al., 2017) and others the loads and torque on the rolls (Silvestre, Mendiguren, Argandoña, et al., 2012; Galdos, Argandoña, et al., 2017).

Representations of some of those results can be found on Figure 2.27.

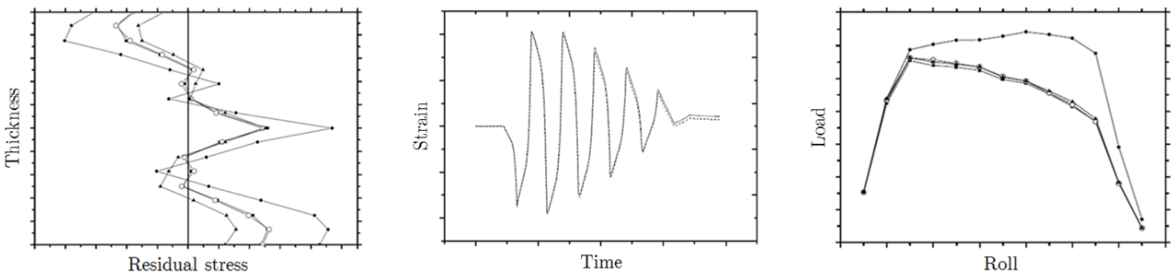

(a) Residual stresses distribution (b) Strain path of superficial node (c) Load on working rolls

Figure 2.27 – Example of roll levelling results evaluation. Adapted from Silvestre, Mendiguren, Galdos, et al. (2013).

2.8 Impact on roll forming

As mentioned in Section 2.1, roll forming processes are suitable to a wide range of geometrical defects, mainly longitudinal bow, springback and end flare. One of the factor which motivates such defects is the accumulation of non-homogeneous residual stresses in the strip during its processing.

Abvabi et al. (2015) studied the effect of cold rolling residual stresses on the quality of a DP780 steel roll formed product. Cold rolling induces the following longitudinal residual stress distribution in the strip: symmetric, positive near the strip surfaces and negative in the central part (Figure 2.28). This phenomena is inflated with the increase of total plastic strain, which is almost constant across thickness. From this work, it is possible to extrapolate some conclusions about the need to simulate roll levelling previously to a roll forming simulation, when metal strips are submitted to a roll levelling pre-processing.

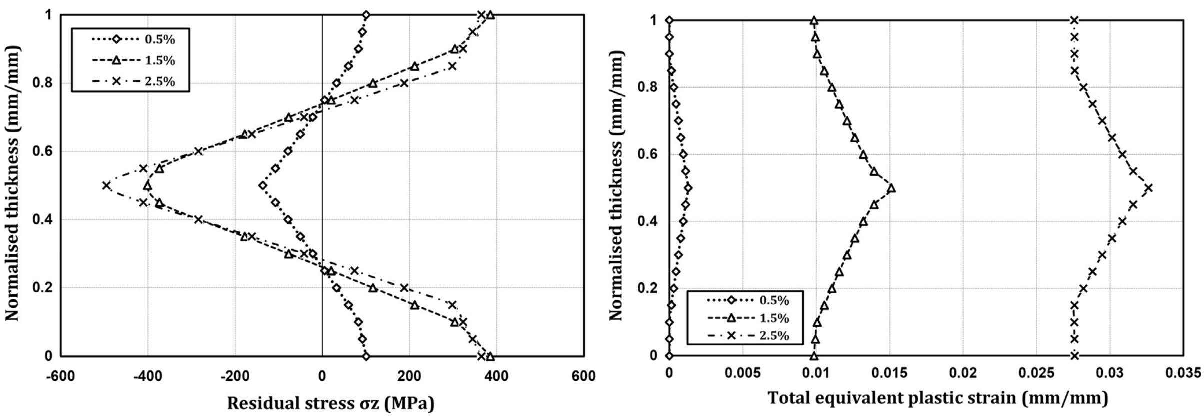

(a) Longitudinal residual stress (b) Accumulated plastic strain

Figure 2.28 – Cold rolled steel strip state distribution across thickness (Abvabi et al., 2015).

After roll forming a V-profile, it was observed that knowing the levelled state of the strip leads to an insignificant impact on the springback prediction, which mainly depends on the yield stress of the material (which increases with total plastic strain due to hardening effect). For his work, Abvabi et al. (2015) considered that the material would be characterised after cold rolling and that introducing the true strength of the material would be enough to improve the springback prediction.

However, for the present work, this consideration is not valid. If one wants to predict the effect of roll levelling in further forming processes, it may not be feasible to experimentally characterise the material for each combination of material, geometry and machine setting. Thus, if only the properties of the raw material are known, roll levelling simulations are expected to have a positive impact in the accuracy of further forming process simulations.

On the other hand, the longitudinal bow and end flare decrease for higher initial strains and residual stresses (Abvabi et al., 2015). As they are highly dependent on initial residual stresses, their prediction is expected to be positively affected by a previous roll levelling simulation.

Therefore, it is of the highest interest to better understand and characterise roll levelling FEA and study the feasibility of implementing roll levelling pre-processing in commercial roll forming FEA software.

Chapter 3

Modelling of roll levelling process

During this work, an in depth roll levelling modelling study is proceeded using finite elements analysis COPRA® FEA RF software. After having executed a literature review on roll levelling, in this chapter a summary of the finite element models and main topics under scope throughout the next chapters can be found. Some of the topics are workpiece modelling, material constitutive models, tooling deformation and initial defects modelling. The modelling study is of major importance due to the fact that a good compromise between simulation quality and computation time.

3.1 Analysis planning

Several roll-levelling finite element analyses are proceeded throughout the next two chapters. During each analysis, a particular characteristic of the model is under scope and the resulting observations are used to refine and improve further analyses.

Table 3.1 – Sequence of roll levelling analyses.

	Analysis stage								
	1	2	3	4	5	6	7	8	9
Dimension									
2D	●	●	●	●	●	●	●	○	○
3D	○	○	○	○	○	○	○	●	●
Material									
Swift law	●	●	○	○	○	○	○	○	○
Combined hardening	○	○	●	●	●	●	●	●	●
Constant modulus	●	●	●	○	●	●	●	●	●
Chord modulus	○	○	○	●	○	○	○	○	○
Tooling									
Rigid rolls	●	●	●	●	○	●	●	●	○
Deformable rolls	○	○	○	○	●	○	○	○	●
Other									
Gravity	○	●	○	○	○	○	○	○	○
Entry gap	○	○	○	○	○	●	○	○	○
Initial curvature	○	○	○	○	○	○	●	○	○

Table 3.1 resumes the proceeded sequence of analyses. The first studied characteristic is the meshing method, followed by the material modelling. A simplified 2D rolls' deformation study is also proceeded. Later, when a three dimensional model is analysed, it is possible to study in detail working rolls' deflection and backup rolls effect in the final product. Initial defects' impact on the final product is also analysed.

3.2 Analysis dimension

During the first stages of the current work, a two dimensional model (2D) is developed and studied, since it is exected to provide a good approximation of the real process within a short computation time. In this model, the plane-strain condition is assumed in order to simulate a very wide strip. Therefore, rolls deflection is simplified to a vertical displacement. In order to better understand the effect of working rolls' deflection and addition of backup rolls, a three dimensional (3D) model is required.

Another reason to explore a 3D roll levelling model is due to the compatibility with roll forming process simulations. Due to the high complexity of roll forming, most finite element analyses of this process are proceeded in three dimensions. Therefore, after an extensive 2D study on roll levelling finite element modelling is performed, the process is modelled in 3D and integrated in a combined roll levelling and roll forming FEA.

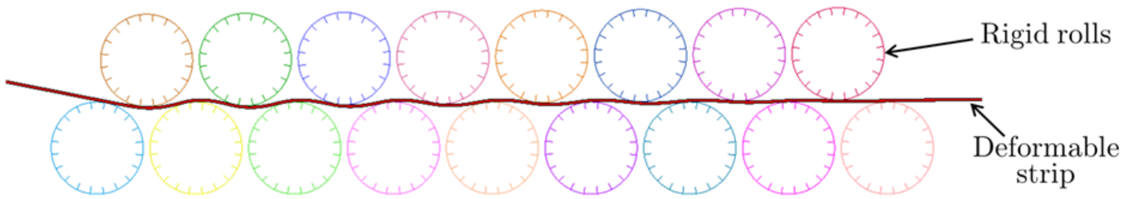

(a) 2D model with rigid rolls (plane strain condition).

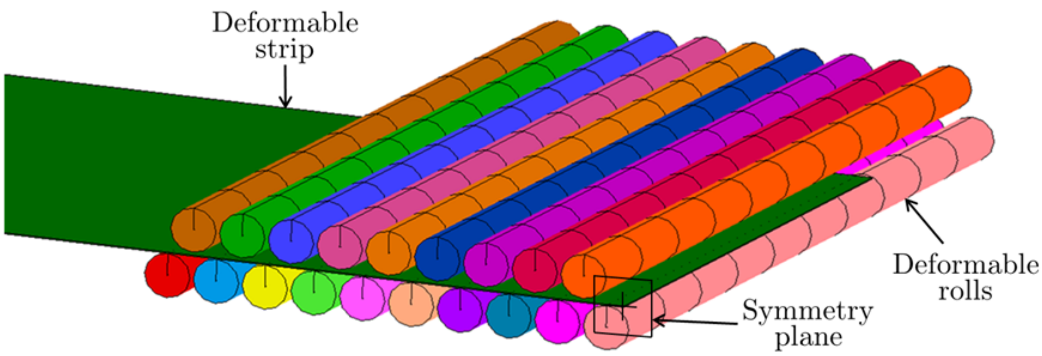

(b) 3D model with deformable rolls (symmetry condition).

Figure 3.1 – Roll levelling finite element models, developed in COPRA® FEA RF.

3.3 Workpiece

During the roll levelling analyses, the workpiece (metal strip) is modelled as a deformable body with 1.5 mm thickness and 1500 mm width. The length is chosen to be three times the machine length (≈1500 mm). In 2D simulations, as the plane-strain condition is considered, the width of the strip has no influence in the stress-strain results under scope when the working rolls are modelled as load controlled geometrical bodies.

When a combined roll levelling and roll forming FEA is executed, the strip width is reduced to approximately 100 mm in order to fit the dimensions of the roll formed profile.

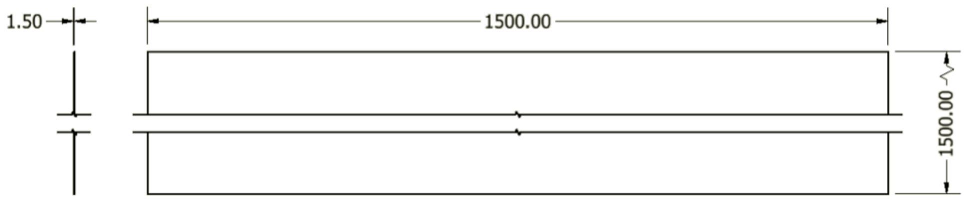

Figure 3.2 – Workpiece dimensions (roll levelling models) (dimensions in mm).

3.3.1 Element type

Depending whether the roll levelling model is two dimensional or three dimensional, different element types are used to model both the strip and deformable rolls, whenever considered.

3.3.1.1 2D modelling

Taking into account the expertise of data M Sheet Metal Solutions GmbH and MSC Marc® user manual (MSC Software Corporation, 2018), the element type used in all 2D simulations is an arbitrary quadrilateral plane-strain element, available in COPRA® FEA RF software as "Element 11".

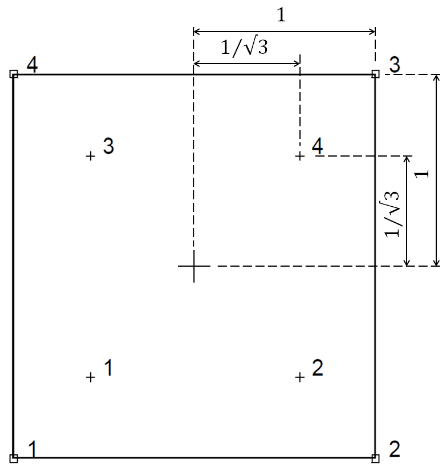

Figure 3.3 – Element type 11, with nodes (square boxes) and integration points (plus signs). Adapted from MSC Software Corporation (2018).

This element type has four integration points and is preferred over high-order elements when the analysis has particular focus on contact (e.g. roll levelling FEA). The output of results from this type of element is available at the centroid or at its four nodes (MSC Software Corporation, 2018).

Analysing a strip meshed with a finite number of elements along thickness has a particular impact on the evaluation of plastic rate (PR, defined in Equation 2.3), which is the thickness percentage which has plasticised during roll levelling. By quantifying the plastic rate according to the strain values in the nodes, there is an uncertainty (e) associated with the discretisation along thickness direction, which is defined in Equation 3.1. An illustration of the before mentioned uncertainty concept can be found in Figure 3.4.

$$e(\%) = \frac{2}{\text{N}^{\text{o}} \text{ elements through thickness}} \cdot 100 \quad \Rightarrow \begin{cases} e = 25.00\% & \text{, 8 elements} \\ e = 16.67\% & \text{, 12 elements} \\ e = 12.50\% & \text{, 16 elements} \end{cases} \tag{3.1}$$

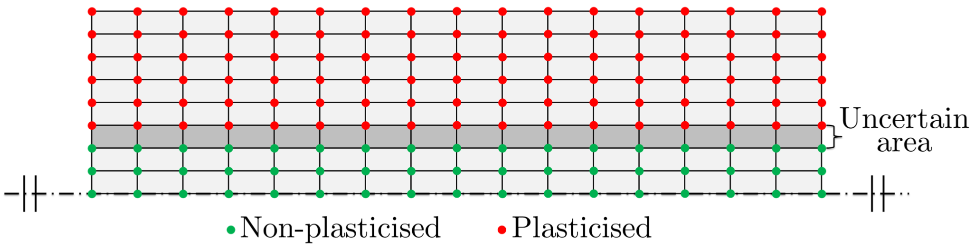

Figure 3.4 – Illustration of the uncertainty (e) when measuring plastic rate in the nodes.

Since each element has four integration points, which are not shared between elements, by analysing the results directly in the integration points it is possible to increase the PR resolution and, thus, enable a deeper understanding on the stresses and strains distribution through thickness. However, such procedure is not automatic and requires an extra effort from the user and, therefore, should only be considered when the results resolution is a priority.

Knowing that the integration points are located at (x_i, y_i) with $x_i, y_i \in \{-1/\sqrt{3}, 1/\sqrt{3}\}$ for an element which nodes are located at (x_n, y_n) with $x_n, y_n \in \{-1, 1\}$, as illustrated in Figure 3.3, it is possible to calculate the global position of the integration points (Adeeb, 2019). Two different distances can be measured between two consecutive integration points, depending whether the points belong to the same element or not. Therefore, for a certain discretisation, two different PR measurement uncertainties are possible, as can be seen in Figure 3.5 - a maximum (e_{max}) and minimum (e_{min}) uncertainty.

$$e_{max}(\%) = \frac{2/\sqrt{3}}{\text{N}^{\text{o}} \text{ elements through thickness}} \cdot 100 \quad \Rightarrow \begin{cases} e_{max} = 14.43\% & \text{, 8 elements} \\ e_{max} = 9.62\% & \text{, 12 elements} \\ e_{max} = 7.22\% & \text{, 16 elements} \end{cases} \tag{3.2}$$

$$e_{min}(\%) = \frac{2 - 2/\sqrt{3}}{\text{N}^{\text{o}} \text{ elements through thickness}} \cdot 100 \quad \Rightarrow \begin{cases} e_{min} = 10.57\% & \text{, 8 elements} \\ e_{min} = 7.04\% & \text{, 12 elements} \\ e_{min} = 5.28\% & \text{, 16 elements} \end{cases} \tag{3.3}$$

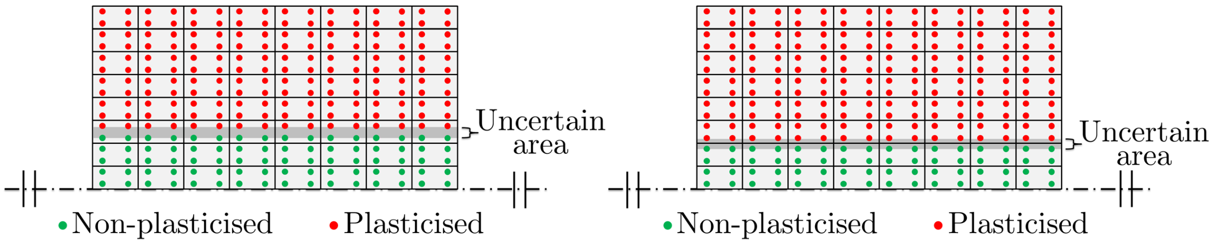

(a) Maximum uncertainty (e_{max}). (b) Minimum uncertainty (e_{min}).

Figure 3.5 – Illustration of the uncertainty when measuring plastic rate in the integration points.

3.3.1.2 3D modelling

In 3D finite element modelling two main element types are used: solid for the strip and beam elements to model deformable rolls. The solid element type is identified in COPRA® FEA RF as "Element 7" and is chosen by taking into account the expertise of data M Sheet Metal Solutions GmbH and MSC Marc® user manual (MSC Software Corporation, 2018). It has eight nodes, eight integration points (Figure 3.6) and uses trilinear integration functions.

In this work, this element is modelled with both imposed constant dilatation strain and assumed strain integration formulation in order to improve its bending behaviour and avoid the hourglass effect.

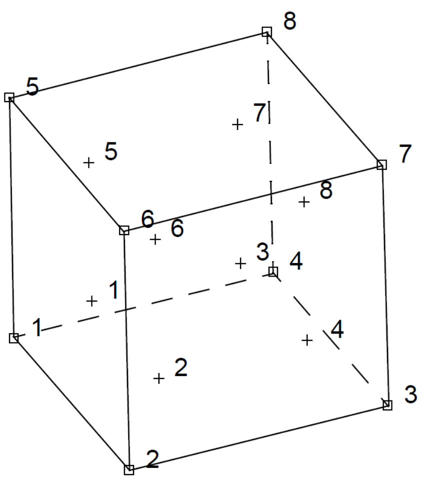

Figure 3.6 – Element type 7, with nodes (square boxes) and integration points (plus signs) (MSC Software Corporation, 2018).

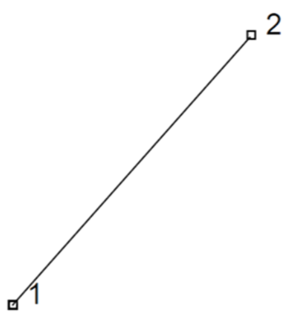

Figure 3.7 – Element type 98, with nodes (square boxes) (MSC Software Corporation, 2018).

In order to model deformable rolls in a time-efficient way, all rolls are modelled as beam elements. This type of element, identified as "Element 98", is an elastic straight beam which has only one integration point and two nodes (Figure 3.7). It uses linear interpolation for axial, transverse and rotation displacements.

Taking into account that deflection is the main deformation phenomena in the rolls, beam elements are chosen due to its simplicity and possibility to establish contact either with other beam and solid elements. It only requires both the inertia moment and contact radius to be defined.

3.3.2 Mesh sensitivity

Taking into account that both final geometry, residual stress distribution and strain distribution are studied (as mentioned in Section 3.6), it is of the highest importance to have a reliable discretisation.

Therefore, during the first analysis an appropriate mesh is searched. This mesh should provide a good balance between the following points:

- Accurate representation of the final geometry;
- Detailed representation of the stress distribution, in particular the longitudinal residual stress component distribution across thickness;
- Detailed representation of the strain distribution, in particular the final accumulated plastic strain distribution across thickness;
- Accurate representation of the steady state condition of continuously reverse bending;
- Require a reasonable computation time.

In the subsequent analyses, different meshing strategies are studied, such as regular, locally refined (e.g. Figure 2.26) and locally refined with elements of different thickness (non-uniform). Also, the refined area length is under scope.

3.3.3 Material modelling

As in the present work the objective is to better understand the particularities of roll levelling FEA, only one material is studied. This material is DP1000 steel, which is a dual-phase advanced high strength steel (AHSS) with an yield stress of 700 MPa and tensile stress of 1000 MPa. A Poisson's ratio, ν, of 0.3 is assigned to steel and used throughout this work.

Dual-phase steels present an excellent combination between strength and formability, due to their microstructure of hard martensitic phase on a soft ferritic matrix. This type of steel shows a high strain hardenability, due to the formation of mobile dislocations in the matrix, which favours a proper strain redistribution (ArcelorMittal, 2018). The mechanical properties can be further increased if the material undergoes a bake hardening (BH) process (Pereloma et al., 2017).

3.3.3.1 Young's modulus model

As the Young's modulus (E) of steel is a very stable and well known parameter, the simplest way to model it is by considering a constant value. This strategy is used in most models with the value of $E = 210$ GPa.

A more detailed analysis can be done by taking into consideration Young's modulus degradation by means of chord modulus (Yoshida et al., 2002; Sun et al., 2011), which presents the updated Young's modulus for a certain pre-strain. It is calculated as the slope between the loaded and unloaded state in a stress-strain plot, as illustrated in Figure 2.25 and analytically modelled in Equation 3.4. This modelling strategy is evaluated in Section 4.5.2.

Sun et al. (2011) simplify the above mentioned equation with $K = E_0 - E_a$ and characterise DP980 steel with the parameters of Table 3.2. Due to the resemblance between DP980 and DP1000 steels, the parameters are considered equivalent between both materials.

$$E = E_0 - (E_0 - E_a) \cdot \left[1 - \exp\left(-\xi \cdot \varepsilon_0^p\right)\right] \tag{3.4}$$

where E is the chord modulus, E_0 the initial Young's modulus, E_a the Young's modulus for infinitely large pre-strained materials, ξ a constant and ε_0^p the pre-strain. E_0, E_a and ξ are material parameters (Yoshida et al., 2002).

Table 3.2 – Chord modulus parameters of DP980 steel (Sun et al., 2011).

Parameter	Value	Unit
E_0	208	GPa
K	56200	MPa
ξ	175	-

* $K = E_0 - E_a$.

3.3.3.2 Hardening model

As discussed in Section 2.7.3.1, diverse models are used to model the work hardening of DP1000 steel. In this section, the different hardening models to be analysed are explained. The von Mises yield criterion is considered in all material models.

In an initial stage, a power function is fitted to the experimental results from a uniaxial tensile test of DP1000 and, thus, a hardening Swift law (Equation 3.5) with the parameters of Table 3.3 is considered.

$$\sigma_y = K \cdot \left(\varepsilon_{y,init} + \overline{\varepsilon^p}\right)^n \tag{3.5}$$

where σ_y is the updated yield stress, $\varepsilon_{y,init}$ the initial yield strain, $\overline{\varepsilon^p}$ the accumulated plastic strain and K and n the material parameters.

Table 3.3 – Isotopic hardening parameters of DP1000 steel.

Parameter	Value	Unit
K	1100	MPa
n	0.10	-
ε_0	0.29	%

Since in the roll levelling process the material is under cyclic loads, it is important to take cyclic hardening into account when choosing the work hardening model. This can be achieved for most materials with an isotropic hardening model. However, as mentioned by Silvestre, Galdos, et al. (2014), DP1000 steel shows a pronounced Bauschinger effect. Therefore, to better model DP1000 behaviour, it is necessary to take into account not only the isotropic but also the non-linear kinematic hardening.

A combined isotropic/kinematic hardening model, proposed by Lemaitre et al. (1990), is also analysed. This model is defined by Equations 3.6, 3.7 and 3.8 and the material parameters found in Table 3.4, as suggested by Silvestre, Mendiguren, Galdos, et al. (2015).

$$\Phi(\boldsymbol{\sigma}, \boldsymbol{X}, R, \sigma_{y,0}) = \sigma_{eq,vonMises} - \sigma_{y,Chaboche} = J_2(\boldsymbol{\sigma} - \boldsymbol{X}) - (R - \sigma_{y,0}) \leq 0 \qquad (3.6)$$

$$dR = b \cdot (Q - R) \cdot d\overline{\varepsilon^p} \qquad (3.7)$$

$$d\boldsymbol{X} = \frac{2}{3} \cdot C \cdot d\boldsymbol{\varepsilon}^p - \gamma \cdot \boldsymbol{X} \cdot d\overline{\varepsilon^p} \qquad (3.8)$$

where Φ expresses von Mises' elastic domain, $\boldsymbol{\sigma}$ is the stress tensor, $\boldsymbol{X}$ the deviatoric backstress tensor, R is the isotropic hardening, $\sigma_{y,0}$ the initial yield stress, J_2 the second main tensor invariant, Q the isotropic hardening material limit, $\boldsymbol{\varepsilon}^p$ the plastic strain tensor, $\overline{\varepsilon^p}$ the accumulated plastic strain, , b the isotropic hardening material parameters, and C and γ the kinematic hardening material parameters.

Table 3.4 – Combined hardening parameters of DP1000 steel (Silvestre, Mendiguren, Galdos, et al., 2015).

Parameter	**Value**	**Unit**
Q	-280.16	MPa
b	124.73	-
C	26276.72	MPa
γ	34.88	-

Despite being able to provide some insights on the kinematic hardening effect on the final properties of the levelled strip, the above-mentioned material models are very different and it would be also interesting to study the isolated effect of kinematic hardening in roll levelling of DP1000.

COPRA® FEA RF software provides a simple way to take into account a combined material hardening model. This material model only requires an isotropic hardening model, which is well defined by the Swift law mentioned in Table 3.3, and a kinematic factor (α). If α=0 the model is purely isotropic, if α=1 it is purely kinematic and if $0<\alpha<1$ it is a combined model. By changing the kinematic factor parameter, it is possible to isolate and study the kinematic hardening effect.

3.3.3.3 Uniaxial tension-compression test

Despite having selected in Tables 3.3 and 3.4 the material parameters for the DP1000 steel, the models come from references. Therefore, before proceeding with the evaluation of material modelling effect on roll levelling FEA, the hardening models are compared by a simple uniaxial tension-compression test, as illustrated in Figure 3.8.

The tension-compression test is executed by modelling a single element (eight-noded 3D solid element) with the correspondent material properties and submitting the element to a cyclic uniaxial load

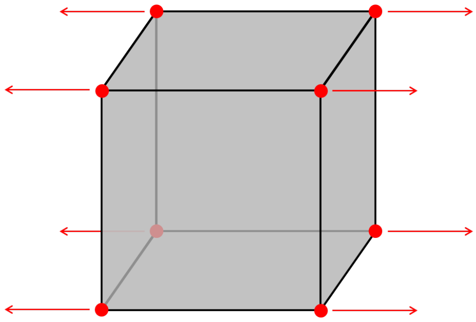

Figure 3.8 – Uniaxial tension-compression test diagram.

which induces a strain magnitude of 2.1%, alternating between tension and compression, in a similar way to what happens in the real roll levelling process.

3.4 Tooling

Tool modelling consists in modelling both machine, working and backup rolls' geometry, kinematics and structural behaviour. As the contact is a property of the workpiece/working rolls set, it is also described in this section.

3.4.1 Geometry

The roll levelling equipment consists on a 6-high roll levelling mill with 17 working rolls, 19 intermediate rolls and 9 backup rolls. The working rolls have a diameter (D_w) of 55 mm, a distance between consecutive rolls (d) of 59 mm and are displayed as illustrated in Figure 3.9. The intermediate rolls have a diameter of 50mm. All rolls have a length of 2200 mm and are made of tool grade steel, with a Young's modulus (E) of 210 GPa and Poisson's ratio (ν) of 0.3.

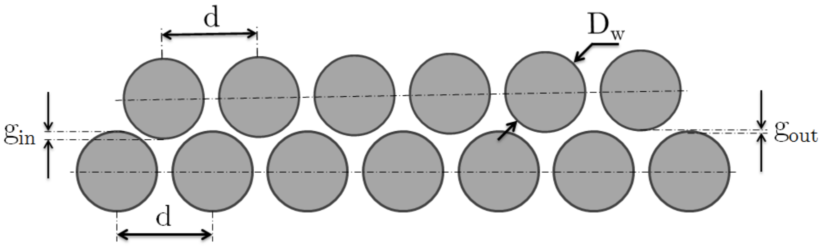

Figure 3.9 – Roll levelling setting parameters (only working rolls are displayed).

Throughout this work, the exit gap (g_{out}) is fixed to 1.23 mm and the entry gap (g_{in}) is set to -2.77 mm. Later, the entry gap effect on the plastic rate (PR) is assessed. Therefore, an empirical experiment is proceeded with several roll levelling FEA, with different machine settings, being executed.

3.4.2 Deformable and rigid rolls

As mentioned before, deformable rolls are only considered in some simulations. In most of the work, no rolls' deformation is considered as they are modelled as rigid bodies (geometrical).

In 2D models, deformable rolls only represent deformation in the cross-section, since a plane-strain condition is considered. In order to take into account rolls' deflection, an approximation has to be made. By constraining the position of the rolls with a spring (with the equivalent stiffness of the roll (K_{eq}) at a certain transverse position (x)), it is possible to approximate the real rolls' deflection as the vertical displacement of the 2D rolls. Appendix B describes the before mentioned concept and details the equivalent stiffness calculation procedure.

When considering deformable rolls in the 3D model, also a simplification is made. Only the working rolls are modelled, however, the stiffness contribution of both intermediate and backup rolls is taken into account by increasing the stiffness of the working rolls. This is achieved by assigning a material with an equivalent Young's modulus value, since the geometry of the working rolls can not be changed. This procedure is also explained in Appendix B.

3.4.3 Contact

Roll levelling is a process where contact is very important in finite element analysis. Not only the strip is driven directly by the working rolls, but also the contact points are multiple and in constant change. Friction is modelled throughout the work using the Coulomb friction model and a constant friction coefficient (μ) of 0.16, adequate for steel-to-steel contact.

Initially, contact settings are established as node-to-segment touching contact. Other contact settings, such as segment-to-segment contact algorithm and analytical description of elements' segments, also known as smooth boundary, are analysed. Figure 3.10 illustrates the before mentioned contact settings.

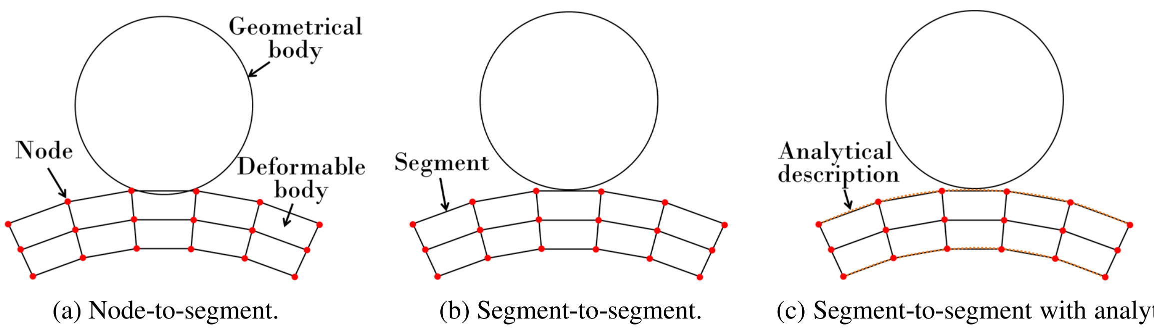

(a) Node-to-segment. (b) Segment-to-segment. (c) Segment-to-segment with analytical description.

Figure 3.10 – Some contact algorithms available in COPRA® FEA RF software.

3.5 Initial defects

During this work, a search for the impact of initial defects on roll levelled strips is performed. Therefore, two types of steel strips are levelled: stress-free flat strips and stress-induced deformed strips.

In order to induce coil set pre-stress and deformations in the strips, the originally flat strip is bent to a certain curvature radius before entering the levelling equipment, similarly to what is suggested on Section 2.7.5. The induced bent aims to represent coil set, which is a typical defect that requires levelling.

In Figure 3.11 the bending process is illustrated. During the simulation, the strip is pressed against a curved surface by two bending rolls. After closing the levelling equipment and before feeding the strip, one of the bending rolls moves along the curved surface so that the initial curvature is set. The remaining length is bent continuously during the simulation. No friction is considered between the metal strip and both the bending rolls and curved surface.

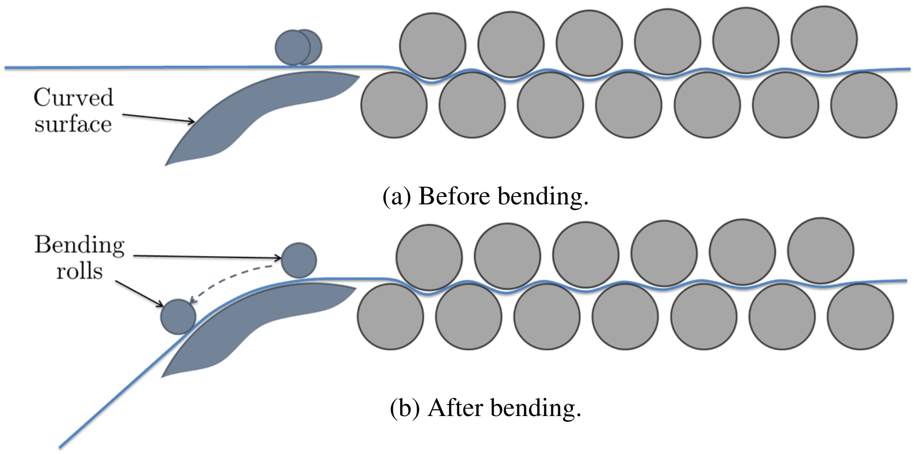

(a) Before bending.

(b) After bending.

Figure 3.11 – Illustration of initial defects' induction (only working rolls are displayed).

3.6 Results evaluation

The final results to be evaluated from the roll levelling FEA are the final geometry, residual stress distribution across thickness, plastic strain distribution across thickness and strain path through the levelling process.

Different evaluations should be proceeded with the simulation results, as the following list enumerates. Each evaluation method is detailed in the following subsections.

1. Flatness quantification, by measuring strip's residual curvature radius and maximum vertical displacement;
2. Analysis of residual stress distribution across thickness, executed in an excerpt of the strip where results are consistent;
3. Analysis of accumulated plastic strain distribution across thickness and plastic rate (PR) measurement;
4. Analysis of strain path of a surface node throughout the levelling process.

3.6.1 Final geometry

Since one of the main objectives of roll levelling is to achieve a flat metal strip, it is important to proceed a flatness evaluation. This evaluation is done by comparing the curvature radius of the strip, at the exit of the machine. The maximum vertical displacement is also measured, in order to provide further insight on the final geometry. During the roll levelling FEA, the aim is to achieve a straight strip, which is confirmed by a large curvature radius.

The curvature radius is measured by fitting a circle in 3 nodes of the upper surface of the strip. These nodes are placed as illustrated by red dots in Figure 3.12. The final curvature radius is equivalent to the circumference radius.

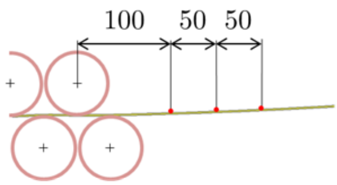

Figure 3.12 – Curvature radius measurement procedure (dimensions in mm).

The maximum vertical displacement (Δy_{max}) is measured as the vertical displacement of the front end of the metal strip, as Figure 3.13 suggests.

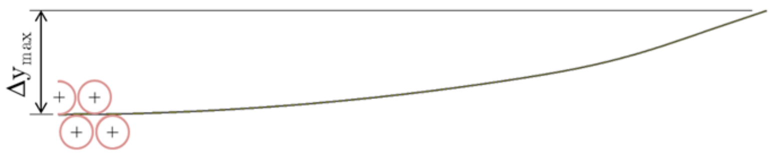

Figure 3.13 – Maximum vertical displacement measurement procedure.

3.6.2 Residual stress and strain distributions

The control of residual stress distribution is another main objective of roll levelling. Therefore, during the pre-process finite element analysis one should look for the final residual stress distribution as of main importance. It is desirable to achieve an homogeneous residual stress distribution across thickness, for the stress components both in length and thickness directions.

It is also of great interest to understand how does that distribution changes from cross-section to cross-section, i.e. how does the residual stress distribution across thickness changes through the length direction. Ideally, the distribution should not change from cross-section to cross-section, meaning that the results achieved a steady state. Several measurements are proceeded in multiple cross-sections (S_1, S_2, ..., S_n), such as illustrated in Figure 3.14.

The strain distribution across strip's thickness and its evolution along the length direction are also analysed, in a similar way as performed for residual stress evaluation. The accumulated plastic strain is expected to present a thickness distribution that is symmetric and zero in the centre part of the strip (fibres in the elastic range, review Figure 2.17).

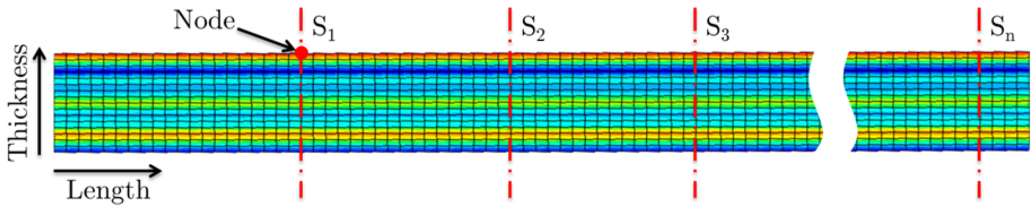

Figure 3.14 – Residual stress (first component of stress) distribution across thickness and its evolution.

3.6.3 Stress and strain evolution through levelling

Despite being a secondary analysis objective, it is interesting to analyse how the stress and strain paths influences the final properties and state of the levelled material, particularly to study the effect of different material constitutive models, contact and machine settings. The path is measured in a top surface node (e.g. the node highlighted in Figure 3.14), where the stress and strain are of higher magnitude when compared to the remaining nodes across thickness, and plotted in function of time. The first component (rolling direction) of total stress and strain are assessed and plotted in function of time and the position in the levelling process. Working roll's are taken as reference and numbered (Figure 3.15) in order to illustrate the position of the strip.

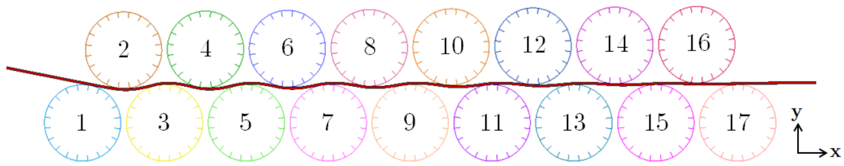

Figure 3.15 – Working rolls' numbering.

Due to the fact that roll levelling submits the strip to a consecutive reverse bendings (Yan et al., 2008), it is expected that the strain in a surface node follows a positive-negative cyclic path, with a local maximum (or minimum) value when in contact with the working rolls, as exemplified in Figure 2.27b.

Chapter 4

2D roll levelling analysis

Following the finite element modelling summary available in Chapter 3, the 2D roll levelling model is exploited and the effect of different parameters on the quality of simulation results is assessed with the goal of acquiring knowledge on roll levelling finite element modelling and extract conclusions that are used for further development of the pre-process simulation. The meshing strategy is studied so that a compromise between computation time and results' resolution is found. Different material models are modelled, considering that roll levelling submits the material to tension-compression load cycles. Levelling rolls' deformation is analysed as well, where deflection approximated by a 2D vertical displacement. Also machine settings, contact type and initial defects are studied.

4.1 Geometry and boundary conditions

Following the description in Chapter 3.4.1 of the levelling equipment, a finite element model is developed. The dimensions are the same as previously mentioned (55 mm diameter working rolls and 59 mm between centre of rolls). The exit gap is set to 1.23 mm and the entry gap to -2.77 mm, however the later is changed during the machine settings study (Section 4.7). The steel strip is modelled with 1.5 mm thickness and 1500 mm length, in order to provide a good continuity of results.

The bottom working rolls are fixed at the same horizontal position, while the top working rolls are linearly aligned from the first until the last one. Their position is achieved by three conditions: preserve the entry and exit gaps, horizontally centre the last top working roll between the two last bottom working rolls and keep a distance of 59 mm between centre of two consecutive rolls.

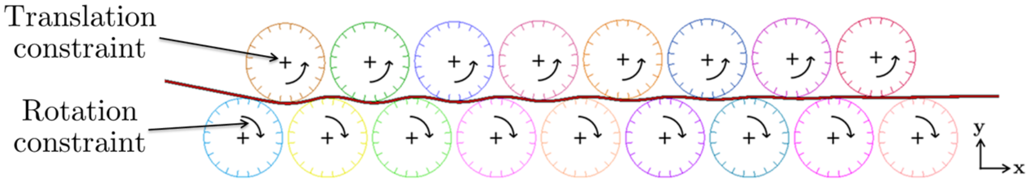

Figure 4.1 – Boundary conditions in the 2D model.

Since the strip is only constrained in the 2D plane-strain analysis, all boundary conditions in this model are applied on the rolls. The boundary conditions, illustrated in Figure 4.1, are translation inhibitions, both in x and y direction, and a constant rotation of 300 rpm, which drives the sheet strip at a velocity of $\approx$51.8 m/min.

4.2 Mesh sensitivity

During the literature review, it was observed that roll levelling simulations are long lasting (Silvestre, Argandoña, et al., 2014) and that this fact is more pronounced when a fine analysis through thickness is required, which applies to this work. Therefore, some authors suggest the use of a locally refined mesh (i.e. mesh with 2 distinguishable areas: coarse and refined, having the latest the smaller elements as exemplified in Figure 2.26) as a good approach to achieve feasible results with a shorter computation time (Silvestre, Mendiguren, Galdos, et al., 2013).

4.2.1 Regular mesh

In order to determine an appropriate locally refined mesh, a sensitivity study is proceeded with different regular meshes (constant element size, as illustrated in Figure 4.2). During this study it is desired that two meshes are found: a coarse one, which provides an acceptable representation of the final geometry, and a fine one, which provides an acceptable representation of stress and strain distributions through thickness.

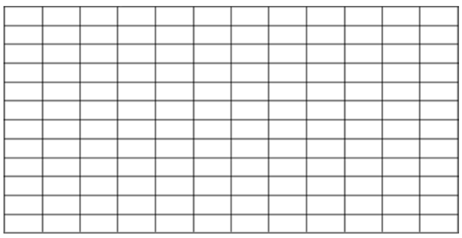

Figure 4.2 – Regular mesh with 12 elements through thickness.

The following simulations are proceeded and the geometrical results are measured as suggested in Section 3.6.1 and represented both in Table 4.1 and Figure 4.3.

Table 4.1 – Simulations proceeded during regular mesh sensitivity analysis.

Elements p/ thickness	Aspect ratio	Curvature radius (mm)	Max. vertical displ. (mm)	CPU time (h)
2	0.75	477.11	853.18	0.34
3	0.50	3744.85	218.80	0.50
4	0.50	3038.80	232.27	0.77
8	0.50	2855.29	248.11	5.93
12	0.50	4242.84	191.08	20.70
16	0.50	5160.05	169.85	41.00

Considering that a discretisation with 2 elements over the thickness provides unexpected geometrical results and that the geometrical results' variation observed when more than 4 elements over the thickness are modelled does not justify the penalty on the computation time, it is possible to conclude that a coarse mesh with 3 or 4 elements through the thickness provides the best compromise solution to assess the geometry of the strip.

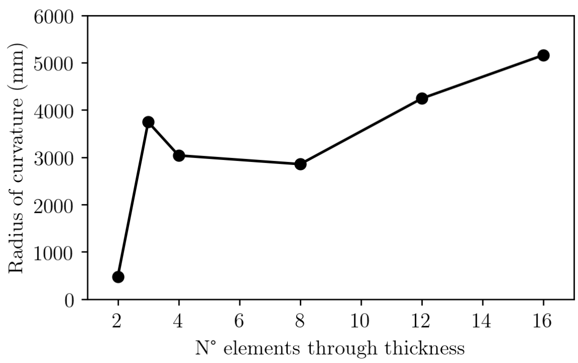

(a) Curvature radius.

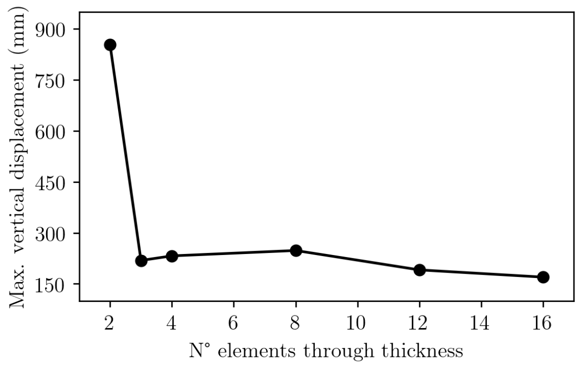

(b) Vertical displacement.

Figure 4.3 – Effect of thickness refinement in the final geometry.

When it comes to a detailed representation of stress and strain distribution through thickness, further analyses are required. Figure 4.4 represents the distribution through thickness after levelling of residual stress (by means of the longitudinal of stress (Comp11), as explained in Appendix A) and of the total equivalent plastic strain, which are some of the most important variables to evaluate.

The residual stress and accumulated plastic strain distribution across thickness are studied several times throughout this work and, therefore, it becomes important to generally understand how they are analysed. The residual stress distribution alternates repeatedly between tensile and compressive across thickness, achieves the highest magnitudes in the top/bottom surface of the strip and is close to point symmetric. This distribution is further explained in Appendix A.1 and is related with the fact that the process submits the strip to consecutive reverse bendings with a decreasing curvature. Regarding the accumulation of plastic strain, it is expected to have 2 distinct zones: purely elastic and plasticised zones. Close to the centre of the strip no plastification is expected to occur during the reverse bending cycles, since a neutral fibre is expected near the middle of the thickness. In the plasticised zone (remaining thickness) the distribution behaves linearly achieving a maximum value in the top/bottom surface of the strip. In this result, it is important to have an accurate representation of the transition between the different zones in order to calculate the plastic rate (view Equation 2.3).

If one observe the resolution of both Figure 4.4a and 4.4b, it is understandable that a mesh with 8 elements through thickness (or even less) is not suitable for a in-deep analysis of the accumulated plastic strain, as it has an unsuficient resolution to represent an elastic area in the centre of the strip. On the contrary, a mesh with 12 elements through thickness stands as a good compromise of time and results quality. A finer mesh of 16 elements through thickness provides a better resolution with a significant

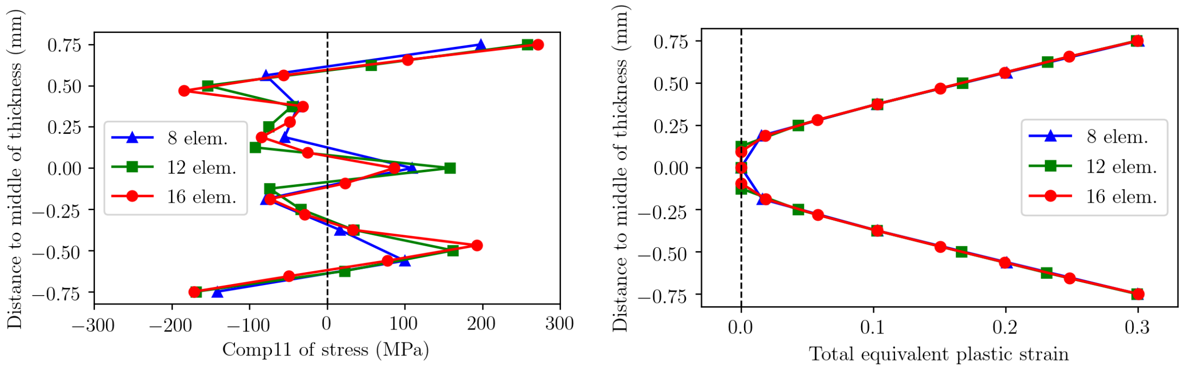

(a) Residual stress. (b) Accumulated plastic strain.

Figure 4.4 – Results' thickness distribution after levelling (regular meshes).

penalty on the computation time. The results from the FEA with a regularly meshed strip with 16-elements through thickness are taken into account as reference during the remaining mesh sensitivity analysis.

Therefore, three locally refined meshes stand-out as promising solutions: 3-to-12, 4-to-12 and 4-to-16 elements through thickness. Further mesh sensitivity analyses are required to validate the final choice for a locally refined mesh.

4.2.2 Locally refined mesh

In this section, models with the before mentioned locally refined discretisations are developed and several FE analyses proceeded. The refined area has a length of approximately 100 mm, which is more than 1.5× the distance between the centre of rolls. This length is used so that, during the levelling process, a smooth transition between bending/unbending is achieved. In Figure 4.5, it is possible to observe the different transitions used.

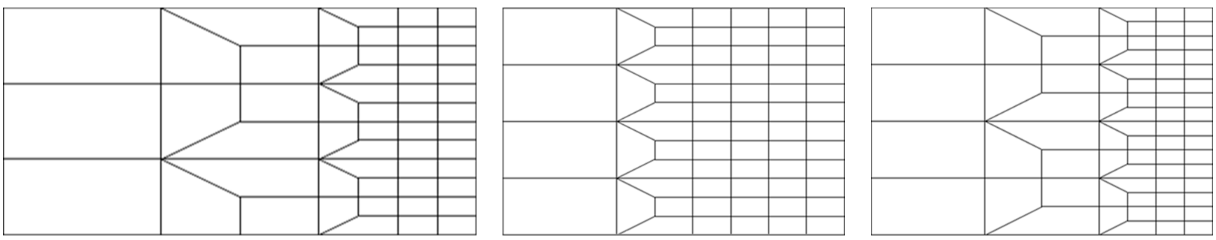

(a) 3-to-12 elements. (b) 4-to-12 elements. (c) 4-to-16 elements.

Figure 4.5 – Transition of different locally refined meshes under analysis, identified by the number of elements through thickness.

The geometrical results and computation time of such simulations are measured as suggested in Section 3.6.1 and resumed in Table 4.2. From the geometrical results displayed in Figure 4.3a, it is observed that the curvature radius of a levelled strip with a 3-to-12 locally refined mesh is completely out of the expected, when compared with the results of regularly meshed models. This unexpected result is justified by a poor transition, which is asymmetrical through thickness direction. On the other hand, both 4-to-12 and 4-to-16 locally refined discretisations provide geometrical results similar to what was expected.

Table 4.2 – Simulations proceeded during locally refined mesh sensitivity analysis.

Mesh	**Curvature radius (mm)**	**Max. vertical displ. (mm)**	**CPU time (h)**
3-to-12	58685.20	229.97	3.8
4-to-12	3183.64	230.32	5.9
4-to-16	3311.73	229.54	8.3

When analysing the thickness distribution of residual stress and accumulated plastic strain (measured in the refined area and represented in Figure 4.6), no significant impact from the coarse area is observed. Regarding the fine area, both meshes with 12 and 16 elements through thickness provide an accurate representation of residual stress and accumulated plastic strain thickness distribution, when comparing to the reference results from the FEA of a regularly meshed model with 16-elements through thickness.

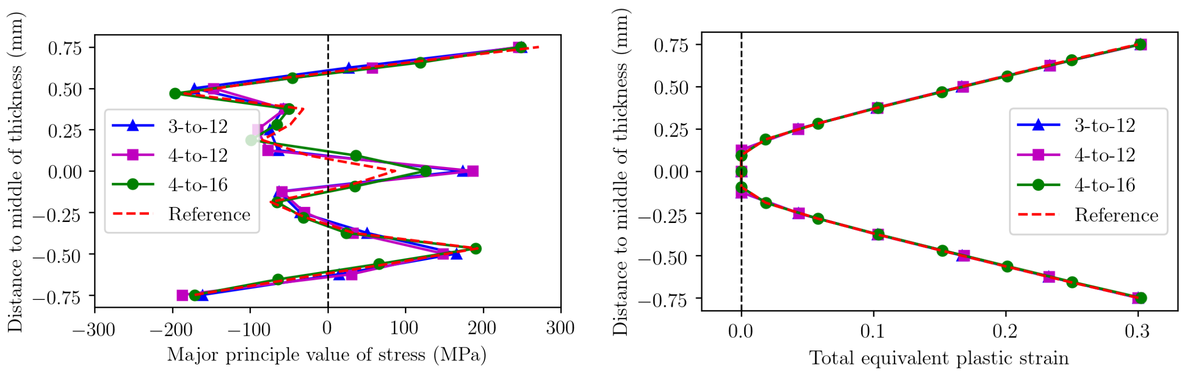

(a) Residual stress.

(b) Accumulated plastic strain.

Figure 4.6 – Results' thickness distribution after levelling (locally refined meshes).

Considering that the main objective of the present work is to study the effect of different variables (such as initial machine settings) on the final strip stress and strain state and that an important parameter to quantify is the plastic rate (PR, defined in Equation 2.3), results resolution through thickness is of high importance. As mentioned in Section 3.3.1, discretisations of 8, 12 and 16 elements through thickness lead to a PR uncertainty of 25.00%, 16.68% and 12.50%, respectively, when analysed in the nodes of the elements.

Taking into account both the computation time, results quality and resolution, the 4-to-12 locally refined mesh is selected as the most adequate mesh for the next numerical chapters presented in this work.

4.2.3 Non-uniform locally refined mesh

The analysis of non-uniform discretisations through thickness is also performed. Such analysis considers elements with different thicknesses, in order to better fit the distribution of results through thickness or reduce the computation time.

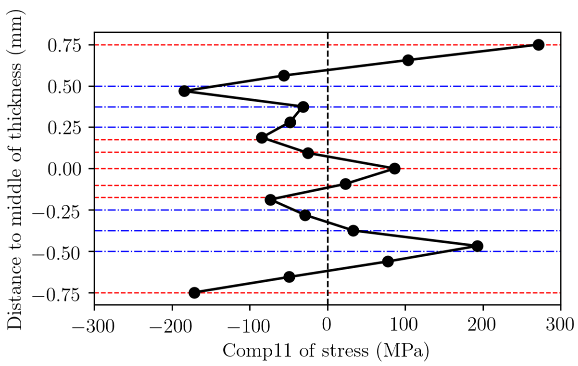

(a) Residual stress.

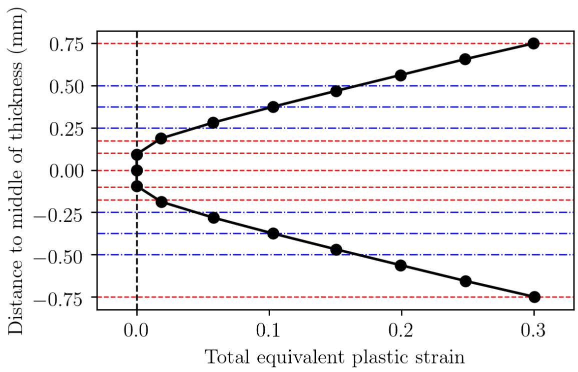

(b) Accumulated plastic strain.

Figure 4.7 – Analysis of the required discretisation through thickness.

Figure 4.7 displays the results from a regularly meshed model with 16-elements through thickness, which is taken as reference for this analysis. Despite having a distribution of accumulated plastic strain which evolutes linearly through the majority of thickness, the distribution of residual stress is not as easily represented. The horizontal lines represent a discretisation that properly fits the results. The red lines (dashed lines) indicate the nodes required to represent the strain distribution, particularly the transition between plasticised and non-plasticised zones, and the blue lines (dotdash lines) to represent the stress distribution.

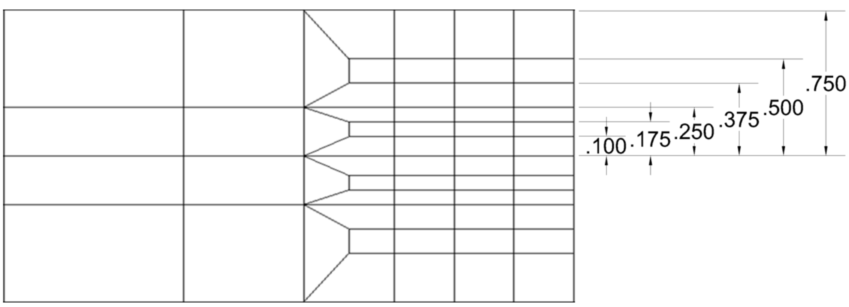

Figure 4.8 – Chosen non-uniform 4-to-12 elements locally refined mesh (dimensions in mm).

As one can observe, in order to improve the representation of both stress and strain distributions, a non-uniform discretisation with 12 elements through thickness can be used. Therefore, a FE analysis of a model with non-uniform 4-to-12 elements locally refined mesh is performed. In Figure 4.8 it is possible to observe the chosen thickness discretisation and transition, which aims not to reduce the computation time but to improve the resolution of results through thickness, particularly in the critical area for plastic rate (PR) measurement.

When comparing the geometrical results of both the uniform (U) and non-uniform (NU) locally refined models with the reference model (regularly meshed model with 16 elements through thickness), it is possible to conclude that the non-uniform locally refined model does not provide a feasible representation of the final geometry. On the other hand, as concluded in Section 4.2.2, a uniform locally refined model with 4-to-12 elements through thickness guarantees acceptable geometrical results. Table 4.3 and Figure 4.9 illustrate the before mentioned comparison.

Table 4.3 – Simulations proceeded during non-uniform mesh sensitivity analysis.

Mesh	**Curvature radius (mm)**	**Max. vertical displ. (mm)**	**CPU time (%)**
Uniform	3183.64	230.32	100
Non-uniform	5869.74	471.16	97

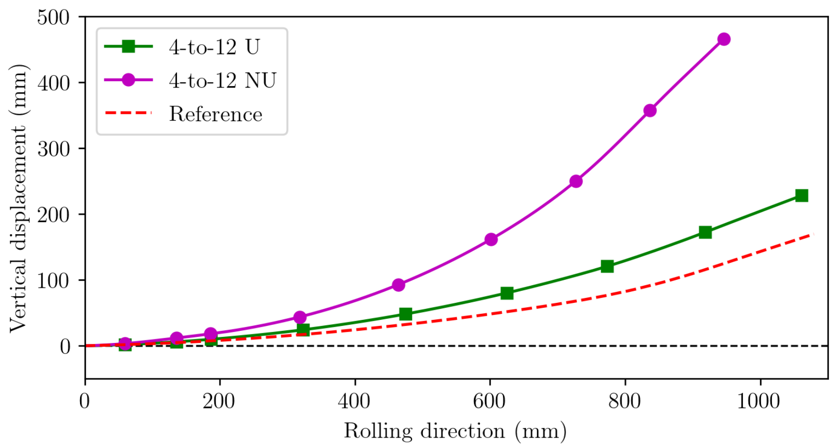

Figure 4.9 – Strip geometry after levelling.[1]

In Figure 4.10, the thickness distribution of both residual stress and accumulated plastic strain is plotted. It is recognizable that, overall, both the non-uniform and uniform models lead to a feasible fitting of the results' distribution provided by the reference model.

However, the advantage of using a discretisation which is non-uniform through thickness becomes obvious when the accumulated plastic strain distribution is under detailed analysis. As mentioned in Section 3.3.1, the PR uncertainty is determined by the thickness of the element where the transition between non-plasticised and plasticised occur. Therefore, when using the chosen non-uniform locally refined model instead of the uniform one, the PR uncertainty is reduced from 16.67% to 10.00%, when analysed in the elements' nodes. Figure 4.11 highlights the uncertain area (defined in Figure 3.4) of both the non-uniform and uniform models.

Since both non-uniform and uniform models provide a proper representation of stress and strain with a similar computation time, but the non-uniform model fails to accurately predict the final geometry of the strip, hereinafter, all models will have a uniform 4-to-12 elements locally refined mesh. The

[1]More data points are analysed than those signed with markers.

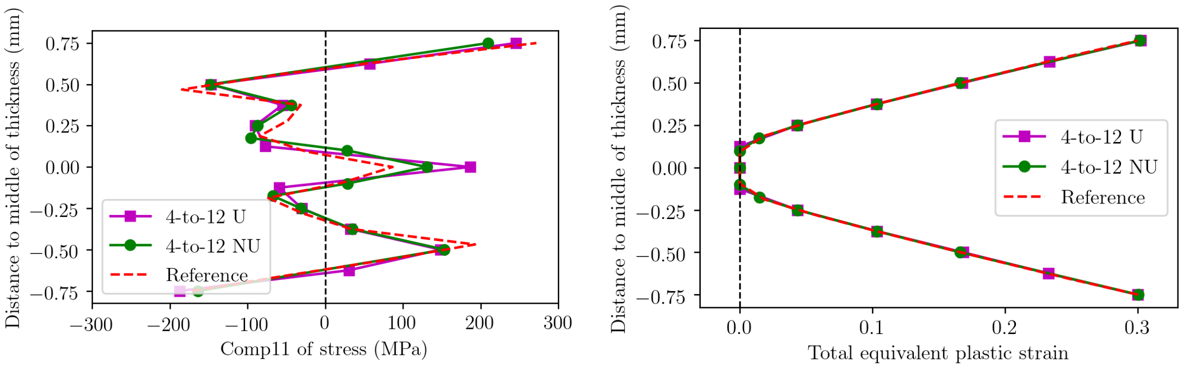

(a) Residual stress. (b) Accumulated plastic strain.

Figure 4.10 – Results' thickness distribution after levelling (non-uniform and uniform meshes).

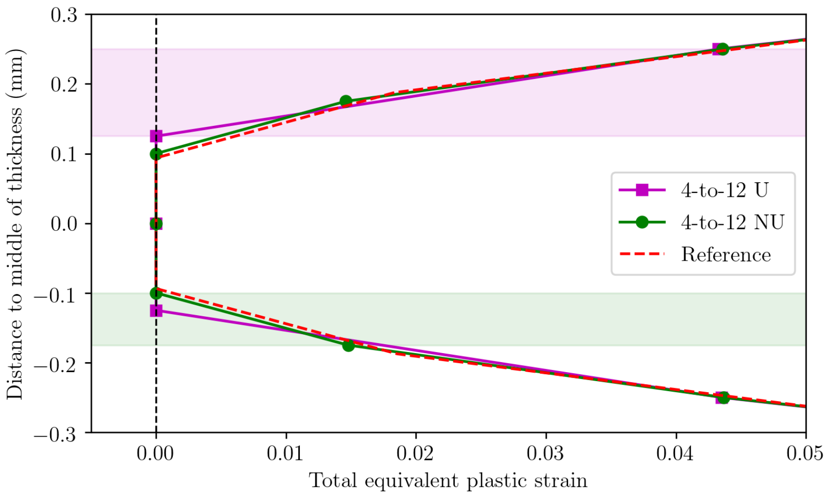

Figure 4.11 – Plastic rate uncertain areas, provided by models with non-uniform (green) and uniform (magenta) meshes.

downside of this choice is that the PR uncertainty is limited to 16.67%, when measured in the nodes of the elements.

4.2.4 Length of refined area

The last point of analysis in this mesh sensitivity study is the length of the refined area. As mentioned in Section 4.2.2, the length of the refined area in all locally refined models analysed previously is 100mm, in order to provide a smooth transition between bending and reverse bending by ensuring continuous contact between the refined mesh and, at least, 3 working rolls.

This is a conservative approach and it is interesting to analyse how does reducing the length of the refined area affects the FEA results. The goal of this study is to improve the efficiency of the model, by providing a better balance between results' quality and computation time.

Therefore, multiple simulations were proceeded with uniform 4-to-12 elements locally refined meshes, which only differed in the length of their refined area. Table 4.4 resumes the respective geometrical results and computation time.

Table 4.4 – Simulations proceeded during the analysis of the refined area length.

Refined length (mm)	**Curvature radius (mm)**	**Max. vertical displ. (mm)**	**CPU time (%)**
100	3183.64	230.32	100
85	3081.47	231.84	94
70	2958.21	233.02	87
55	2981.50	234.07	80
40	3258.08	234.77	74
25	4261.75	234.44	68
10	19974.20	234.41	61

When taking into consideration the geometrical results from the regular mesh sensitivity study (Table 4.1) and comparing them with the previous table, it becomes clear that changing the refined area length from 100mm to 40mm has an irrelevant impact on the final geometry. Also, from the analysis of results distribution through thickness (Figure 4.12), it is confirmed that all models are able to accurately represent both the stress and strain distributions taken as reference.

Consequently, since it is a requisite to have a model able to provide feasible results within the least CPU time, a refined area length of 40 mm will be used in every model from now on, rather then using a similar locally refined mesh with a refined area length of 100mm. This represents a 26% reduction on the computation time.

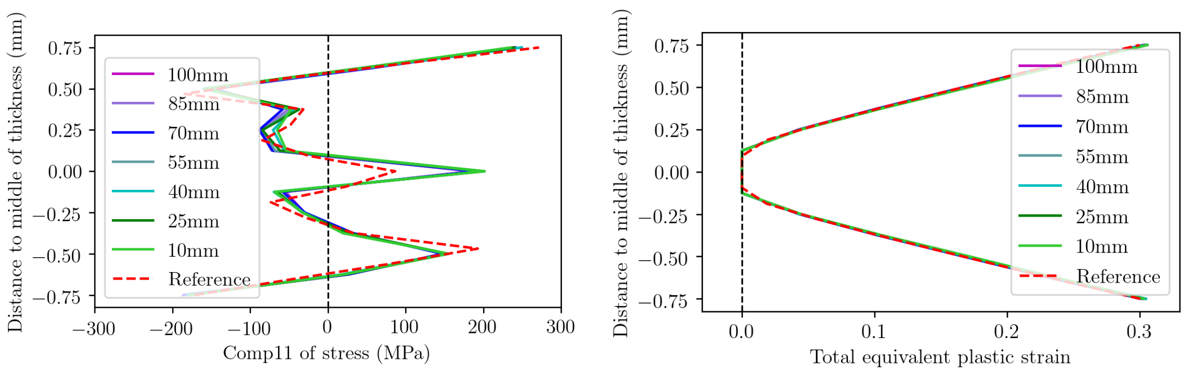

(a) Residual stress.

(b) Accumulated plastic strain.

Figure 4.12 – Results' thickness distribution after levelling (length of refined area).

4.3 Contact modelling

In this section, the performance of three different contact settings in roll levelling FEA is analysed through multiple simulations. As mentioned in Section 3.4.3, roll levelling models with node-to-segment (used until now) and segment-to-segment contact algorithms are modelled, analysed and compared. Also the effect of the analytical segment description is studied.

According to the expertise of MSC Software Corporation, the node-to-segment (N2S) algorithm may lead to stress discontinuities in the contact area. Therefore, it is important to analyse the segment-to-segment (S2S) algorithm performance and the impact of segments' analytical description.

When analysing the final geometry and computation time of both contact models (Table 4.5), no advantage on using either S2S contact algorithm or analytical description of segments is found. On the contrary, the computation time is increased by ≈50% when using S2S. This is mainly due to the fact that, in order to successfully run the simulation with S2S algorithm, smaller step sizes are required.

Table 4.5 – Simulations proceeded during contact modelling analysis.

Contact algorithm	**Segment description**	**Curvature radius (mm)**	**Max. vertical displ. (mm)**	**CPU time (%)**
N2S	Discrete	3252.08	234.44	100
S2S	Discrete	3066.32	231.52	147
S2S	Analytical	3109.26	231.26	148

Regarding the stresses and strains, it is important to have a model able to provide a feasible thickness distribution of results. Since the contact modelling is under scope, it becomes also interesting to analyse the impact of changing the aforementioned contact settings on the stress and strain path throughout the levelling process. Figure 4.13 displays the distribution of results through thickness and Figure 4.14 the stress and strain path of a superficial node throughout the process.

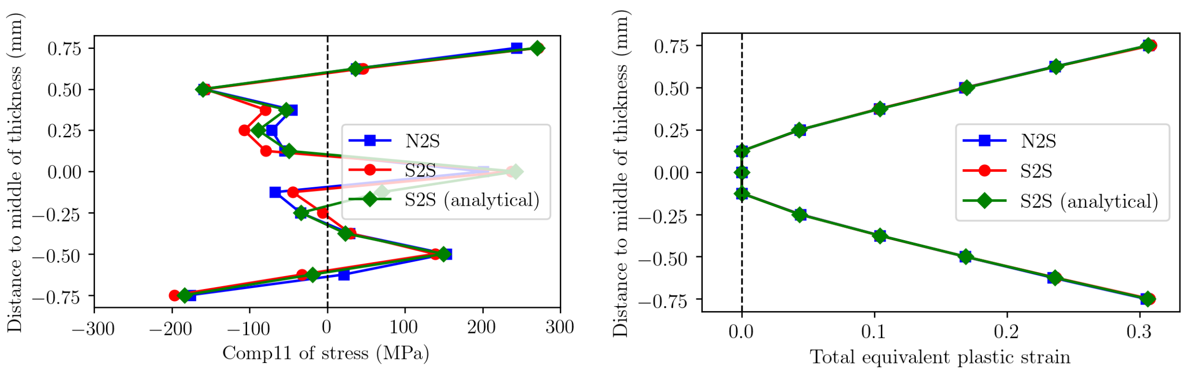

(a) Residual stress.

(b) Accumulated plastic strain.

Figure 4.13 – Results' thickness distribution after levelling (different contact models).

Since all three models under scope are able to accurately represent the distribution of residual stress and accumulated plastic strain through thickness and their path throughout the levelling process, until this analysis stage no reason was found to use segment-to-segment contact algorithm or an analytical description of segments.

In order to corroborate that the N2S algorithm and discrete segments' description are the appropriate choice to model contact on a roll levelling FEA, one last analysis is proceeded to evaluate the hypothesis

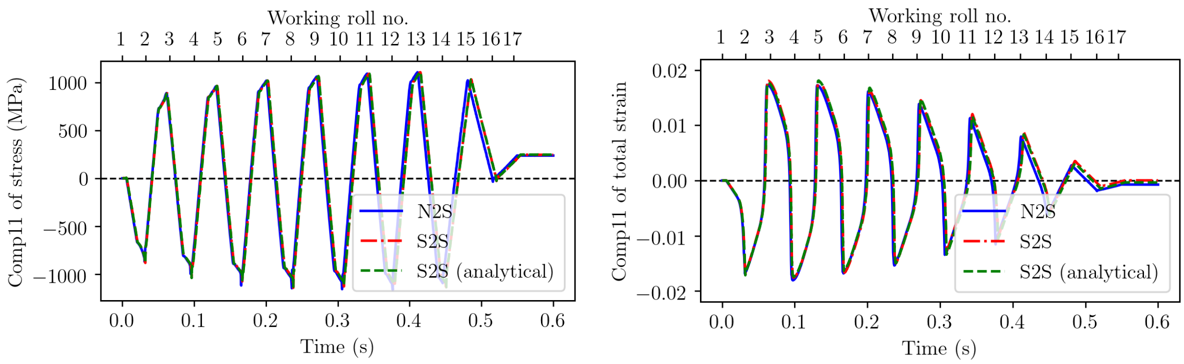

(a) Stress path. (b) Strain path.

Figure 4.14 – Stress and strain path throughout the levelling process (different contact models).

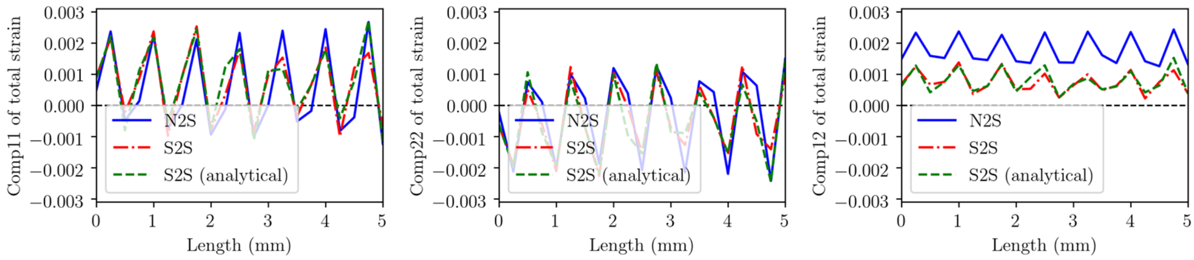

(a) Normal strain (rolling). (b) Normal strain (thickness). (c) Shear strain.

Figure 4.15 – Total strain consistency.

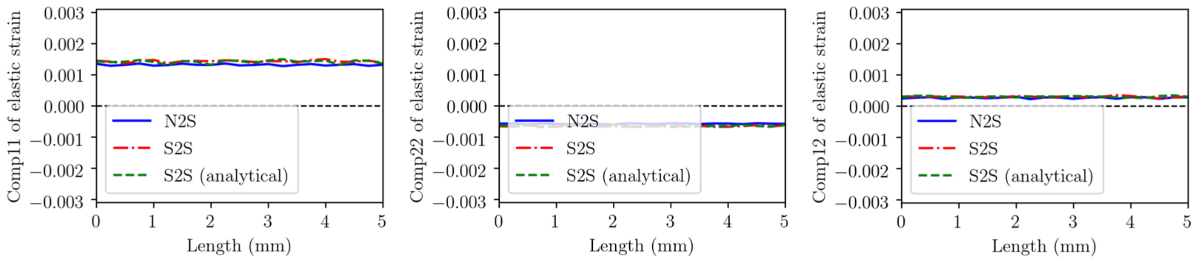

(a) Normal strain (rolling). (b) Normal strain (thickness). (c) Shear strain.

Figure 4.16 – Elastic strain consistency.

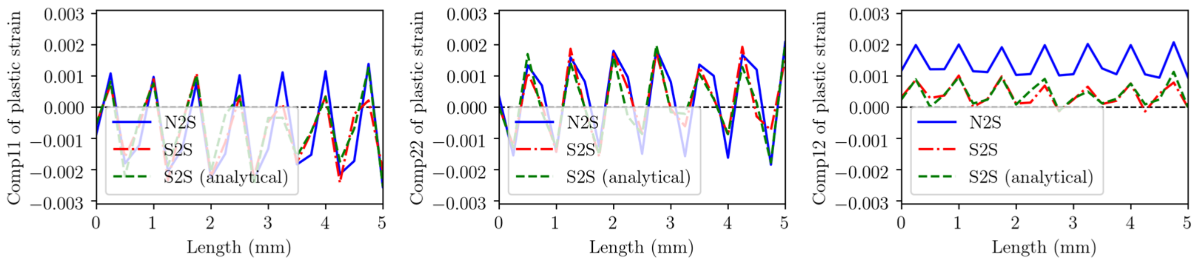

(a) Normal strain (rolling). (b) Normal strain (thickness). (c) Shear strain.

Figure 4.17 – Plastic strain consistency.

that S2S contact algorithm provides more consistent results. A sample set of consecutive superficial nodes from the refined area are selected and their strain results are studied on detail. Figures 4.15, 4.16 and 4.17 display the components of total, plastic and elastic strain.

It becomes clear that there is a periodical fluctuation of the results, which is visible both on the plastic and elastic components of strain. Despite sharing the same frequency, the fluctuation magnitude is insignificant for the elastic strain and significant for the plastic strain. In particular for plastic strain, it is observable that when the strip is under tensile strain in the rolling direction, it undergoes a compressive strain in the thickness direction, due to the fact that no volumetric variation is expected, and *vice versa*.

Even considering that by changing the contact algorithm there is a change of $\approx$0.1% on the total shear strain value, it is fair to conclude that the node-to-segment contact algorithm and discrete segment description provide appropriate geometrical results and stress-strain results, both in terms of distribution through thickness and evolution during the levelling process. It is also possible to add that it is the option that requires less computational effort and that no improvement in the consistency of results was observed, neither by using the segment-to-segment contact algorithm nor analytical segments' description. Thus, hereinafter the node-to-segment contact algorithm and discrete segments' description are used.

4.4 Gravity

Despite gravity loads have been neglected throughout this work, in this chapter, its effect on roll levelling FEA is evaluated. The decision of neglecting gravity in the previous analyses was taken according to the knowledge and experience of data M Sheet Metal Solutions GmbH, since gravity is disregarded in roll forming FEA. However, it is interesting to confirm if such assumption is also valid for roll levelling FEA and what are the effects of gravity in the levelled strip.

Two simulations are executed, with and without gravity loads. Gravity loads are modelled considering the density of DP1000 steel (ρ=7800 kg/m^3) and gravity acceleration (g=9.8 m/s^2).

After analysing the computation time and final geometry of both FEA, at a first instance one would say that the results are completely different. On one hand, taking into account gravity leads to a penalty of $\approx$40% on the computation time but the final geometry is almost flat (curvature radius of 10230 mm), and, on the other hand, neglecting gravity leads to a final geometry with a significant residual curvature radius of 3252 mm (Figure 4.18).

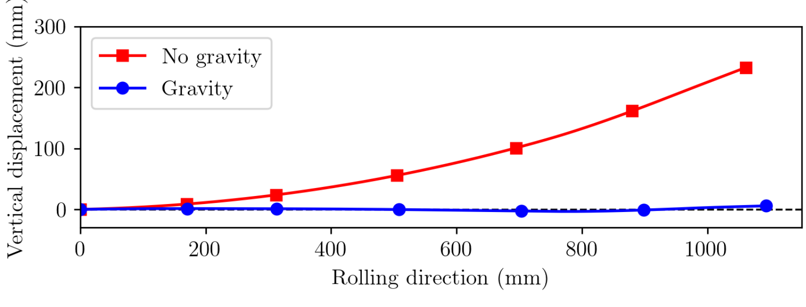

Figure 4.18 – Strip geometry after levelling.[2]

[2]More data points are analysed than those signed with markers.

Regarding the results distribution through thickness after levelling (Figure 4.19), both models provide similar results. The model with gravity displays a higher magnitude of residual stresses in the nodes close to the surface, however this difference is due to the elastic deformation induced by the weight of the strip.

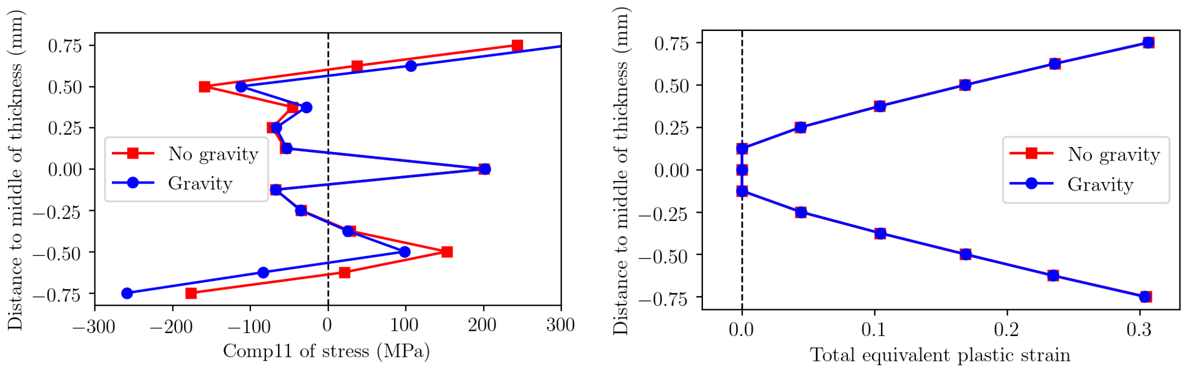

(a) Residual stress. (b) Accumulated plastic strain.

Figure 4.19 – Results' thickness distribution after levelling (gravity effect).

Considering gravity during the process simulation also has no significant impact on the stress and strain evolution throughout the levelling process. In Figure 4.20, one can observe the stress and strain paths of a surface node from the refined area of the strip. The only differences between the two models are observed when the strip is outside the machine, before and after levelling. When gravity loads are considered, a stress offset is induced by the weight of the suspended strip. This effect is not visible when the strip is being levelled, as the strip is constrained by the working rolls.

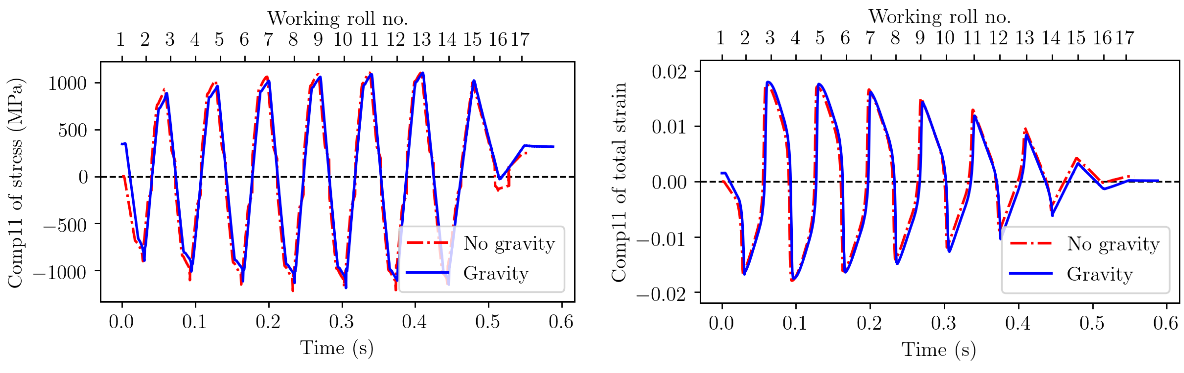

(a) Stress path. (b) Strain path.

Figure 4.20 – Stress and strain path throughout the levelling process (gravity effect).

The only reason to take gravity into account when proceeding a roll levelling FEA is to achieve a final geometry closer to reality, which enables a flatness quantification according to ASTM A1030. However, no significant impact is observed on the final stress-strain state of the strip and an increase of ≈40% on the CPU time is expected. Therefore, gravity loads should only be taken into consideration when flatness quantification is required.

4.5 Material modelling

As mentioned in Section 3.3.3, different material models are used throughout this work. Until this analysis stage, only a material model with a constant Young's modulus of 210 GPa and an isotropic hardening law (Swift law) was used.

In this section, the kinematic hardening effect and Young's modulus degradation of DP1000 are studied, in order to understand how this phenomena affects roll levelling simulation results.

4.5.1 Hardening model

As pointed in Section 3.3.3.2, DP1000 steel exhibits a strong kinematic hardening behaviour. Therefore, it is particularly important to take this hardening mechanism into account when analysing a roll levelling process, where cyclic loads are applied. For this study, a constant Young's modulus of 210 GPa and two different hardening models are used: an isotropic model (Swift law) and a combined hardening model (Chaboche-Lemaitre model), defined in Table 3.3 and Table 3.4 respectively.

Since the hardening models' parameters are obtained from different sources, in a first instance the models are compared in a simple uniaxial tension-compression test, described in Section 3.3.3.3. The goal of this test, is to verify if both models are representative of the same material.

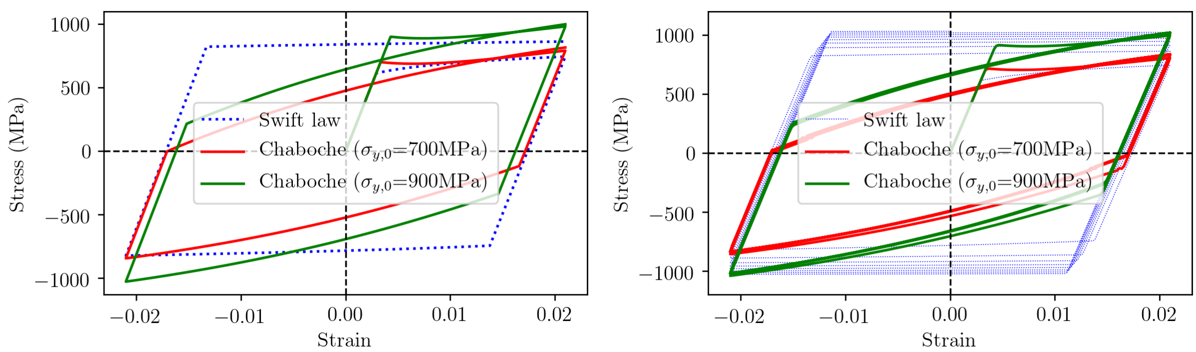

(a) Cyclic load (×1).

(b) Cyclic load (×8).

Figure 4.21 – Stress-strain curve from different hardening models (tension-compression test).

The resultant stress-strain curves are presented in Figure 4.21. Despite displaying different behaviours in the initial stages of the cyclic load, the models fit properly after one cycle, considering $\sigma_{y,0}$=700 MPa. However, for a high number of load cycles, the isotropic hardening effect (represented by the Swift law model) leads to the expansion of the yield surface. Therefore, in order to have a proper fitting between both models when the number of load cycles is high, higher yield stress values should be considered (e.g. $\sigma_{y,0}$=900 MPa). Taking into account that the initial yield stress ($\sigma_{y,0}$) of DP1000 steel is ≈700 MPa and that roll levelling process involves many load cycles, the results are expected to vary significantly when the hardening model is changed.

After validated, the hardening models are implemented in two finite element analyses of the roll levelling. In Table 4.6 it is possible to observe the required computation time of each analysis and in Figure 4.22 the final geometry. The results distribution through thickness are displayed in Figure 4.24.

Table 4.6 – Simulations proceeded during hardening modelling analysis.

Type of model	**Hardening model**	**Curvature radius (mm)**	**Max. vertical displ. (mm)**	**CPU time (%)**
Isotropic	Swift law	3127.99	234.78	100
Combined	Chaboche-Lemaitre	5034.24	-154.51	136

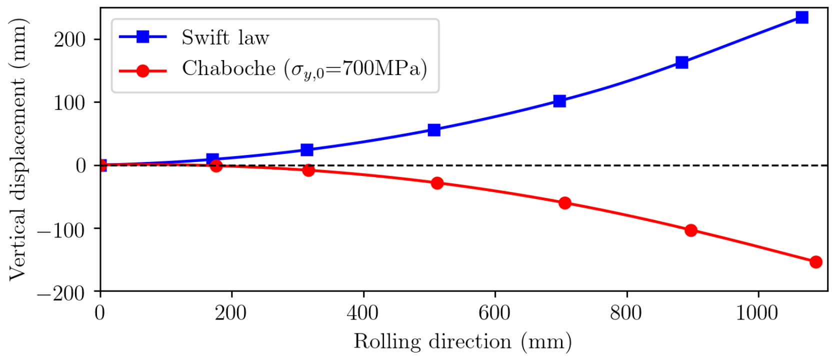

Figure 4.22 – Strip geometry after levelling.[3]

As expected, the results are different. Particularly in the geometrical results, a severe difference is observed as Chaboche-Lemaitre hardening model leads to a negative vertical displacement of the front end of the strip. On the contrary, in all previous simulations (in which Swift law is used), the front end of the strip exhibited a positive vertical displacement.

This observation can be justified by different levels of plastic strain accumulated during roll levelling. Since the hardening models are different, the yield strain is not the same. Therefore, it is important to understand how is plastic strain accumulated in both models.

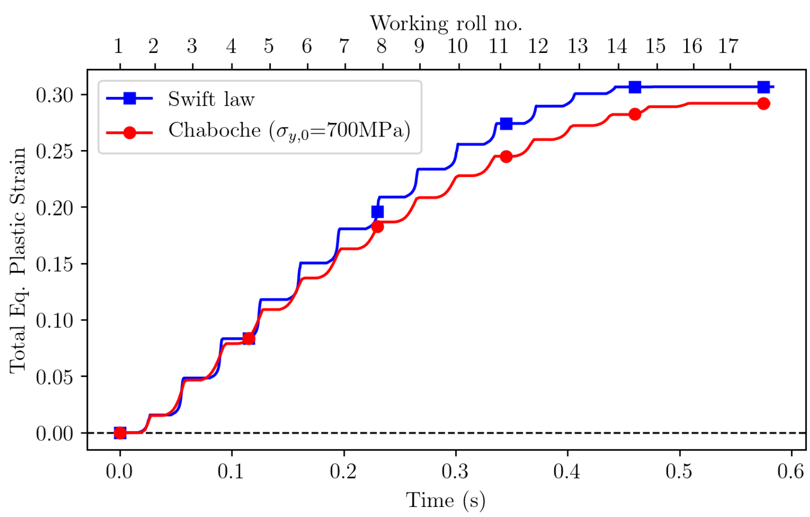

Figure 4.23 – Plastic strain accumulation throughout the levelling process (different hardening models).[3]

[3]More data points are analysed than those signed with markers.

Figure 4.23 resumes the cumulative function of equivalent plastic strain throughout the levelling process. By analysing it, one can understand that the Swift law model leads to a harder material (i.e. higher yield stress), for a high accumulated plastic strain. As a consequence, plastification only occurs until the 14$^{\text{th}}$ working roll, while it takes place until the 16$^{\text{th}}$ roll when the combined hardening law is considered. However, the combined hardening model provides a harder material for a small accumulated plastic strain. Since the material is tractioned and compressed repeatedly, the accumulation of different amounts of plastic strain during the levelling process leads to different geometries.

Another possible justification for different final geometries is the residual stress distribution (Figure 4.24a), which is also related with the hardening model. Despite both models leading to a mean value of residual stress close to zero, the stress distribution of each simulation is point symmetric relatively to the neutral fibre. Therefore, an elastic bending is expected. However, this elastic deformation is not relevant and can be neglected, when compared to the plastic deformation.

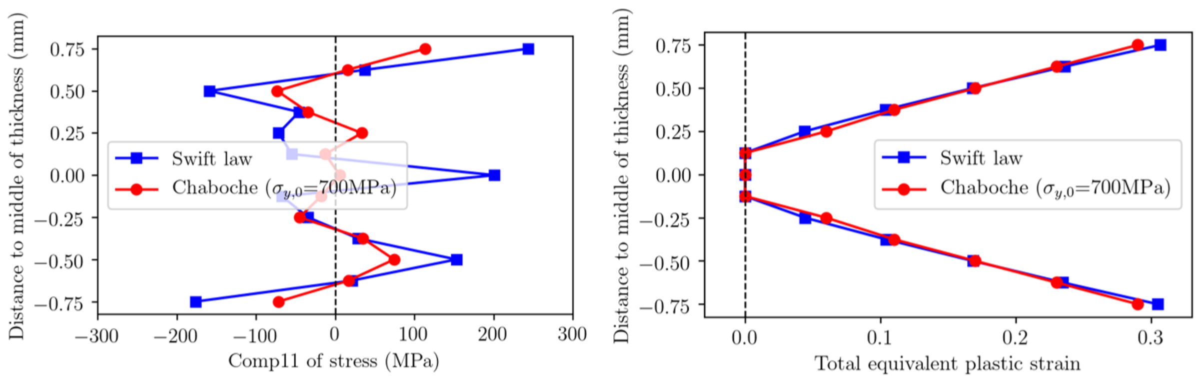

(a) Residual stress. (b) Accumulated plastic strain.

Figure 4.24 – Results' thickness distribution after levelling (different hardening models).

Regarding the stress and strain path throughout the levelling process (Figure 4.25), it is also noticeable that the Swift law model leads to higher levels of stress. The difference between both models increases during the process due to the isotropic hardening, a consequence of the increase of accumulated plastic strain.

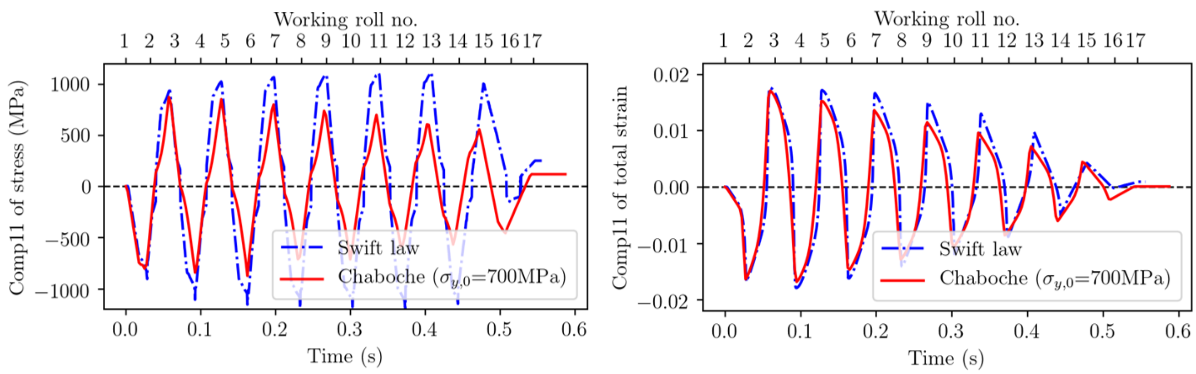

(a) Stress path. (b) Strain path.

Figure 4.25 – Stress and strain path throughout the levelling process (different hardening models).

When the stress-strain evolution of a top surface node is assessed and compared between both models, the isotropic and kinematic hardening effects become visible.

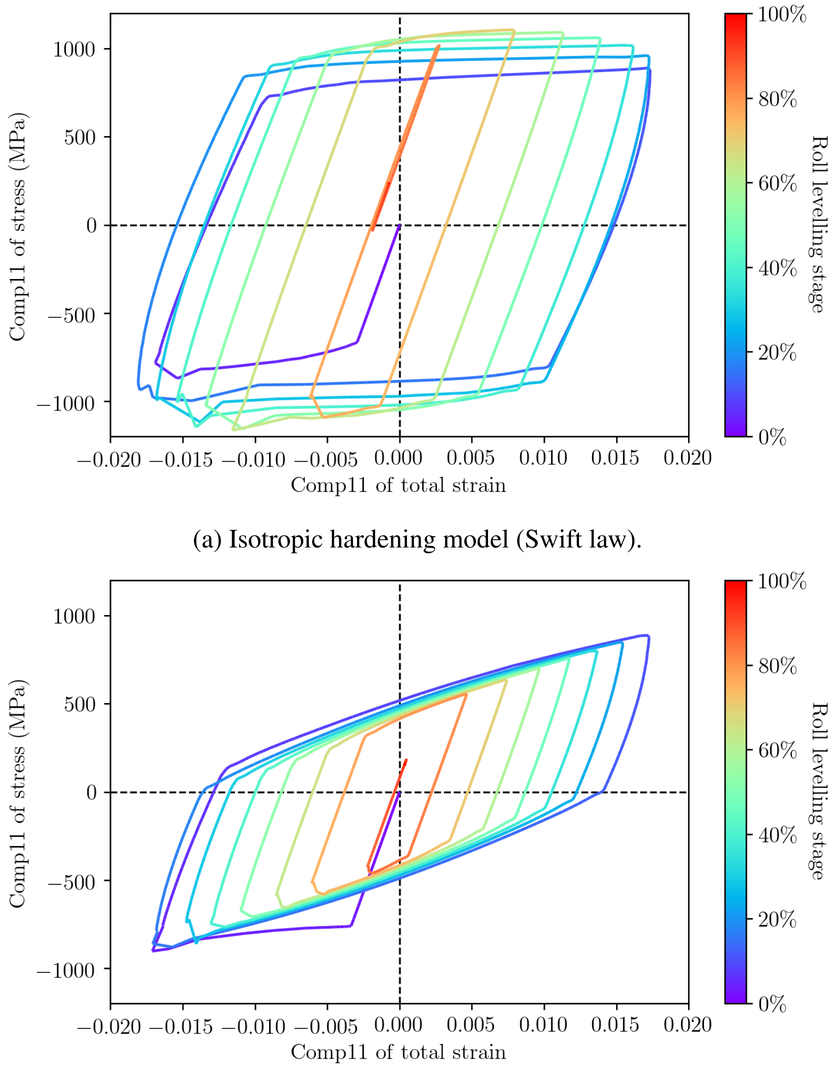

(a) Isotropic hardening model (Swift law).

(b) Combined hardening model (Chaboche-Lemaitre).

Figure 4.26 – Stress-strain curve from different hardening models (roll levelling process).

Figure 4.26a displays the hardening behaviour from the Swift law model. Since it is an isotropic hardening model, the yield surface expands with the accumulation of plastic strain, as can be seen by a near continuous increase of the yield stress during the process.

On the other hand, Figure 4.26b exhibits the behaviour of a combined hardening model. Due to the negative isotropic hardening limit, a reduction of the yield surface with the accumulation of plastic strain is expected and a smooth reduction of the yield limit is observed. The kinematic hardening component leads to the translation of the yield surface, which is represented by the slope on the yield limit. Since the reduction of the yield limit with the increase of plastification is very smooth, it is possible to confirm that this combined model is close to a pure-kinematic hardening model.

Considering that the combined hardening model was adjusted by Silvestre, Mendiguren, Galdos, et al. (2015) to fit experimental results from a cyclic tension-compression test of the material under scope, it is considered an appropriate model to characterise the DP1000 steel hardening behaviour during a roll levelling process. On the other hand, the isotropic model parameters were chosen in order to fit a stress-strain curve from an uniaxial tensile test of a DP1000 sample. According to the observations made in this section, both models provide different results and, therefore, the Swift law model is not suitable to characterise the behaviour of the material under cyclic loads.

Hereinafter, all models will consider the Chaboche-Lemaitre combined hardening model, available in Table 3.4.

4.5.1.1 Kinematic hardening effect

Since both previously studied hardening models are very different, it becomes difficult to understand the isolated effect of kinematic hardening in the material behaviour, during a roll levelling process. In this subsection another material hardening strategy, besides the Swift law and Chaboche-Lemaitre model, is exceptionally evaluated.

By defining the material behaviour with an isotropic hardening model and a kinematic factor (α), COPRA® FEA RF enables a simple and fast material combined hardening modelling strategy. If the previously used Swift law is chosen to characterise the isotropic behaviour, the kinematic effect can be studied by varying the α value. Therefore, several roll levelling finite element models with multiple kinematic factor values are developed and analysed. Table 4.7 resumes the executed analyses and their computation time.

Table 4.7 – Simulations proceeded during kinematic hardening analysis.

Isotropic model	**Kinematic factor (α (%))**	**Curvature radius (mm)**	**Max. vertical displ. (mm)**	**CPU time (%)**
Swift law	0	3127.99	234.78	100
Swift law	20	1713.07	231.39	93
Swift law	40	10255.70	-101.37	99
Swift law	60	754.37	-612.25	99
Swift law	80	750.88	-573.35	101
Swift law	100	2155.73	-262.27	89

As one can notice, the impact α has on the computation time is insignificant, considering that the same hardening model has been used only by changing the kinematic factor between each analysis.

On the other hand, as predicted before, kinematic hardening has a strong effect on the final geometry. In Figure 4.27 it is possible to observe that a small kinematic factor (e.g.α=20%) leads to a small geometrical variation, when compared with the isotropic model (α=0%). However, if a pure kinematic model is considered (α=1), the final strip has the opposite curvature. The maximum geometrical results deviation from the isotropic model is achieved when $60\% \leq \alpha \leq 80\%$.

If the geometrical results of the combined hardening model are reviewed, no proper fitting is possible with any of the kinematic factors analysed. The best approximation is achieved with α=40% or α=100%.

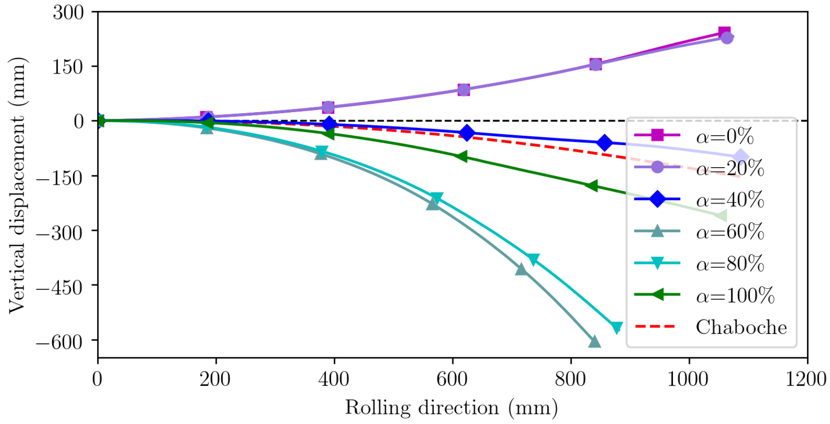

Figure 4.27 – Strip geometry after levelling (kinematic hardening effect).[4]

The accumulation of plastic strain during the roll levelling FEA (Figure 4.28) also has a behaviour similar to the one predicted before, as the isotropic model provides a harder material (i.e. higher yield stress) for high accumulated plastic strain. This conclusion can be justified by the fact that, when no kinematic hardening is considered, plastic strain accumulation only occurs until the 14th working roll. With the increase of kinematic factor, the accumulation of plastic strain extends up to the 16th working roll. Since the strain induced in each bending is constant (i.e. constant machine settings), only hardening justifies such difference in the accumulation of plastic strain.

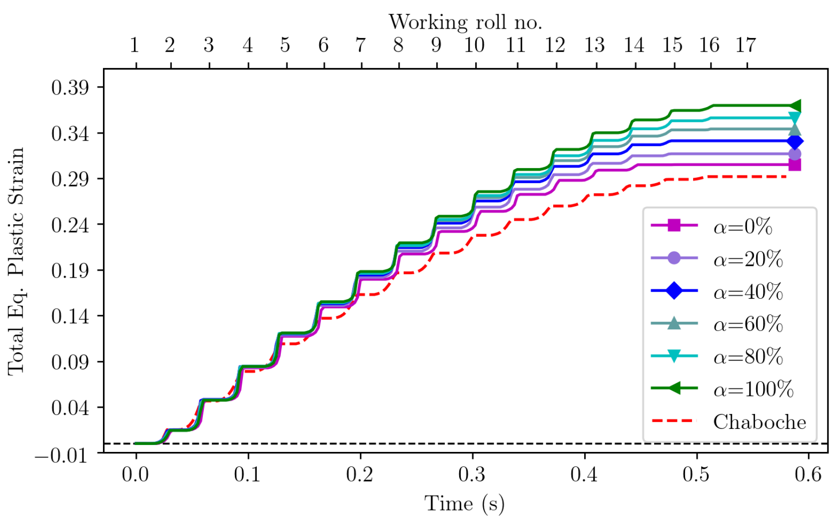

Figure 4.28 – Plastic strain accumulation throughout the levelling process (kinematic hardening effect).[4]

One significant difference is observed between Chaboche-Lemaitre model and these simple combined hardening models. The increase of kinematic factor leads to an increase of the accumulated plastic strain, however, Chaboche-Lemaitre combined hardening model leads to a smaller accumulation of plastic strain when compared to the isotropic alternative, as Figure 4.28 illustrates and as concluded in the

[4]More data points are analysed than those signed with markers.

comparison between Swift law and Chaboche-Lemaitre hardening models.

Therefore, it is possible to conclude that, in this roll levelling process, a kinematic model leads to less hardening than an isotropic nodel. Also, for combined hardening models, a negative isotropic coefficient leads to a reduction of accumulated plastic strain. These observations are mostly visible in superficial nodes and lose relevance as the analyses scope approaches the middle of thickness.

Also, when an analysis is proceeded across strip thickness, no correlation is found between the kinematic effect and residual stress distribution. From Figure 4.29a, which displays the residual stress distribution through thickness, one can observe that intermediate values of kinematic factor (α=40% and α=60%) provide completely unexpected results. However, both purely isotropic and purely kinematic models (α=0% and α=100%) present similar residual stress distributions through thickness, which are also close to the results found with Chaboche-Lemaitre model.

Regarding the distribution of accumulated plastic strain (Figure 4.29b), the only effect of kinematic hardening is the increase of accumulated plastic strain with the increase of kinematic factor. However, as mentioned before, this can be neglected when the analysis is performed close to the middle of thickness and, thus, no change in the plastic rate measurement is expected.

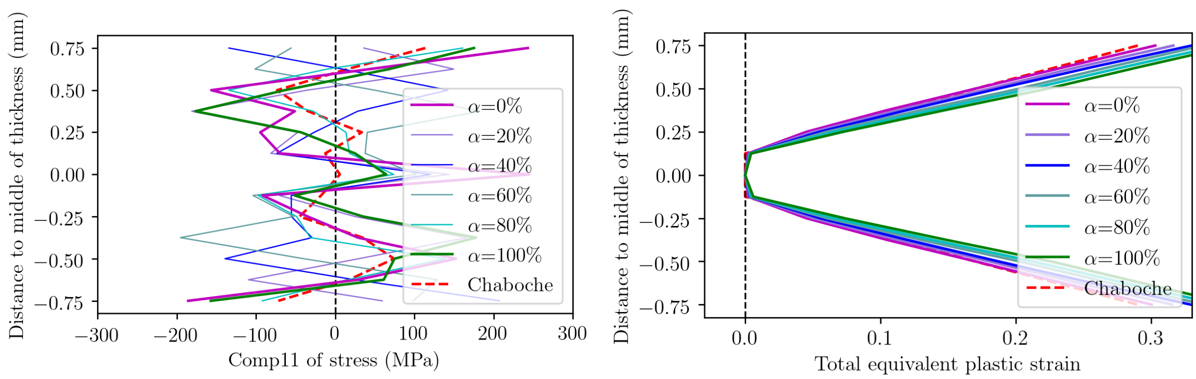

(a) Residual stress.

(b) Accumulated plastic strain.

Figure 4.29 – Results' thickness distribution after levelling (kinematic hardening effect).

By assessing the evolution of stress and strain of a surface node throughout the process, some previously stated observations are corroborated. The strain paths are very similar, which is expected since the machine settings are constant. Also the stress paths are similar, however with higher magnitudes for small kinematic factors and *vice versa*. It is worth to mention that Chaboche-Lemaitre model can be fitted by a pure isotropic model during the first stages of the levelling process and, as the number of load cycles increases, it become closer to a pure kinematic model. Therefore, for roll levelling finite element modelling, one alternative to better fit Chaboche-Lemaitre hardening model with this simple hardening model is to define a variable kinematic factor, dependent on the equivalent plastic strain.

Another interesting result to analyse is the stress and strain relation from the different models, during the roll levelling process. This enables a better understanding of the effect kinematic hardening has the material stress/strain state.

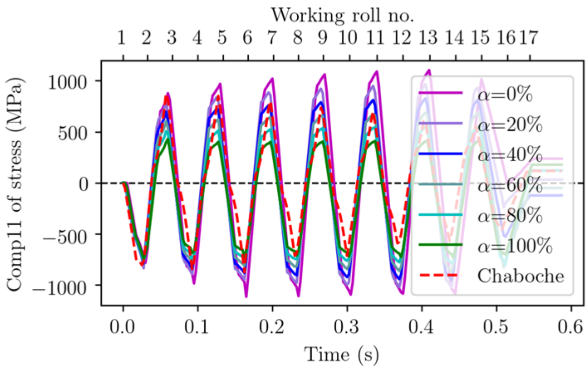

(a) Stress path.

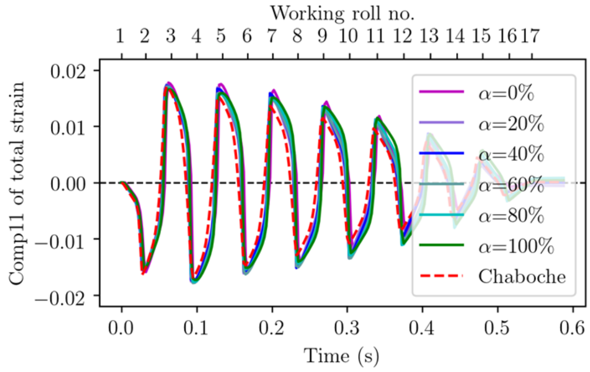

(b) Strain path.

Figure 4.30 – Stress and strain path throughout the levelling process (kinematic hardening effect).

Figure 4.31 displays the material behaviour under the simple combined hardening model, available in COPRA® FEA RF. Each stress-strain curve corresponds to a different simulation and kinematic factor, as resumed in Table 4.7.

It is observed that the pure kinematic model exhibits a reduced hardening effect during roll levelling process and results in a smaller stress amplitude than the pure isotropic model and that the combined hardening models, with intermediate values of kinematic factor, result in intermediate results between the isotropic and kinematic model ones. The fact that isotropic hardening leads to the increase of the yield surface and kinematic hardening to the translation of the yield surface, justify this stress amplitude difference.

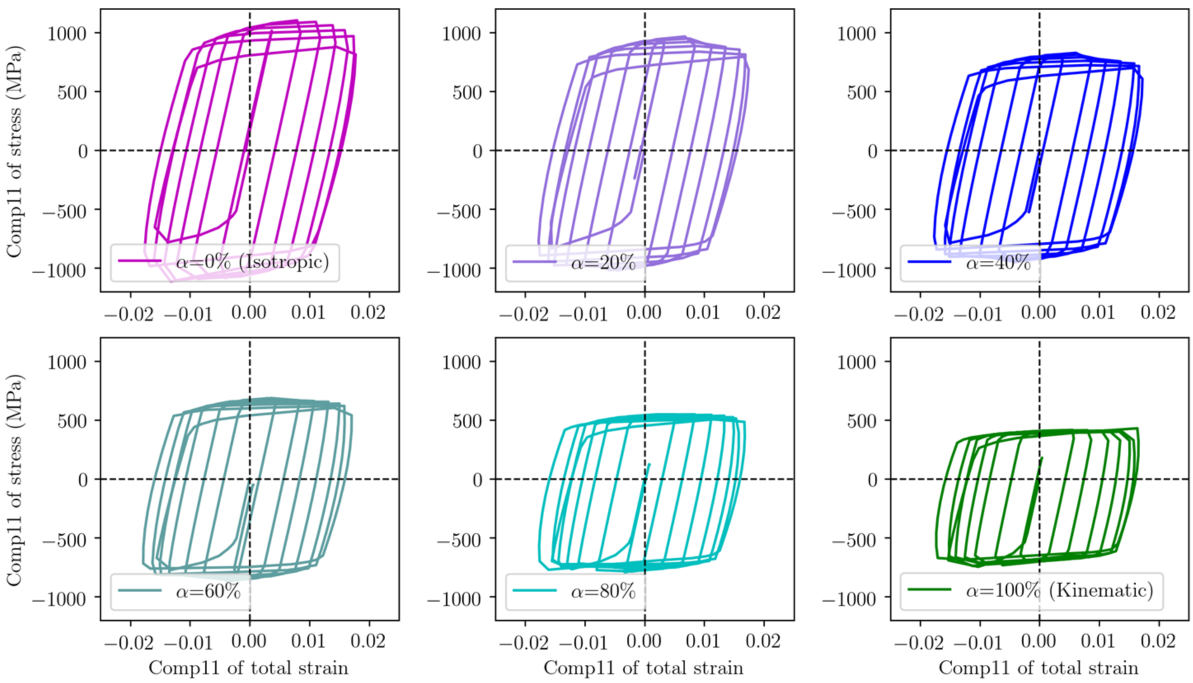

Figure 4.31 – Stress-strain curve from different hardening models (kinematic hardening effect).

4.5.2 Young's modulus

In this section, two material models are compared: one with a constant Young's modulus of 210 GPa and another with a strain-dependent Young's modulus (chord modulus, defined in Table 3.2). Both assume the Chaboche-Lemaitre hardening model, studied in Section 4.5.1.

Since the chosen finite element analysis software does not support a strain-dependent Young's modulus, modelling the chord modulus requires either the development of a subroutine within the FEA software or the creation of a multi-physics model in which a simulation artifice is used. This artifice consists in enabling heat generation from plastic deformation, set the material as non-conductive and adjusting chord modulus' function to be driven by strip's temperature. The later strategy is chosen for this work.

In order to validate this simulation artifice, a simple uniaxial tension-compression test with several cycles is executed. This enables a first comparison between the two Young's modulus models and a better fitting of the theoretical (according to Equation 3.4) and simulated values of chord modulus, as can be seen in Figure 4.32a. Also, Young's modulus degradation is observed when the stress-strain curves of both Young's modulus models are compared (Figure 4.32b).

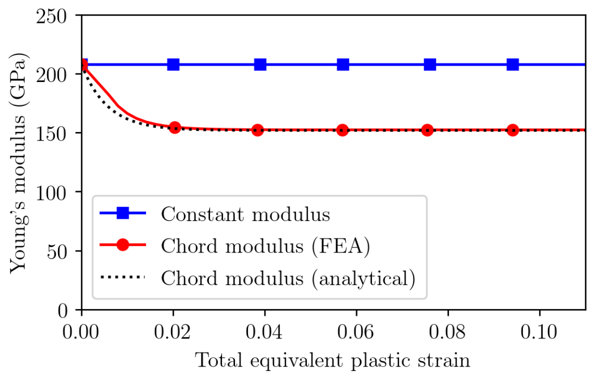

(a) Chord modulus values.[5]

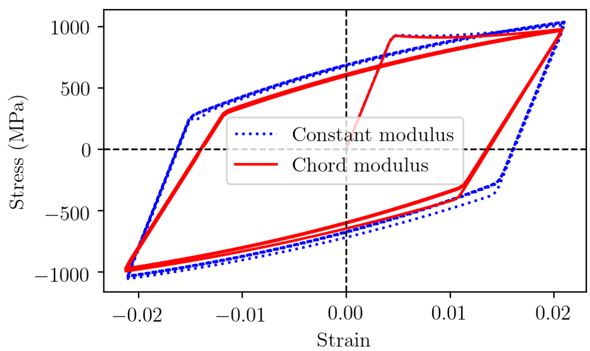

(b) Stress-strain curves.

Figure 4.32 – Chord modulus model analysis, through an uniaxial tension-compression test.

Later, a finite element analysis of the roll levelling process is proceeded, where chord modulus is taken into account and its results are compared with those from a previous analysis with constant Young's modulus.

Table 4.8 – Simulations proceeded during Young's modulus modelling analysis.

Hardening model	Young's modulus model	Curvature radius (mm)	Max. vertical displ. (mm)	CPU time (%)
Chaboche-Lemaitre	Constant modulus	5034.24	-154.51	100
Chaboche-Lemaitre	Chord modulus	9532.20	-15.98	139

From Table 4.8, one can identify two significant differences induced by the Young's modulus models. By taking into account Young's modulus degradation with plastic strain, the resultant strip exhibits a very

[5] More data points are analysed than those signed with markers.

high curvature radius, i.e. its very flat. However, modelling a non-constant Young's modulus represents a penalty of ≈40% on the computation time.

When the distribution of results through thickness is analysed (Figure 4.33), it is possible to observe that the residual stress magnitude suffers no significant impact when chord modulus is considered. Regarding the distribution of accumulated plastic strain, a small reduction of plastification is induced by a non-constant Young's modulus. This phenomena can be easily explained, as the Young's modulus value is reduced with the accumulation of plastic strain and, therefore, the elastic recovery increases during the process.

Despite being evident that a reduction of plastification occurs due to Young's modulus degradation, it is impossible to quantify how much it affects the plastic rate. This limitation is related with an insufficient discretisation through thickness for such a detailed study.

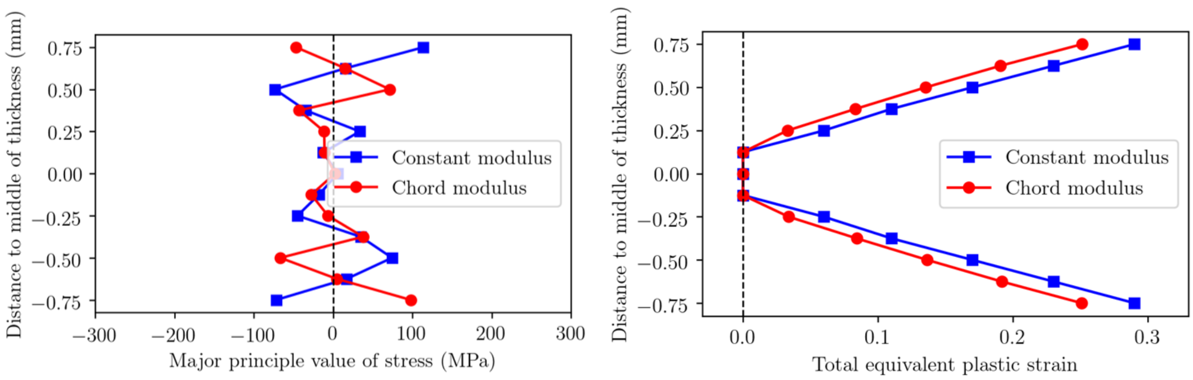

(a) Residual stress. (b) Accumulated plastic strain.

Figure 4.33 – Results' thickness distribution after levelling (different Young's modulus models).

By observing the stress and strain evolution throughout the process of a surface node, the previous observation is corroborated, as similar stress paths result in a different accumulation of plastic strain, when the Young's modulus model is changed (Figure 4.34a).

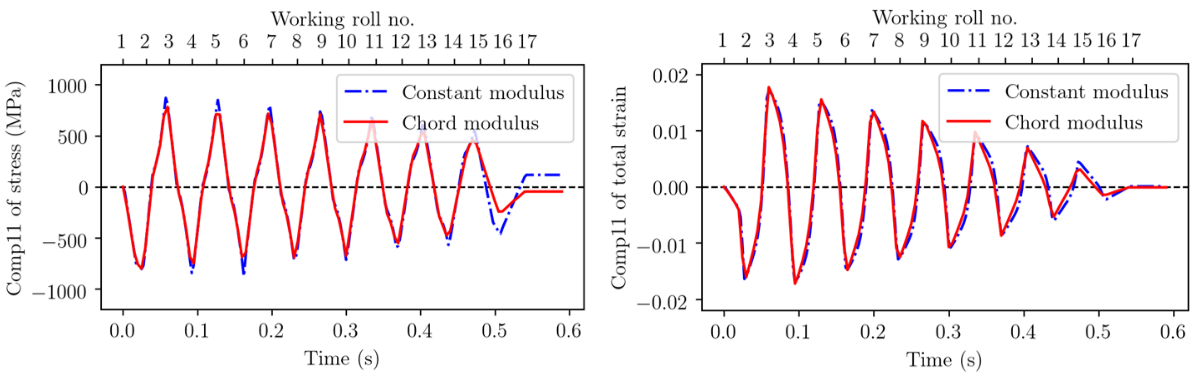

(a) Stress path. (b) Strain path.

Figure 4.34 – Stress and strain path throughout the levelling process (different Young's modulus models).

The degradation of Young's modulus become visible when the stress-strain curve of a surface node is plotted. In Figure 4.35 there are two images, which contain the before mentioned results of a roll levelling FEA with constant Young's modulus and chord modulus, respectively. If the loading/unloading segments' slopes are assessed for each curve, it is possible to quantify the Young's modulus for a certain pre-strain. Thus, it becomes clear that both Young's modulus models have the same initial value.

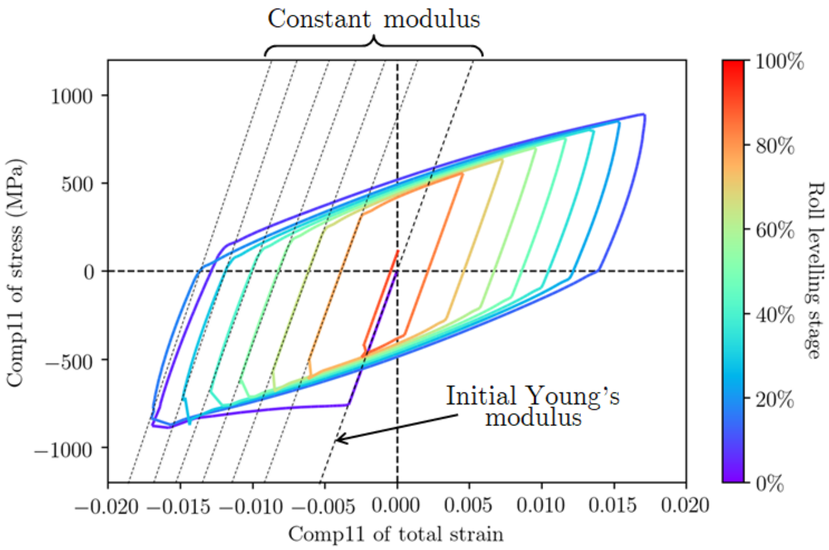

(a) Constant modulus.

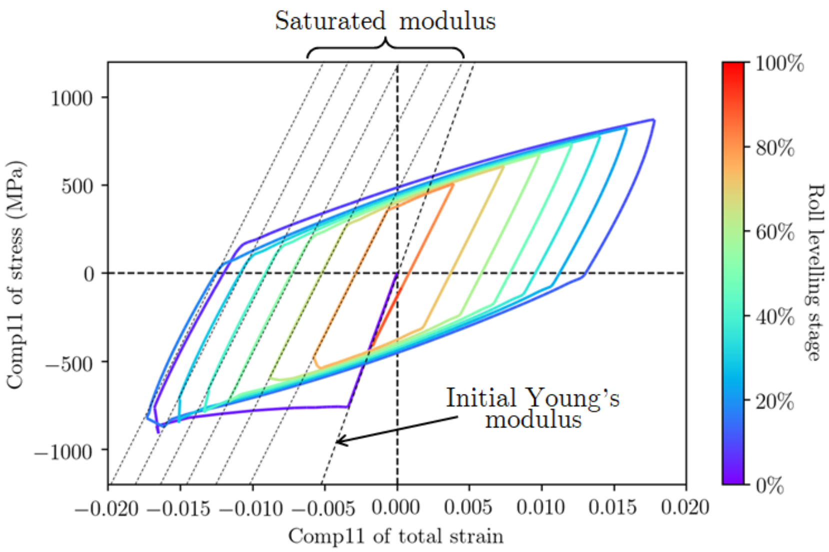

(b) Chord modulus.

Figure 4.35 – Stress-strain curves from different Young's modulus models (roll levelling process).

Throughout the process, constant modulus model assigns the material, as its name suggests, the initial Young's modulus. On the other hand, chord modulus model leads to a significant reduction of Young's modulus as consequence of its degradation. The minimum Young's modulus value of 152 GPa is achieved after ≈2% of accumulated plastic strain, which occurs in the first bending and remains constant afterwards.

Despite providing a better approximation of the real process, chord modulus represents a significant additional computation effort and is not easy to model. Since the impact in both residual stress distribution and plastic rate measurement is not critical, modelling a constant Young's modulus is found to be the best compromise solution. Hereinafter, in all finite element models, DP1000 steel is modelled with a constant Young's modulus value of 210 GPa.

Although not being essential to roll levelling FEA, when analysing subsequent processes it may be important to take into account that degradation of Young's modulus has already occurred.

4.6 Deformable rolls

In this section, different strategies to model deformable rolls in 2D are assessed. Considering that the roll levelling equipment has position controlled working rolls in order to counterbalance the structural deformation of the machine, the only deformations that can affect the roll levelling process and should be analysed through FEA are related with the working rolls: their deflection and flattening.

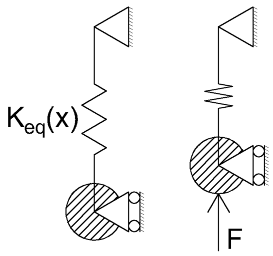

(a) Vertical displacement.

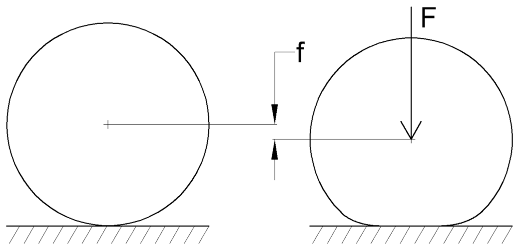

(b) Flattening.

Figure 4.36 – Deformable working rolls illustration.

The deflection of working rolls is induced by the contact force applied by the strip (F) and is reduced in most industrial equipments by using backup rolls. In this 2D analysis no intermediate or backup rolls are modelled, however their contribution to working rolls' stiffness (K_{eq}) is taken into account. The stiffness calculation is explained and proceeded in Appendix B using the Equation 4.1, for different width positions ($x \in [0, L]$) in a machine with backup rolls displaced every 440 mm (L).

$$K_{eq} = \frac{24 \cdot E \cdot I \cdot L}{x^2 \cdot (L - x)^2} \tag{4.1}$$

where E is the Young's modulus and I rolls' equivalent moment of inertia (calculated in Appendix B).

Figure 4.37 illustrates the deflection of a working roll at different x positions.

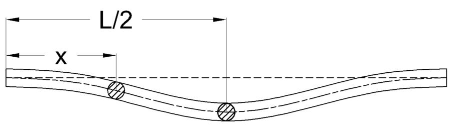

(a) Deflection.

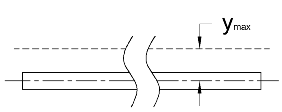

(b) Displacement ($x = \frac{L}{2}$).

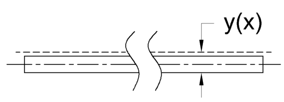

(c) Displacement ($x \neq \frac{L}{2}$).

Figure 4.37 – Deflection representation in 2D models.

In order to model roll's deflection at a certain *x* position, a spring with the equivalent stiffness of the roll (K_{eq}) is used to define its vertical position, in function of the vertical component of contact normal force. This strategy neglects the horizontal component of contact normal force and simplifies roll's deflection to a 2D vertical translation. Figure 4.36a illustrates how such springs are modelled.

Considering that at the location of each backup roll (x=0 and x=L) the equivalent stiffness is considered to be infinite, the rolls are modelled to be rigid in those locations. By proceeding several FEA considering the equivalent stiffness of the working rolls at different *x* positions, it is possible to have an insight on the impact of rolls deflection in the variation of results through width. Rolls' flattening is neglected in this analysis stage. The executed simulations, geometrical results and CPU time are available in Table 4.9.

Table 4.9 – Simulations proceeded during rolls' deflection study.

Position x/L **(%)**	**Equivalent stiffness** K_{eq} **(N/mm)**	**Curvature radius (mm)**	**Max. vertical disp. (mm)**	**CPU time (%)**
0	$+\infty$[a]	5024.24	-154.51	100
25	1864470[a]	3770.39	-154.32	130
50	1048764[a]	3153.61	-153.89	122

[a] Values from Appendix B.

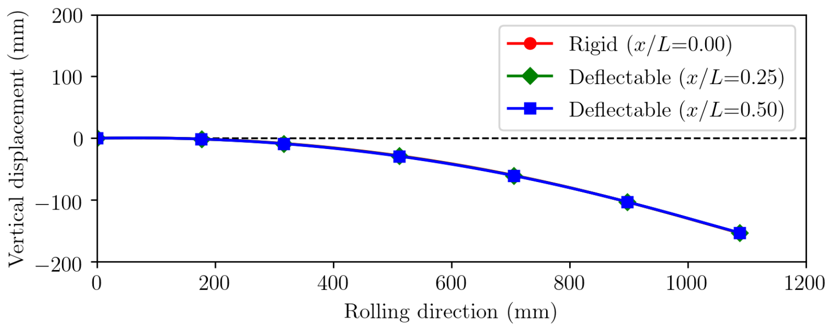

Figure 4.38 – Strip geometry after levelling (deformable rolls).[6]

As can be observed in Figure 4.38, rolls' deflection has no major impact on the final geometry of the strip. The previous results suggest that the levelling equipment is able to correct strip's shape accurately. However, it is still important to analyse the distribution of results through thickness, in order to validate this observation. Also it is interesting to have an insight on rolls' vertical displacement.

Throughout the roll levelling process, rolls' vertical displacement (2D simplification of deflection) changes both between rolls and transverse positions (*x*). As illustrated in Figure 4.39 and in accordance with the literature review, the maximum deflection is observed in the 3rd working roll (enumerated as explained in Section 3.6.3) and then reduces gradually from roll to roll. This observation is also valid for the loads on the rolls, since the vertical displacement is proportional to the vertical component of

[6] More data points are analysed than those signed with markers.

contact force. The maximum deflection of the working rolls is found in the 3rd roll at x/L=0.50 and has a magnitude of 0.026 mm, which corresponds to $\leq$1.5% of the entry gap value (g_{in}).

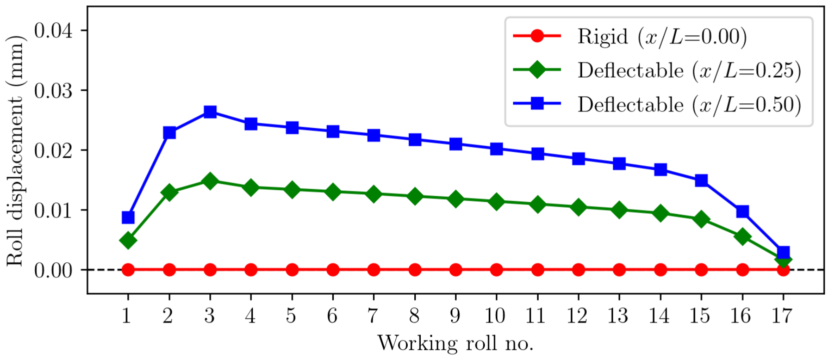

Figure 4.39 – Absolute vertical displacement of each working roll, at multiple cross-sections.

It is expected that when deflectable rolls are modelled in 3D, where no plane-strain condition is considered, larger geometrical variations are observed across strip's width (e.g centre buckles). Nonetheless, it is not possible to quantify those defects with a 2D analysis.

When assessing the impact of rolls' deflection on the final properties of the levelled strip, the distribution of results through thickness is also analysed. The amount of plastic strain induced during the process is approximately constant throughout the width of the strip, as can be seen in Figure 4.40a. Consequence of a constant plastic strain distribution, the plastic rate is very consistent. Regarding the distribution of residual stress through thickness, no significant differences are observed when rolls' deflection is taken into account.

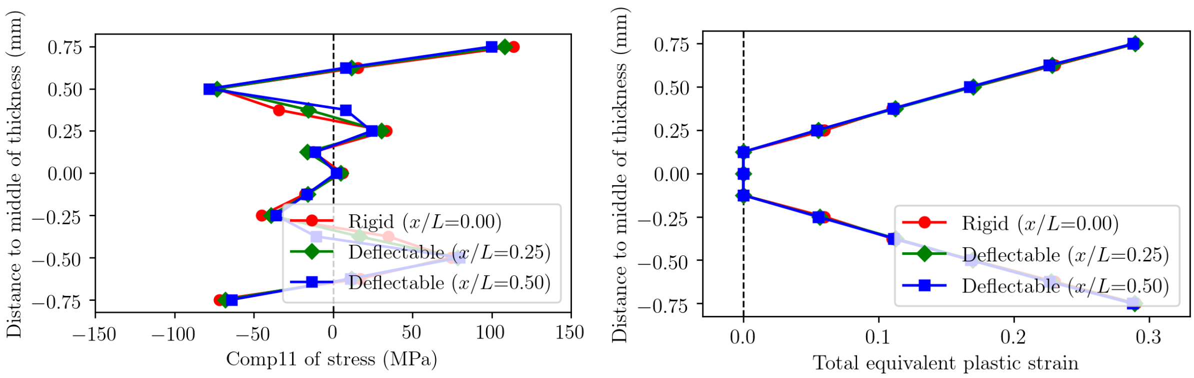

(a) Residual stress.

(b) Accumulated plastic strain.

Figure 4.40 – Results' thickness distribution after levelling (deformable rolls).

Therefore, it is possible to conclude that rolls' deflection has no significant impact in a 2D roll levelling FEA and should be neglected. However, such conclusion may not be valid during a 3D analysis, since no plane-strain condition is considered.

Regarding the geometrical variation of the cross-section, referred as flattening, it is important to quantify how much deformation occurs, understand if the rolls are plastically deformed and if this phenomena should be taken into account when proceeding a roll levelling FEA. It is expected that, due to the contact loads (F) inherent to the process, the working rolls' radius may change locally (f), as illustrated in Figure 4.36b.

The roll where the highest contact load is expected is selected and modelled as a deformable body, with the element type used in the strip - "Element 11". In order to submit the roll to the highest expected load, no deflection is modelled ($K_{eq} = +\infty$). All the other rolls remain rigid bodies, since, as concluded previously from Figure 4.39, it is in the third roll where the highest contact load is expected, approximately 60 N/mm (at x/L=0).

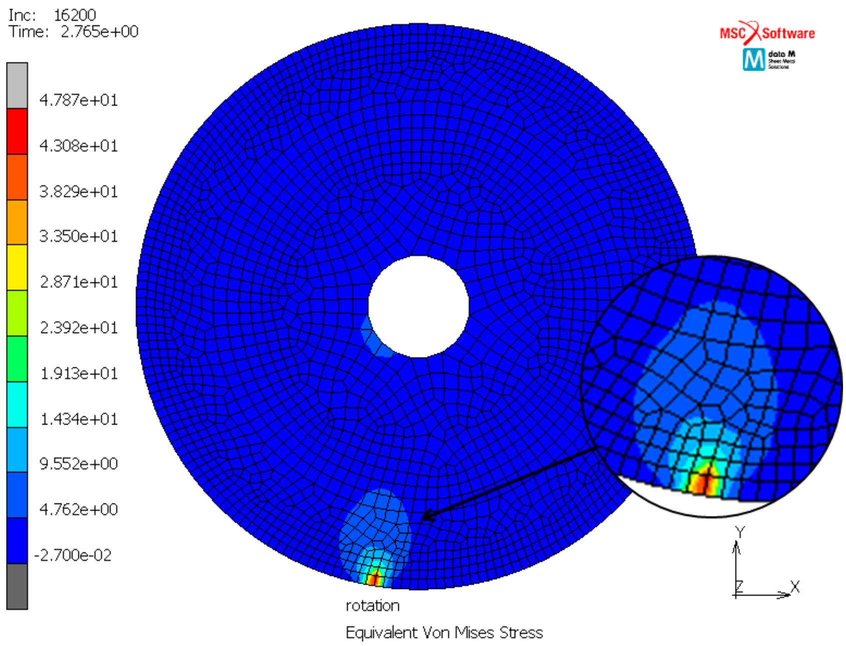

Figure 4.41 – Stress in working roll no.3, during a roll levelling FEA (values in MPa).

As can be seen in Figure 4.41, by proceeding a roll levelling FEA where rolls' flattening is considered, it is possible to quantify the amount of stress and strain induced in the working roll. Since the maximum von Mises equivalent stress found in the roll is ≈50 MPa, no plastification occurs in the 3rd roll. Therefore, it is possible to state that no permanent change in geometry is expected to be found in any working roll.

However, some elastic deformation is expected near the contact point. Such deformation leads to a temporary change in roll's geometry. By measuring the initial radius and minimum radius, when and where the maximum contact load is applied, such geometrical variation is quantified. Table 4.10 sums up the cross-section geometrical changes observed when flattening is evaluated.

From the rolls' flattening study, it is possible to conclude that no permanent deformation is induced in the working rolls. Also, the elastic radius variation is small ($\leq$1.23%) and can be neglected when analysing the roll levelling process, mainly due to the fact that it represents an additional penalty of ≈36%

Table 4.10 – Simulations proceeded during rolls' flattening study.

Flattening	Minimum radius (mm)	Radius variation (%)	CPU time (%)
No	27.50	0.00[a]	100
Yes	27.16	1.23[a]	136

[a] Considering an initial radius of 27.50mm.

on the CPU time. If the radius variation was significant, a finite element model only with deformable deformable should have been developed.

Despite the fact that both rolls' deflection and flattening are neglectable in a 2D analysis, the first is further analysed with a 3D roll levelling simulation (Chapter 5) since the strip is expected to exhibit transverse buckles when the plane-strain condition is not considered. During the remaining 2D analyses, only rigid working rolls are modelled.

4.7 Machine settings

During the previous sections, the same machine settings have been used (mentioned in Section 3.4.1). Since the roll levelling processes aims to achieve a flat metal strip, the strip is required to plasticise. However, the amount of plastification, measured as the plastic rate (PR), should be chosen in order not to be excessive. Thus, it is important to establish the relation between machine settings and PR.

Considering that the roll levelling equipment modelled enables the adjustment of both entry and exit gap, as described in Section 3.4.1, in the current study the exit gap (g_{out}) is fixed to 1.23 mm. On the other hand, different entry gap values (g_{in}) are assessed. Table 4.11 exhibits some of the FEA executed during the machine settings study, their geometrical results and CPU time.

Table 4.11 – Simulations proceeded during machine settings study.

g_{in} (mm)	Curvature radius (mm)	Max. vertical disp. (mm)	CPU time (h)
-0.50	2650.54	-117.68	4.90
-1.50	2654.25	-117.69	4.89
-2.50	3558.41	-133.62	4.71
-3.50	19799.10	-54.44	4.72
-4.50	5039.30	90.65	4.95

From the geometrical results, it is possible to observe that a larger entry gap leads to a higher curvature radius, except for the model with a gap of -4.5 mm which geometrical results are not the expected. This behaviour is displayed in Figure 4.42 and suggests that a geometrical improvement is expected from the increase of plastic rate.

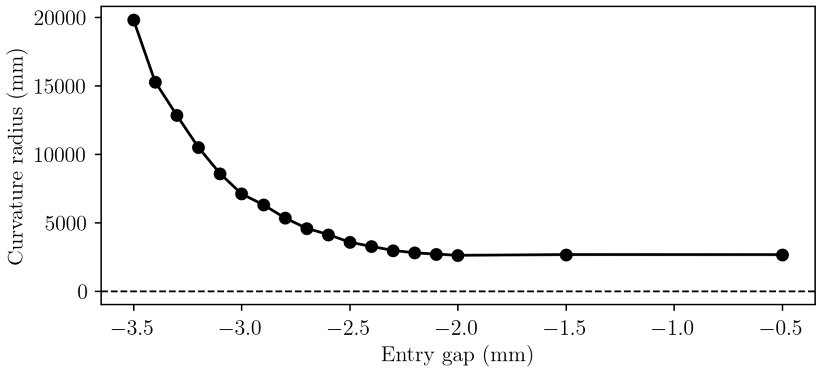

Figure 4.42 – Final curvature for multiple entry gaps.

If one analyses the results distribution through thickness, it is expected to observe that more severe entry gaps lead to higher plastic rates and, consequently, to an improvement on the final geometry. However, such behaviour is not directly observable in Figure 4.43b due to an insufficiency mesh refinement. The results from the machine settings used throughout the work ($g_{in} = -2.77$ mm and $g_{out} = 1.23$ mm) are taken as reference and plotted in the following figures. Regarding the residual stress distribution, the only correlation found is that higher penetrations result in higher stress levels.

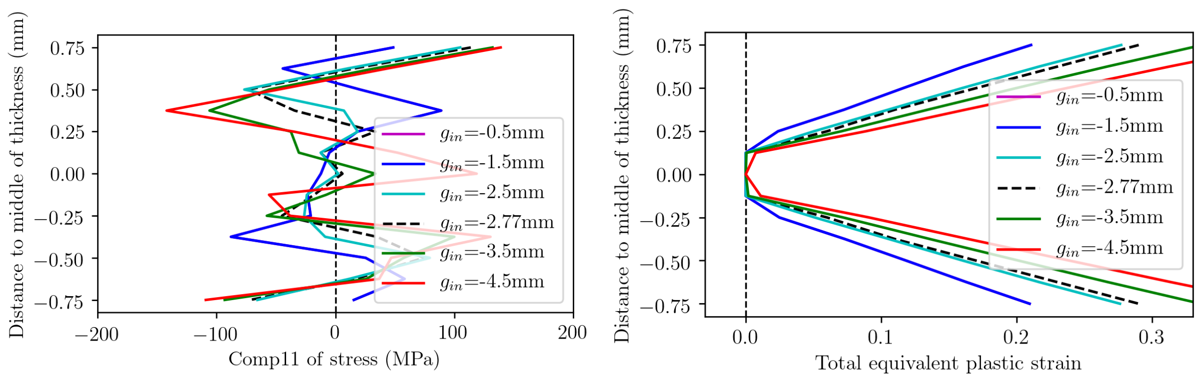

(a) Residual stress.

(b) Accumulated plastic strain.

Figure 4.43 – Results' thickness distribution after levelling (different entry gaps).

In order to increase the resolution through thickness, one may proceed as explained in Section 3.3.1 and measure the results in the integration points. By doing so, the measurement uncertainty is reduced from 16.67% to a maximum of 9.62%. Figure 4.44 displays the thickness distribution of accumulated plastic strain for different entry gap settings, measured in the integration points and zoomed to the critical region for plastic rate measurement.

When it comes to plastic rate measurement, it is necessary to execute a simple data analysis in order to achieve a better measurement, considering that the finite-element analysis provides discrete results. If the accumulated plastic strain results plotted in Figure 4.44 are separated and analysed in three different parts (i.e. results in the elastic region, in the top plasticised region and bottom plasticised region of the strip) it is possible to fit a polynomial function to the data points contained in each plasticised region.

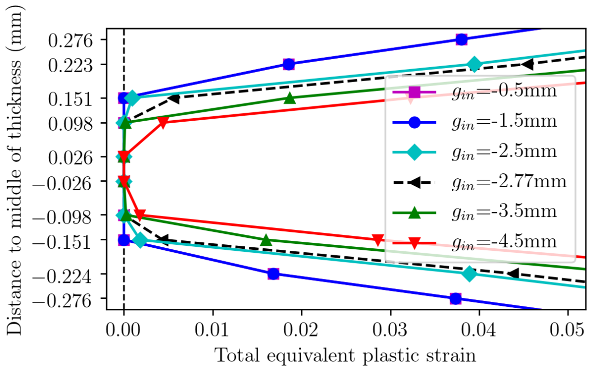

Figure 4.44 – Thickness distribution of accumulated plastic strain for different entry gaps.[7]

The goal of this approach is to fit the discrete set of results with a continuous function. By analysing the resultant functions one can better predict the thickness coordinates where the transition between elastic and plasticised regions occurs and, therefore, better predict the plastic rate (PR, defined in 2.3).

Figure 4.45 illustrates the relation between entry gap (g_{in}) and plastic rate (PR) which exhibits a pronounced trend: as the entry gap becomes more severe the plastic rate increases, approximating the trend described by a second degree polynomial equation ($PR(\%) = 0.6348 \cdot g_{in}^2 + 0.8838 \cdot g_{in} + 78.443$). The experimental results are achieved by following the approach described in the previous chapter.

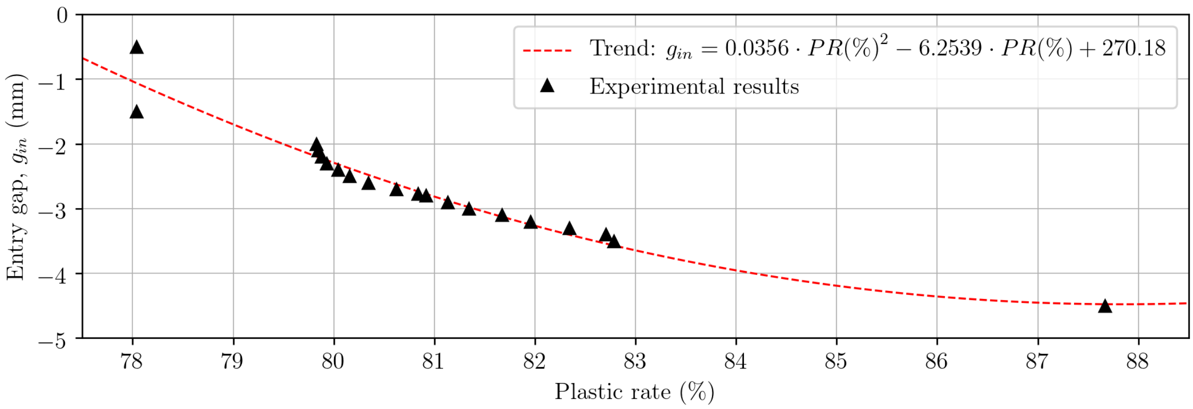

Figure 4.45 – Relation between entry gap (g_{in}) and plastic rate (PR).[7]

The previous figure proves that a detailed prediction of the PR is possible from discrete roll levelling FEA results by means of a simple data analysis.

Regarding the evolution of the stress and total strain state throughout the levelling process, the strain levels reduce with the decrease of g_{in} while the stress levels remain similar (Figure 4.46). This is due to the fact that, on the contrary to the material modelling study, in this section the machine settings are changed and only one material model is used.

The stress levels similarity is justified by the fact that every bend leads to a stress level which surpasses the yield stress and, consequently, similar elastic strain levels. The difference between strain

[7] Results evaluated in the integration points.

levels can be corroborated by the increase of plastic strain with more severe entry gaps, as can also be observed by higher values of accumulated plastic strain in Figure 4.47.

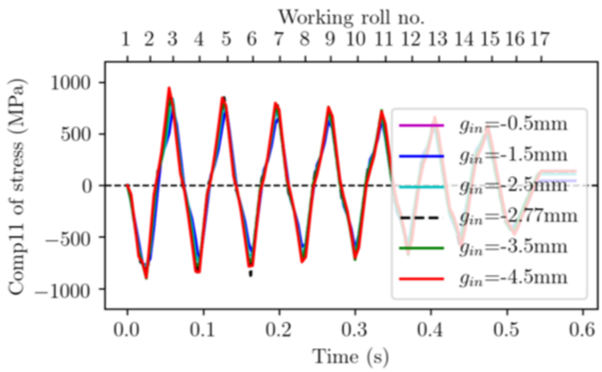

(a) Stress path.

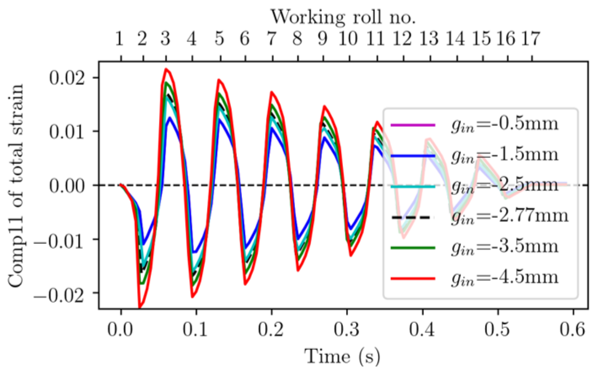

(b) Strain path.

Figure 4.46 – Stress and strain path throughout the levelling process (different entry gaps).

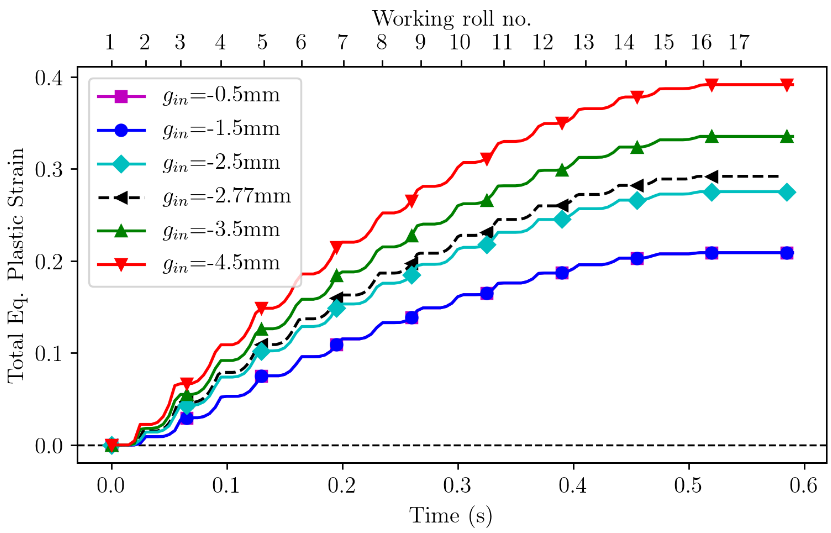

Figure 4.47 – Plastic strain accumulation throughout the levelling process (different entry gaps).[8]

4.7.1 Simplified model - Three point bending

Taking into account that roll levelling finite element simulations take a long calculation time (e.g. 5 to 6 hours) and require a complementary data analysis so that a feasible PR evaluation is proceeded, a compromise solution to determine acceptable initial roll levelling settings with a small computation effort is desired.

In this work, a simplified roll-levelling finite element model is suggested and illustrated in Figure 4.48. The model consists on a small strip of material and 3 curved rigid bodies, which have the same radius of the working rolls and are used to bend the strip. In order to approximate the bending behaviour

[8] More data points are analysed than those signed with markers.

of a long strip being continuously levelled, the boundary conditions are such that in one end of the strip all degrees of freedom are constrained and in the other end only the horizontal translation is free.

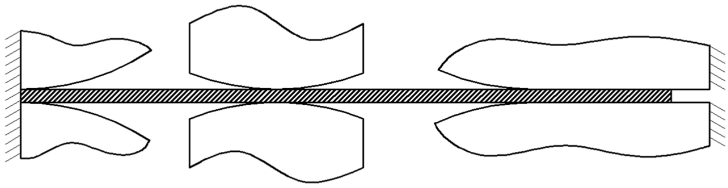

(a) Initial position.

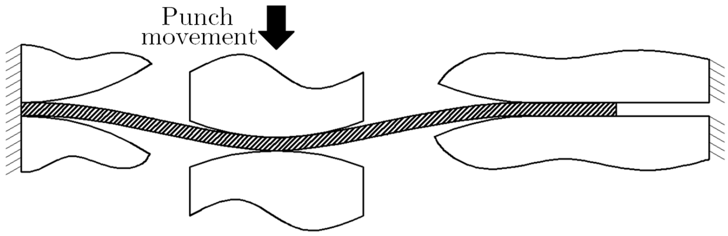

(b) Bent position.

Figure 4.48 – Three-point bending model.

The initial settings are then selected by analysing the evolution of PR in function of movable rigid bodie's penetration, which represents the entry gap. By proceeding an earlier estimation of the machine settings, the number of iterations and time required to proceed a detailed roll levelling FEA are expected to reduce significantly.

Several analyses are proceeded, with different mesh refinements. Their resolution through thickness and computation time are available in Table 4.12. It becomes obvious that this method is very fast, when compared with the CPU time required for a 2D roll levelling FEA ($\approx 7\times$ faster).

Table 4.12 – Simulations proceeded during machine settings study (simplified model).

Elements p/ thickness	**Resolution (%)**	**CPU time (h)**
12	16.67	0.04
24	8.33	0.42
48	4.17	0.68

By analysing the PR evolution in function of punch's penetration, from the simulation with 48 elements through thickness and performing the same data analysis as in Figure 4.45, it is possible to predict the PR *versus* g_{in} curve with the simplified model (Figure 4.49).

It is observable that the plastic rate (PR) increases for more severe entry gaps (g_{in}), however, when compared to the results from the 2D roll levelling FEA, a different trend is suggested. The experimental results follow a trend with a contrary curvature (negative second derivative) and the same PR is achieved with less penetration in the three point bending model. This difference is due to the fact that only the first

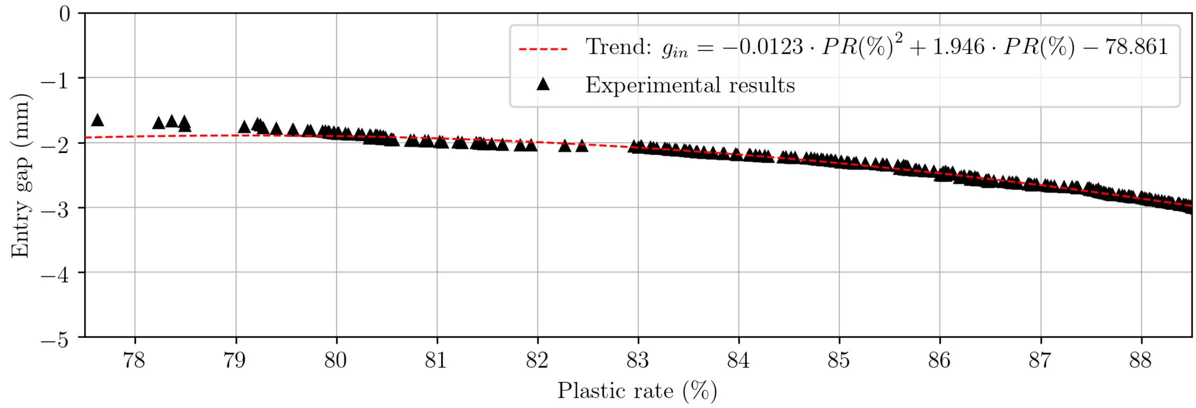

Figure 4.49 – Relation between entry gap (g_{in}) and plastic rate (PR), from a simplified simulation with 48 elements over the thickness.

bending is simulated in the simplified model. Also, a limited length of strip is modelled and boundary conditions are established to approximate the continuity of material.

This simplified three point bending model is believed to be a promising approach to predict the required initial setting for a certain plastic rate (PR), however further development is still required to improve the model and better approximate the roll levelling process.

4.8 Initial defects

Regarding the efficiency of roll levelling process, it is important to understand how different initial defects affect the properties of the levelled strip. In this section, coil set defect is modelled and its impact on the levelled strip analysed. This geometrical defect was chosen considering that it is associated with most coiled materials and, therefore, very common in industry.

For an entry gap of -2.77 mm, several roll levelling FEA are proceeded. In all of them, an initial curvature is induced on the metal strip as illustrated in Figure 3.11. Between consecutive analyses, the induced curvature radius is reduced, in order to model a coil with an outside diameter of 1000 mm and an inside diameter of 400 mm. The objective of this study is to better understand how the final properties of the strip change during a real roll levelling process, where the strip is feed from a finite length coil. It is also important to conclude if coil set defect should be taken into account when analysing the levelling process.

Table 4.13 – Simulations proceeded during initial curvatures study.

Coil set radius (mm)	Curvature radius (mm)	Max. vertical disp. (mm)
$+\infty$	5024.24	-120.03
500	5049.46	-115.34
400	5022.48	-115.30
300	5081.27	-115.27
200	5050.24	-115.39

Table 4.13 resumes the before-mentioned analyses and presents the respective geometrical results. It is observable that coil set defect has no impact in the geometrical properties of the levelled strip, as Figure 4.50 corroborates.

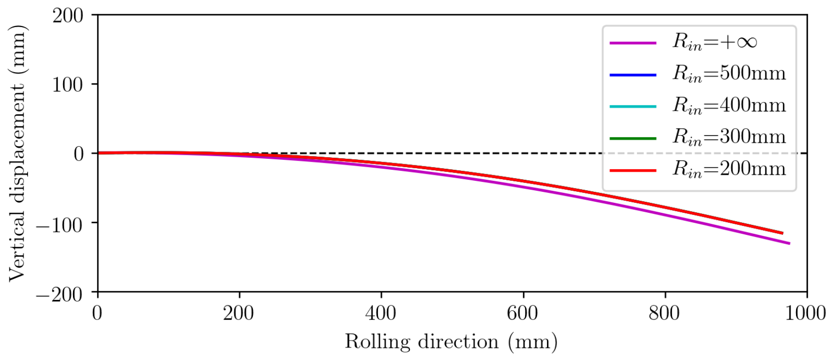

Figure 4.50 – Strip geometry after levelling (different initial curvatures).

By analysing the final distribution of results through thickness (Figure 4.51), it is also possible to state that the residual stress and total accumulated plastic strain thickness distributions are not influenced by any initial curvature radius. This leads to the conclusion that roll levelling is able to correct, at its best extent, coil sets from coils of DP1000 steel with a thickness of 1.5 mm and a minimum coil diameter of 400 mm. This conclusion can be extended to all coil sizes, as smaller coils are not common and larger diameters represent an easier challenge to level.

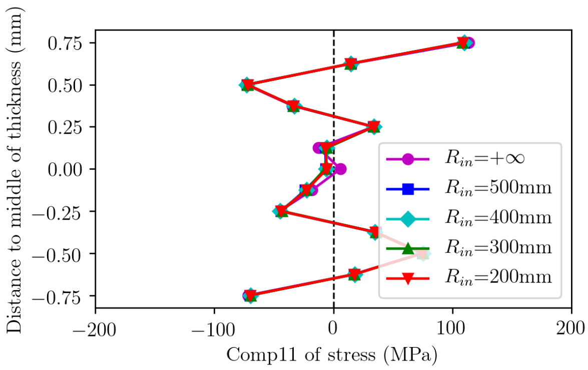

(a) Residual stress.

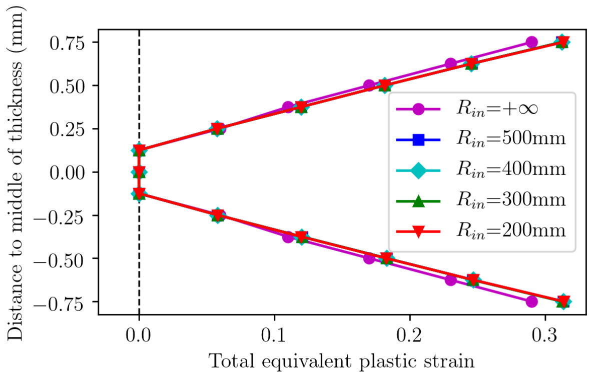

(b) Accumulated plastic strain.

Figure 4.51 – Results' thickness distribution after levelling (different initial curvatures).

The only visible effects of coil set are non-zero initial stress and strain (visible in Table 4.14), which are only present until the levelling process starts and have magnitudes within the order of those observed during roll levelling. In Figure 4.52 it is noticeable that from the moment the first bending takes place (working roll no.2), strip's properties become undistinguishable from those of a strip with no initial curvature.

Due to coil set, stress and strain pre-states are induced in the strip. Table 4.14 resumes the initial stress, total strain (longitudinal component) and the accumulated plastic strain of a node from the top surface of the strip.

Table 4.14 – Initial stress and strain state induced by coil set.

Coil set radius (mm)	Stress (MPa)	Total strain (%)	Accum. plastic strain (%)
+∞	0.00[a]	0.000[a]	0.000
500	589.46[a]	0.885[a]	0.732
400	589.12[a]	0.886[a]	0.733
300	587.52[a]	0.882[a]	0.730
200	583.65[a]	0.904[a]	0.848

[a] Longitudinal component (Comp11).

It is visible that the stress magnitude is similar for different initial curvatures and, therefore, that the yield stress was surpassed. Also, the non-null accumulated plastic strain corroborates this observation. Despite leading to a higher accumulation of plastic strain and, therefore, to an earlier hardening of the material, the hardening effect is not reflected on higher stress levels throughout the process (Figure 4.52a), due to the fact that DP1000 steel exhibits a reduced isotropic hardening behaviour.

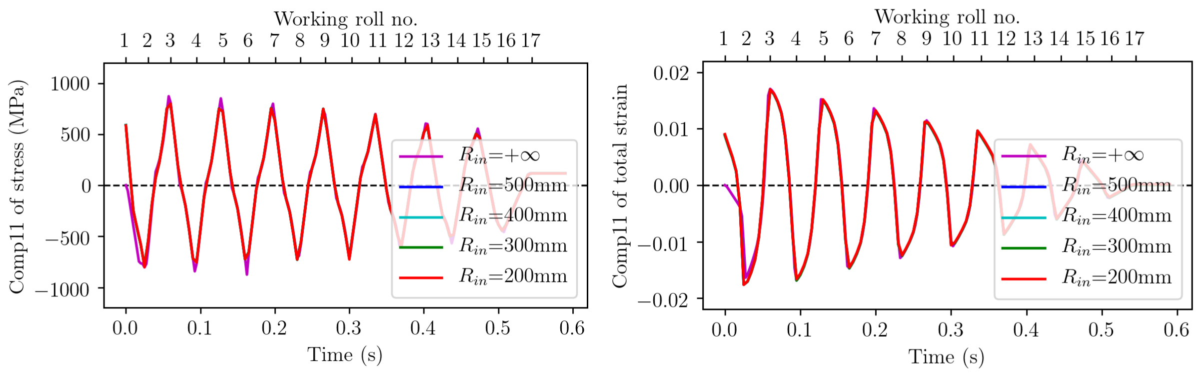

(a) Stress path. (b) Strain path.

Figure 4.52 – Stress and strain path throughout the levelling process (different initial curvatures).

From this study and particularly for DP1000 steel, it is possible to conclude that coil set defects can be neglectable in roll levelling FEA and are corrected, up to the best capabilities of the levelling equipment, during the roll levelling process.

4.9 Conclusions

From the 2D roll levelling finite element modelling study performed in this chapter, some conclusions are drawn and considered throughout the remaining work.

The first topic under scope is the mesh sensitivity. Taking into account that one desires a good compromise between computation time and quality of results, the use a locally refined mesh to model the strip is found to be an adequate strategy. Therefore, a strip with $\approx 3\times$ the machine length is regularly meshed with 4 elements through the thickness, keeping an aspect ratio of 1:2. At 1/3 of the strip length (in rolling direction), a refined area with 12 elements through thickness is also considered. Such refined area has a minimum length of 40 mm and respects the before mentioned aspect ratio. This represents a computation time reduction of 80%, when compared to a regular mesh with 12 elements through thickness.

Contact modelling is also studied, since it is very important in roll levelling FEA. It is observed that, in a 2D analysis where the working rolls are modelled as geometrical bodies, no advantage is found in using a segment-to-segment (S2S) contact algorithm instead of the node-to-segment (N2S) one. On the contrary, by using the S2S contact algorithm, an increase of $\approx$50% on the CPU time is expected. Also for 2D analyses, defining elements' segments analytically has no beneficial impact in results' quality.

Another observation during this chapter is that gravity can be neglected in roll levelling FEA. Despite leading to a strip with a very different geometry, the strains induced due to gravity loads are purely elastic and have no impact on process' effectiveness.

Regarding material modelling, several conclusions are drawn. Being roll levelling a process where cyclic tension-compression loads are applied, conventional isotropic hardening models are not suitable to characterise materials which display a significant kinematic hardening behaviour. Since DP1000 steel exhibits an almost pure kinematic hardening behaviour, a combined isotropic/kinematic hardening model is ideal to perform a roll levelling FEA. The model suggested by Silvestre, Mendiguren, Galdos, et al. (2015) and characterised in Table 3.4 is found to be a proper way to characterise DP1000's hardening behaviour in roll levelling FEA.

Concerning the Young's modulus of the material, DP1000 steel exhibits a significant Young's modulus degradation. A simple way to characterise Young's modulus drop with the accumulation of plastic strain is to use chord modulus model, defined in Table 3.2. However, no major impact on the final properties of the levelled strip are observed and chord modulus model required a higher computation effort. Therefore, the best compromise solution is to model DP1000 with Chaboche-Lemaitre hardening model and a constant Young's modulus of 210 GPa.

The impact machine deformation has on the levelled strip is another topic investigated in this chapter. This is particularly interesting since, on the contrary to the previously mentioned topics, no research on levelling rolls' deformation was found on literature. Since in the 2D analyses a plane-strain condition is considered, it is possible to approximate working rolls' deflection by a simple 2D model where geometric rolls are position controlled by a spring, with the equivalent stiffness of both working, intermediate and backup rolls calculated for a certain transverse position.

During this study, the importance of intermediate and backup rolls becomes clear, since a huge "deflection" is expected if no support rolls are considered. However, for the machine settings analysed in this work, rolls' deflection is concluded to be neglectable in 2D analyses when the structural contribution of both intermediate and backup rolls is taken into account. Nevertheless, neglecting rolls' deflection may not be valid in a 3D analyses since no plane-strain condition is considered and, thus, a 3D analysis is required.

In addition to rolls' deflection, also rolls' section variation (referred as flattening) is studied. Since no significant deformation is observed, the rolls should be modelled as geometrical bodies.

In order to understand how machine settings affect the process effectiveness and the properties of the levelled strip, a machine settings study is proceeded. By varying the entry gap value, it is possible to observe that the more severe the entry gap is, the flatter the strip becomes. However, increasing the entry gap also leads to higher residual stress magnitudes.

One objective of this study is to find a correlation between entry gap (g_{in}) setting and plastic rate (PR), however, a detailed correlation is limited by the resolution through thickness. By analysing the results on the integration points (and, therefore, improving thickness resolution) and fitting a continuous polynomial function to the discrete results, it is possible to estimate a relation between g_{in} and PR.

Alternatively to the time costly roll levelling FEA, it is possible to study machine settings by proceeding a simplified simulation, in which only one bending is modelled. This approximation also leads to a relation between entry gap and plastic rate, however it still requires further development.

The impact initial defects have on the properties of the levelled strip is the last topic under scope in this two dimensional study. It is concluded that the roll levelling process is able to correct the curvatures induced by the whole range of coil radius, since the final geometry and stress-strain state of the strip are not dependent on the initial curvature radius. This conclusion is valid for coil set defects on DP1000 steel strips.

Chapter 5

3D roll levelling analysis

In order to complement the two dimensional roll levelling finite element modelling study proceeded in Chapter 4, different 3D models of the before-mentioned process are developed and analysed throughout this chapter. Since no plane-strain condition is considered in the 3D analyses, topics such as rolls' deflection, distribution of results in width direction and defects generation (e.g. buckles) can be studied in detail. Besides complementing the study on roll levelling finite element modelling, this chapter also serves to develop a 3D roll levelling model which can be later integrated with a standard roll forming finite element model, which is also three dimensional, in a single finite element model.

5.1 Initial considerations

Since this is a cumulative work, some considerations are taken from the two dimensional study and applied in the development of three dimensional roll levelling FE models. The following points enumerate such considerations:

- The machine settings are the same as in most of the 2D analyses: g_{in}=-2.77 mm and g_{out}=1.23 mm, as described in Section 4.1;
- Knowing that a plastic rate of $\approx$80% is expected for the above mentioned machine settings (Section 4.7), a coarse mesh (relatively to the one used in 2D analysis) can be adjusted to provide an acceptable insight on results' distribution through thickness;
- DP1000 steel is modelled considering a constant Young's modulus of 210 GPa and Chaboche-Lemaitre's combined hardening law, characterised in Section 3.3.3 and analysed in Section 4.5;
- When rigid rolls are modelled, the node-to-segment (N2S) contact algorithm is used, as concluded in Section 4.3. When deformable rolls are modelled, other contact algorithms are explored;
- No rolls' flattening (change in section's geometry) is expected and, therefore, can be neglected (Section 4.6);
- Gravity acceleration is neglected (Section 4.4);
- No coil set defects are taken into account, as concluded in Section 4.8.

5.2 Geometry and boundary conditions

In this chapter, the levelling equipment is modelled in three dimensions with the same dimensions and machine settings as in the 2D model, as mentioned in Section 3.4.1 and Section 4.1.

There are 17 working rolls, which have 55 mm diameter, 2200 mm length and a spacing of 59 mm between centre of rolls. The exit gap is set to 1.23 mm and the entry gap to -2.77 mm. The steel strip has 1.5 mm thickness, 1500 mm width and 1500 mm length, in order to provide a good continuity of results. Also, a table of rolls is added at the exit of the levelling machine since the 3D simulation exhibited instabilities at the end of the process.

Regarding the boundary conditions, an illustration can be found in Figure 5.1. Each roll has the longitudinal (x) and vertical (y) translations constrained in its extremities (highlighted in blue). Also their transverse (z) rotation is controlled in the same location, inducing a driving speed of 300 rpm ($\approx$ 51.8 m/min). In order to have a time-efficient simulation, only half the width of both rolls and strip is modelled. Such consideration is made by constraining the transverse (z) translation of solid elements' nodes (strip) and, whenever deflectable rolls are modelled, the transverse (z) translation, longitudinal (x) rotation and vertical (y) rotation of beam elements' nodes (deflectable working rolls) which are placed in the middle-width of the machine (highlighted in red).

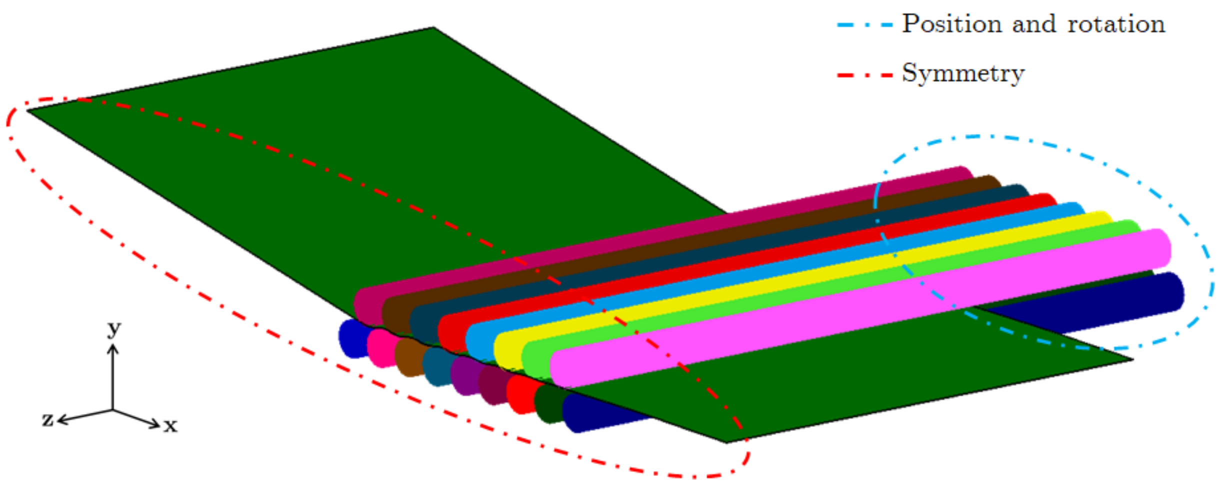

Figure 5.1 – Boundary conditions in the 3D model.

When deformable rolls are considered, a new material with a Young's modulus of 517.95 GPa is assigned to the working rolls. This is a modelling artifice has the purpose of better representing the real process by assigning the combined stiffness from both working and intermediate rolls to the working rolls. This simplification is explained and calculated in Appendix B, similarly to the procedure followed in the 2D analysis of deformable rolls (Section 4.6). Backup rolls' effect is modelled by means of several boundary conditions constraining both x and y translations of each working roll, in the same width position where the backup rolls would be placed. The distance between two consecutive backup rolls is considered to be 440 mm.

5.2.1 Full roll levelling model

A more realistic roll levelling model was also developed. This model had both working, intermediate and backup rolls modelled with beam elements, as illustrated in Figure 5.2. Each working roll is supported by two intermediate rolls with a length of 2200mm and a diameter of 50mm. On the other hand, each intermediate roll is supported by several backup rolls which are position controlled, have a diameter of 55mm and are placed every 440mm. They alternately support each side of the intermediate rolls, leading to a deformed shape of the working rolls which is not planar. In this model a symmetry boundary condition is established in the plane highlighted in Figure 5.2.

This complex model was developed in order to avoid modelling simplifications when analysing working rolls' deflection. However, such model is associated with severe beam-to-beam and beam-to-solid contact instabilities and, therefore, no successful simulation was possible.

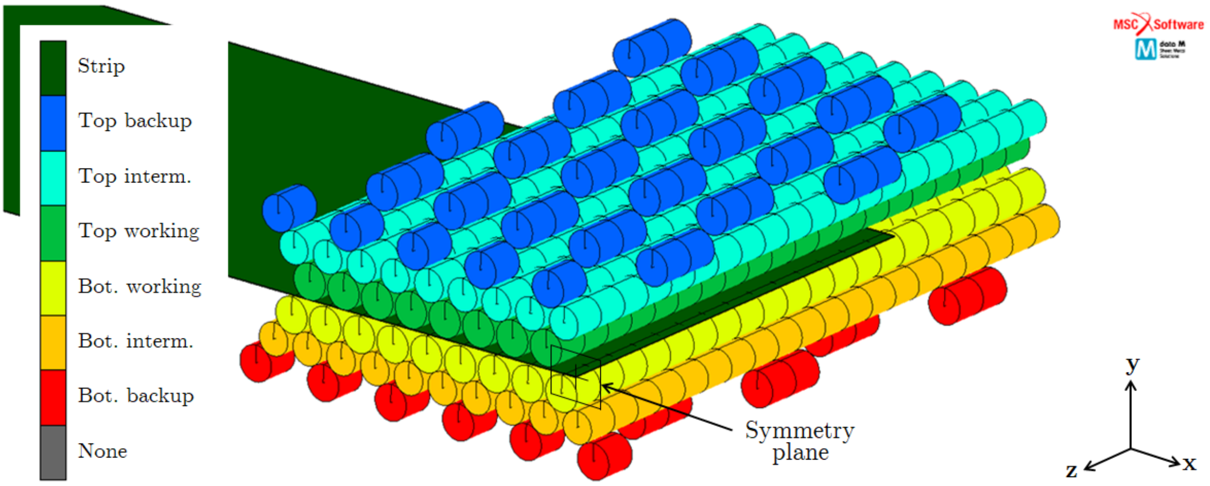

Figure 5.2 – Illustration of the 3D full roll levelling model (symmetric).

From this attempt to perform a simulation with deformable working, intermediate and backup rolls it is possible to conclude that further research on beam elements contact modelling is required. Hereinafter, only the models described in Section 5.2, which are simplified in order to avoid modelling both intermediate and backup rolls, are analysed.

5.3 Rigid rolls

Considering that the three dimensional simulation is expected to require a much higher computation effort (over 60 h) than the 2D roll levelling model presented in the previous chapter (approximately 5-6 h), only two constant discretisations are used: with 2 and 3 elements through thickness, with each element having 5mm in length and 10 mm in width.

When two elements through thickness are used, each one is modelled with the same thickness (0.75 mm). On the contrary, when three elements are modelled, the middle element is 0.3 mm thick and the remaining ones 0.6 mm. The last discretisation is designed in order to enable a plastic strain measurement of ≈80% from the nodal results, rather than just an information on whether the strip is completely plasticised or not, as provided by an analysis with the first mentioned discretisation.

However, if the results' distributions through thickness are analysed in the integration points, an increased resolution over the thickness is possible. The thickness distributions of residual stress (Figure 5.3a) from the analyses with 2 and 3 elements across thickness are similar, indicate that the strip is mostly under compression in the top half and under traction in the bottom half, and exhibit a maximum stress magnitude within the range observed in the 2D analyses. Regarding the distribution of accumulated plastic strain (Figure 5.3b), both models provide a good approximation of the 2D results, displaying 3 distinct areas: a non-plasticised area in the middle of the thickness and two plasticised areas in the top and bottom part of the strip, where the accumulated plastic strain evolves linearly up to a maximum close to strip's surface.

Note that the results plotted in the before-mentioned figures are the average (in width) of results' distributions through thickness and that the horizontal dashed lines illustrate the position of the integration points, both for the simulation with 2 elements over the thickness (on the bottom half of each plot) and the simulation with 3 elements over the thickness (on the top half of each plot).

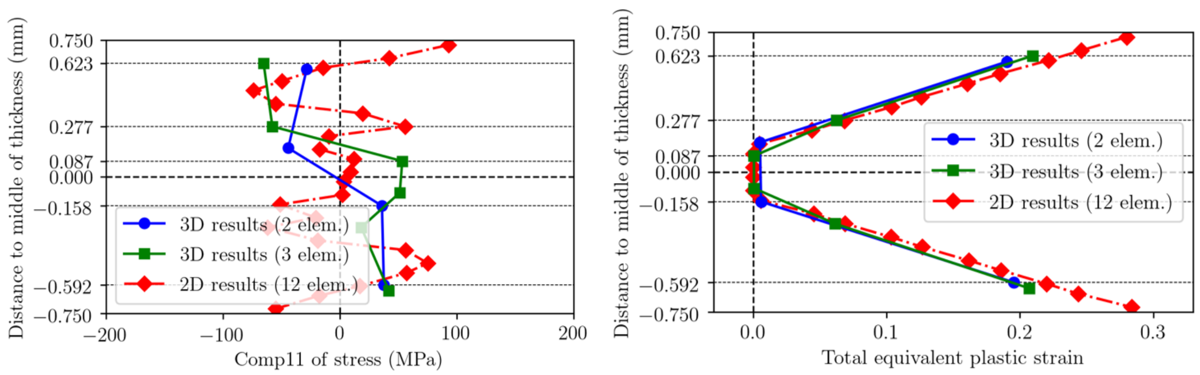

(a) Residual stress. (b) Accumulated plastic strain.

Figure 5.3 – Results thickness distribution after levelling (rigid rolls).[1]

Since a new dimension is under scope during the 3D analyses, it is important to study how the results change across width. Therefore, the results which lead to the average thickness distributions plotted in the previous figures are analysed throughout the width of the strip, as suggested by Figure 5.4.

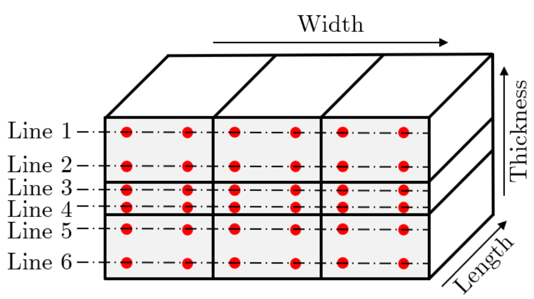

Figure 5.4 – Illustration of results' analysis across width (mesh with 3 elements/thickness).

[1]Results evaluated in the integration points.

Figures 5.5 and 5.6 display the width variation of residual stress and accumulates plastic strain, respectively. Subfigures (a) illustrate the results from the analysis with 2 elements over the thickness and subfigures (b) from the analysis with 3 elements, where each line corresponds to one line of integration points, as suggested in Figure 5.4.

It is observable that the results from both analyses (2 and 3 elements across thickness) are consistent throughout the majority of strip's width. The largest deviation is observed close to the edges of the strip and is more evident in the residual stresses study.

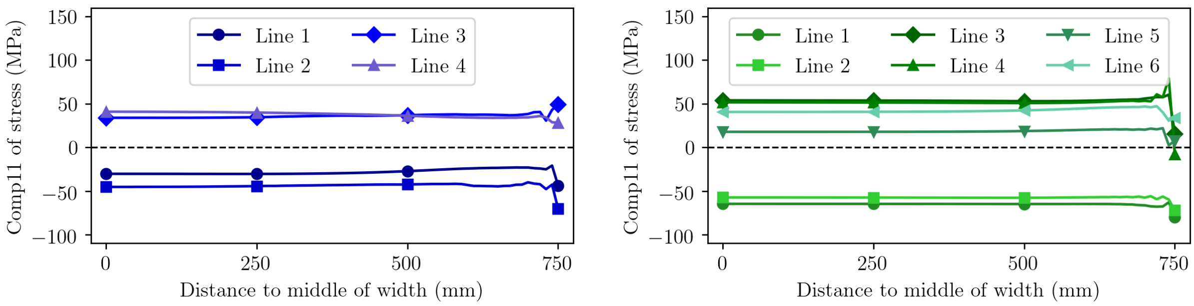

(a) 2 elements/thickness. (b) 3 elements/thickness.

Figure 5.5 – Residual stress width variation after levelling (rigid rolls).[2,3]

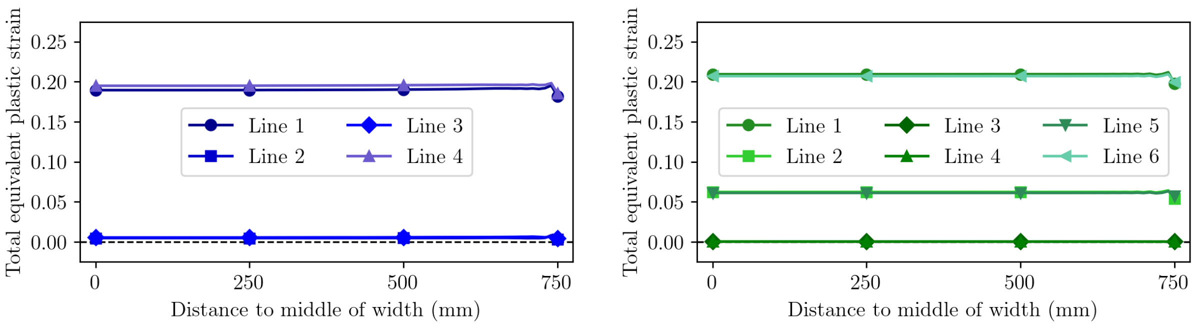

(a) 2 elements/thickness. (b) 3 elements/thickness.

Figure 5.6 – Accumulated plastic strain width variation after levelling (rigid rolls).[2,3]

One can justify the inconsistency of results in the areas closer to the edges due to discontinuity of material. Since the strip has a limited width, it exhibits a different behaviour in the edges (which also occurs in the real roll levelling process). Therefore, the stress and strain levels vary slightly and geometrical deviations are expected in those areas. Consequently, the edge areas should only be analysed when an insight on the defects is desired or when a narrow strip is modelled.

When the final geometry is analysed (Figure 5.7), it becomes very interesting to observe how the three dimensional analysis enables generation of defects in width direction. Despite no rolls' deflection is modelled, the levelled strip exhibits a centre buckle which is induced by the release of residual stresses where the discontinuity of material occurs.

[2] Results evaluated in the integration points.

[3] More data points are analysed than those signed with markers.

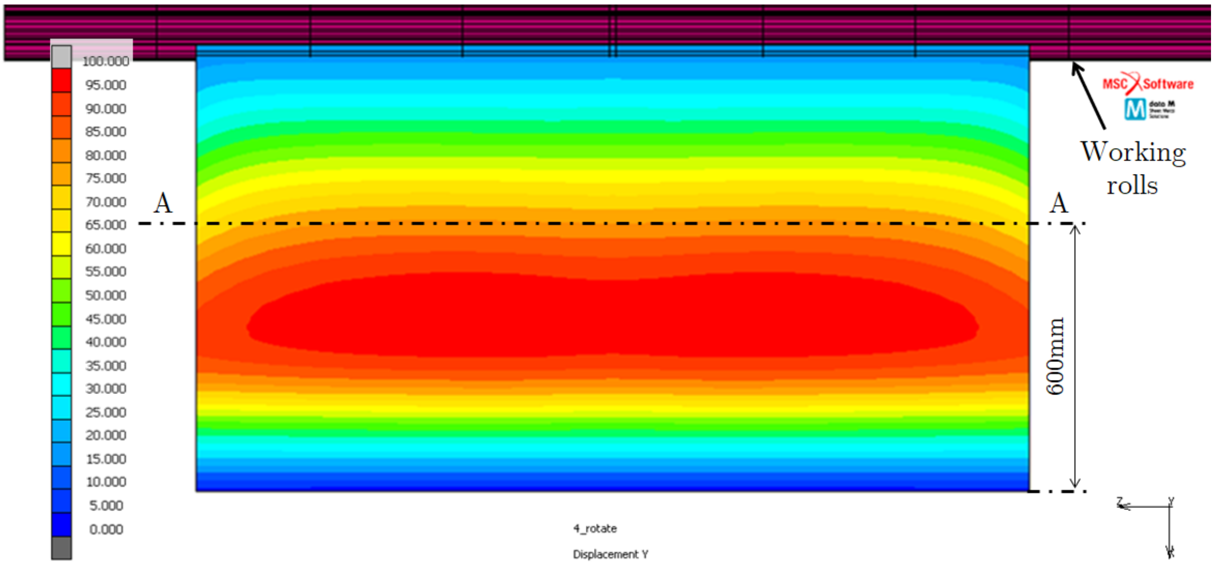

Figure 5.7 – Strip's vertical displacement after levelling (mm). Top view of the analysis with rigid rolls.

By plotting the position of each node from the path indicated in Figure 5.7 (at ≈600 mm from the front end of the strip), it is possible to measure the maximum vertical distances between two nodes. Figure 5.8 illustrate the before-mentioned concept, from where it is possible to conclude that the models with 2 and 3 elements through thickness result on buckles with 2.29 mm and 1.08 mm, respectively. Such buckles correspond to less than 0.16% of strip's width and, therefore, can be neglected. When deflectable rolls are modelled, the buckle magnitude is expected to increase.

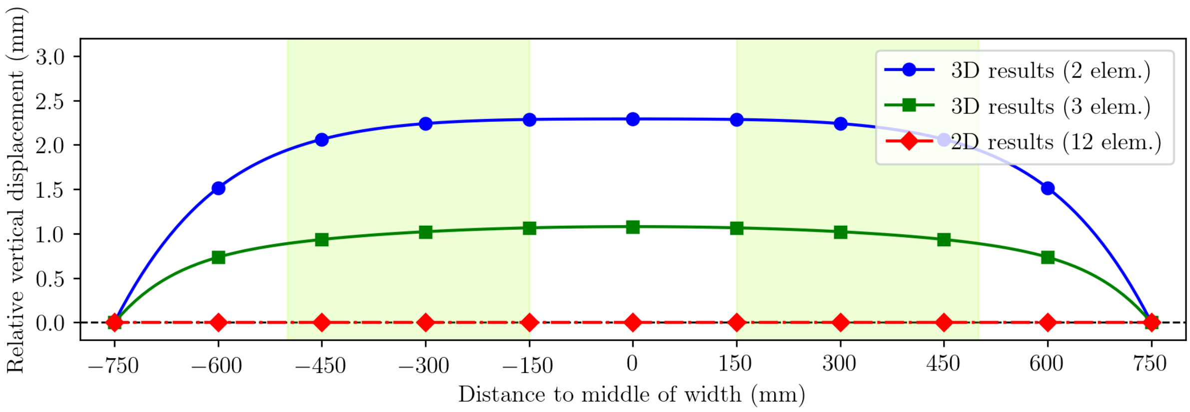

Figure 5.8 – Strip geometry after levelling in width direction (section A-A, from Figure 5.7).[4]

From the analysis with rigid working rolls, it is possible to conclude that a discretization with 3 elements through thickness provides a better insight on the residual stress distribution through thickness. On the other hand, the computation time increases with mesh refinement. Regarding the final geometry, both discretisations provide similar results, considering that the buckle is neglectable. Therefore, at this analysis stage it is not possible to state which discretisation is preferable.

[4]More data points are analysed than those signed with markers.

5.4 Deflectable rolls

In this section, a 3D roll levelling finite element model with deflectable working rolls is analysed with the main purpose of this studying rolls' deflection and its impact on the consistency of results across the width of the strip. By modelling rolls stiffness as mentioned in Section 5.2 and in Appendix B, it is possible to have an in-depth insight on rolls' deflection and the impact on the final properties of the strip.

During the model preparation and analyses execution, two observations are made: modelling deformable rolls represents a strong penalty in the computation time (≈100 h) and establishing contact between beam and solid elements is associated with modelling instabilities. Due to these instabilities, a successful simulation with 3 elements over the thickness was not possible and, therefore, only results from an analysis with 2 elements across thickness are displayed in this section.

By analysing the distributions of results through thickness in the integration points, as proceeded in Section 5.3 where it is also studied how residual stress and accumulated plastic strain results vary in throughout the strip's width after levelling, one can conclude that rolls deflection significantly affects the residual stress distribution (Figure 5.9). On the other hand, no significant impact is observed in the distribution of accumulated plastic strain (Figure 5.10).

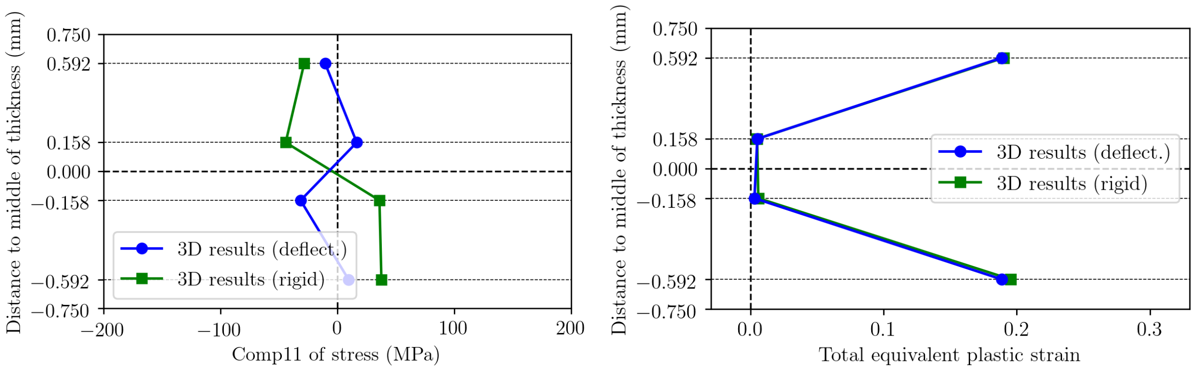

(a) Residual stress. (b) Accumulated plastic strain.

Figure 5.9 – Results thickness distribution after levelling (deformable rolls).[5][6]

When compared to the results from the 2D and 3D FEA with rigid rolls, the average distribution of residual stresses (Figure 5.9a) is very different. This is due to the fact that rolls' deflection leads to buckles in the strip and, consequently, to an alternate tension-compression state at multiple width positions. Nonetheless, the maximum residual stress magnitude is similar to the observed in the analysis with rigid rolls. Regarding the distribution of accumulated plastic strain, rolls' deflection has no impact in the final results.

the results are consistent over the width and no impact of rolls' deflection is observed. Thus, no significant impact on PR measurement is expected.

On the contrary to what was observed in the analysis with rigid rolls, the distribution of residual stress (Figure 5.10a) exhibit an irregular behaviour throughout the full width of the strip, not only in the

[5] Results evaluated in the integration points.

[6] Sub-figure (b) illustrates more data points than those signed with markers.

areas close to the edges of the strip. The fluctuation of results appears to have a frequency related with the distance between backup rolls and suggests that residual stress distribution is very sensitive to rolls' deflection. On the other hand, the accumulated plastic strain is approximately constant across the full width of the strip and, thus, rolls' deflection has no significant impact on plastic rate (PR) measurement.

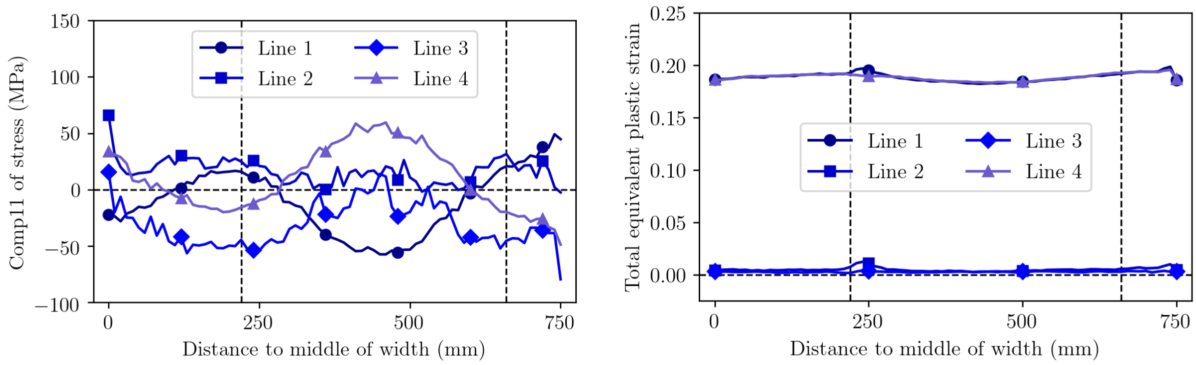

(a) Residual stress. (b) Accumulated plastic strain.

Figure 5.10 – Results width variation after levelling (deflectable rolls).[7][8]

When the final geometry of the strip is observed (Figure 5.11), it becomes clear that the strip exhibits several buckles, as predicted during the residual stresses analysis. Figure 5.12 illustrates the vertical position of a node path in a cross section located at 600 mm from the front end of the strip, as suggested in the following figure.

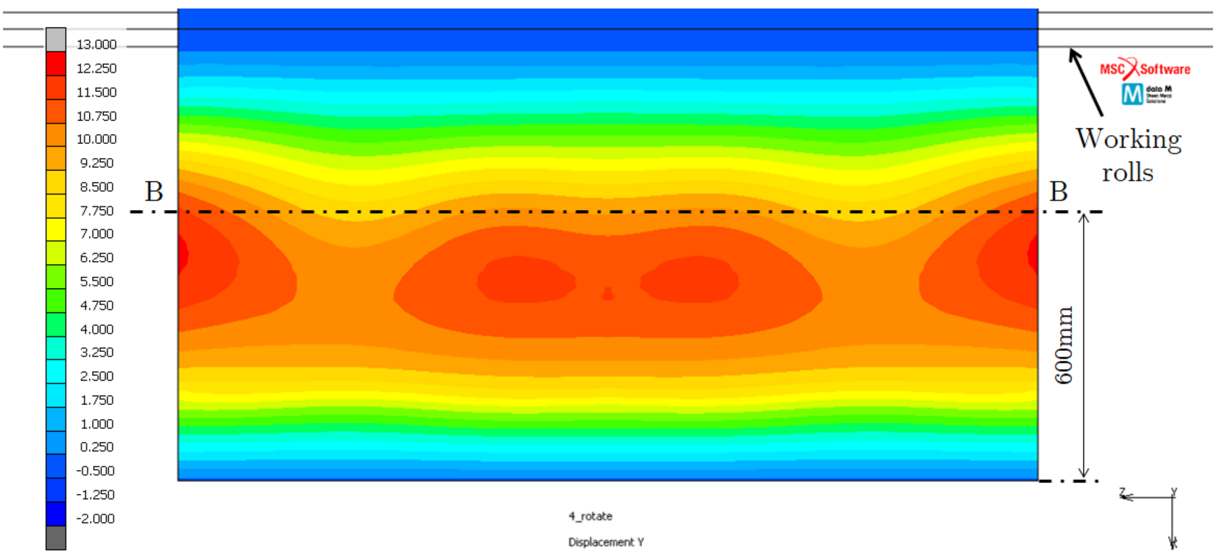

Figure 5.11 – Strip's vertical displacement after levelling (mm). Top view of the analysis with deflectable rolls.

Since the working rolls deflect between two consecutive backup rolls (which positions are identified by dashed lines in Figure 5.12), the levelled strip displays one buckle between each pair of backup rolls.

[7] Results evaluated in the integration points.
[8] Sub-figure (b) illustrates more data points than those signed with markers.

The largest buckle is characterised by a maximum vertical variation of 2.54 mm, which is less than 0.17% of strip's width and, therefore, is not significant. It also becomes interesting to confirm if the buckles are consistent with rolls' deflection.

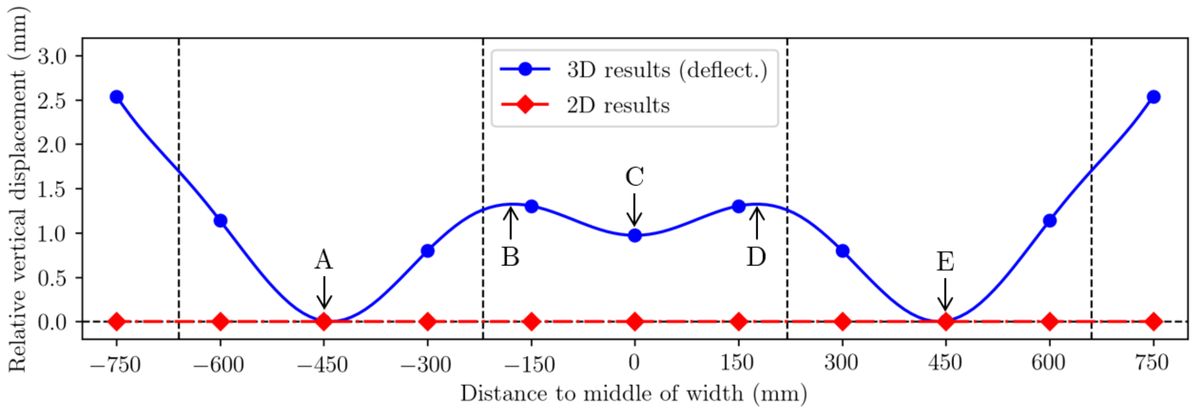

Figure 5.12 – Strip geometry after levelling in width direction (section B-B, from Figure 5.11).[9]

According the previous figure, the IU definition is applied to two segments of the strip: B-D and A-E, considering that points A, B, C, D and E are local maximums. Each segment is approximated by a sinusoidal wave characterized by the following length and height (l_{wave} and h_{wave}, respectively):

$$\begin{cases} h_{wave,BD} = y_B - y_C = 0.356\,mm \\ l_{wave,BD} = x_D - x_B = 360\,mm \end{cases} \quad \text{and} \quad \begin{cases} h_{wave,AE} = y_B - y_A = 0.356\,mm \\ l_{wave,AE} = x_E - x_A = 360\,mm \end{cases} \tag{5.1}$$

, where x_i is the width position and y_i the relative vertical displacement of point i, $i \in \{A,B,C,D,E\}$.

If the International Unit (IU) definition of flatness (Equation 2.2) is applied to the transverse buckles observed in Figure 5.12, it is possible to compare the levelling quality of the simulated process with common IU values from real shape control processes. Therefore, the IU-value is calculated as follows:

$$IU = \left(\frac{\pi}{2} \cdot \frac{h_{wave}}{l_{wave}}\right)^2 \cdot 10^5 \quad \Rightarrow \quad \begin{cases} IU_{BD} \approx 0.24 \\ IU_{AE} \approx 0.56 \end{cases} \tag{5.2}$$

According to Theis (2002b), common roll levellers enable a minimum IU-value (i.e. maximum flatness) of 5 IU. Therefore, it is possible to confirm that the roll levelling finite element model analysed throughout this work results in a flatter strip than expected in the real roll levelling process. However, if complex initial defects are induced in the strip, the final IU-value is expected to increase.

In the 2D analysis it is observed that the third roll is the one with the highest load and, therefore, the one which deflects the most. By analysing the equilibrium position of the nodes from each working roll, it is possible to plot rolls' relative vertical and horizontal displacement, illustrated in Figures 5.13a and 5.13b, respectively.

[9] More data points are analysed than those signed with markers.

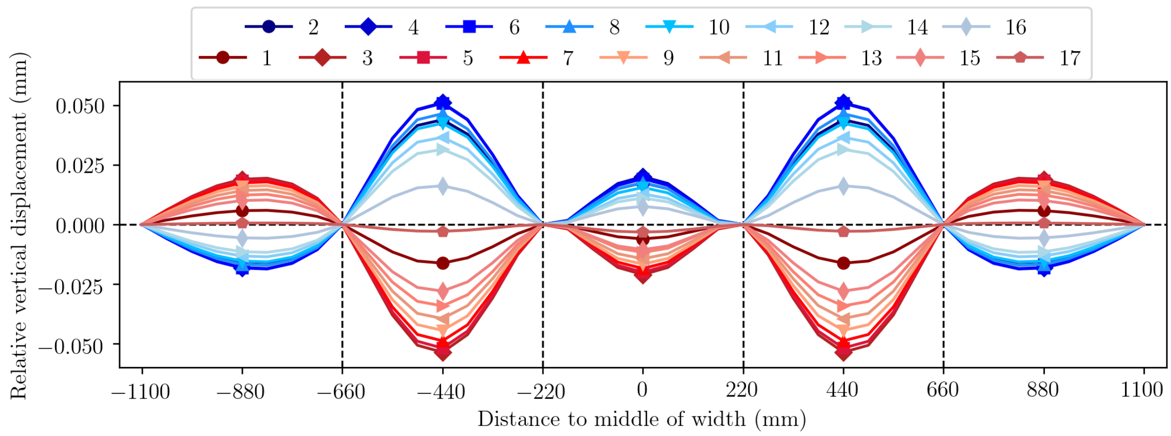

(a) Vertical displacement.

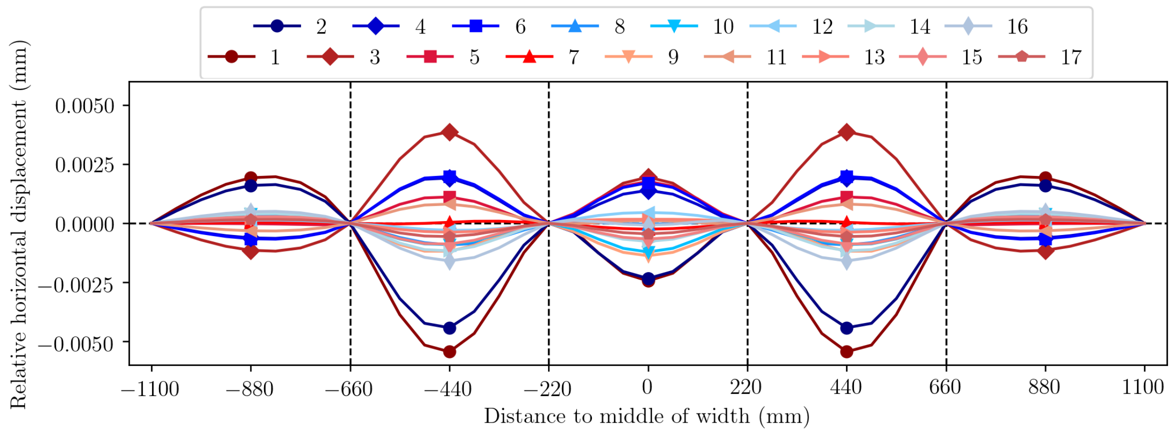

(b) Horizontal displacement.

Figure 5.13 – Working rolls' deflection.[10]

The vertical displacement of the bottom working rolls (identified in Figure 5.13a by odd numbers and hot colours) is concluded to be mostly negative and the one from the top working rolls (identified in Figure 5.13a by even numbers and cold colours) to be mostly positive. This means that the gap between rolls is not constant through width, as it increases locally. Also, it is confirmed that the 3rd working roll deflects the most (0.054 mm) and that strip's buckling frequency is correlated with rolls' deflected shape.

Regarding the horizontal component of deflection (Figure 5.13b), it displays a similar behaviour as the vertical component. The main distinction between both components of deflection is their amplitude, being the horizontal component the one which exhibits smaller values (maximum displacement of 0.005 mm, in the first working roll). Another difference is that it is not possible to correlate the position of the rolls (top/bottom set of rolls) with the horizontal deflection direction (positive/negative).

During this study, the thickness of the strip is also analysed (Figure 5.14) and a maximum variation of approximately 0.001 mm is measured. Considering that such variation corresponds to less than 0.1% of the initial thickness, one can consider that the strip thickness remains constant after roll levelling and is not influenced by working rolls' deflection.

[10]More data points are analysed than those signed with markers.

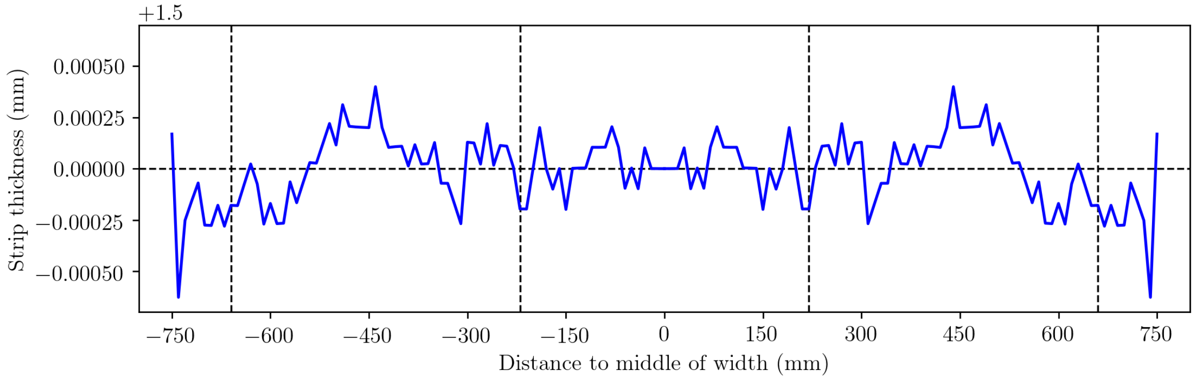

Figure 5.14 – Strip thickness measured in multiple positions across width.[11]

On the contrary to what was expected, the buckles remain insignificant. Therefore, considering that the maximum deflection is only 3% of the entry gap value, rolls' deflection may also be neglected in this 3D roll levelling model. Nonetheless, it is interesting to observe that the number of buckles and their magnitude is related with the number of backup rolls, as few backup rolls lead to a reduced number of higher magnitude buckles and *vice versa*. Therefore, for larger distances between backup rolls it may become important to take into account rolls' deflection.

5.5 Conclusions

From the 3D roll levelling finite element modelling study performed in this chapter, some conclusions are drawn and taken into account throughout the remaining work.

The first conclusions concern the computation time required to perform a three dimensional roll levelling finite element analysis. It is observed that the 3D approach is much more time consuming than the 2D alternative and, therefore, the thickness resolution is penalised so that a feasible computation time is achieved. Nonetheless, modelling the levelling process of a 1500 mm wide strip with 3 layers of elements over the thickness may represent a penalty of over 1000% on the CPU time, when compared to a feasible 2D model. This is a strong motivation to prefer a 2D roll levelling finite element analysis whenever it is possible.

Regarding the final geometry of the strip, in a 3D roll levelling analysis the strip exhibits not only longitudinal but also transverse curvatures, due to the fact that no plane strain condition is assumed in the 3D model. Such curvatures are shape defects, referred as "buckles", and are induced by inconstant stress levels across strip's width, which may be caused by two different reasons: a discontinuity of material (and consequent release of stresses, as observed in the edges) or working rolls' deflection.

Considering that no relevant shape defects are observed for the machine settings analysed during this chapter, it is concluded that rolls' deflection has no significant impact on the final geometry of the strip when a 2D or 3D roll levelling finite element analysis is performed.

[11] More data points are analysed than those signed with markers.

On the other hand, when it comes to the distribution of results across width, it is observed that the residual stresses vary significantly. On the contrary, the accumulated plastic strain is approximately constant throughout the width. When deflectable rolls are modelled, the distribution of residual stresses becomes significantly more irregular across strip's width. As a consequence, it is interesting to understand and quantify the impact of such irregularity on subsequent process simulations. This research question is expected to be most relevant for wide strips (e.g. 1500 mm wide), due to a poorer structural performance of wide levelling equipments.

As mentioned before, levelling rolls' deflection leads to a more irregular distribution of residual stresses across strip's width. However, only rigid rolls are modelled during the next chapter of this work, considering that a narrow strip ($\approx$200 mm wide) is analysed and, as consequence, the levelling equipment is expected to behave stiffer.

From the finite element modelling of deflectable rolls, it is also concluded that beam elements represent a good solution to model deflectable rolls. The downside of this approach is that it is associated with modelling instabilities and a small step size is required so that contact is established between the working rolls and the strip (i.e. beam and solid elements). Difficulties are also found in modelling radial contact between two beam elements and, therefore, an in depth study on beam elements contact modelling is valuable.

Chapter 6

Integration with roll forming FEA

In order to achieve the ultimate objective of this dissertation, a single three dimensional finite element model of roll levelling and roll forming is developed and analysed during this chapter. In a first instance, an appropriate mesh is developed with the goal of providing a compromise solution between results' resolution and computation time. Then, two "U"-shaped profiles are roll formed in DP1000 steel. One profile is formed from an ideal strip (standard roll forming FEA) and the other from a strip which is previously levelled. Both profiles are compared and a search on the impact of roll levelling in roll forming simulations is proceeded. Finally, a time-saving alternative approach to the exclusively 3D roll levelling and roll forming analysis is suggested: a 2D-to-3D mapping, where the pre-process is studied in 2D and its results assigned to a the workpiece of a standard 3D roll forming FEA.

6.1 Initial considerations

For this study, a new finite element model is developed. However, some conclusions from the previous sections are assumed to be valid for this model. Other modelling inputs are considered, taking into account the expertise of data M on roll forming FEA.

- The roll levelling machine settings are the same as in most of the 2D and 3D analyses: g_{in}=-2.77 mm and g_{out}=1.23 mm;
- The roll forming line is designed to produce a symmetric "U"-shaped profile from a strip with 97.19 mm width, which forming flower is illustrated in Figure 6.2;
- A locally refined mesh can be adjusted to provide a feasible compromise solution between thickness resolution and CPU time;
- The mesh should also be valid for roll forming, with a particular focus on the width discretisation of the bending zones;
- DP1000 steel is modelled with a constant Young's modulus of 210 GPa and Chaboche-Lemaitre combined hardening law, characterised in Section 3.3.3;
- Both the roll levelling and roll forming rolls are modelled as rigid bodies;

- Gravity acceleration is neglected;
- No coil set defects is taken into account.

6.2 Geometry and boundary conditions

As mentioned before, the finite element model under scope in this chapter comprises two processes: roll levelling and roll forming (Figure 6.1). The roll levelling part of the model has the same geometry and boundary conditions as explained in Section 5.2.

Regarding the roll forming model, it is a line with six stations displaced every 120 mm, which forms the strip according to the flower illustrated in Figure 6.2. On the contrary to roll levelling, when being roll formed the strip movement is induced by a continuous displacement of the front end. Therefore, no friction is modelled between the strip and the roll forming rolls.

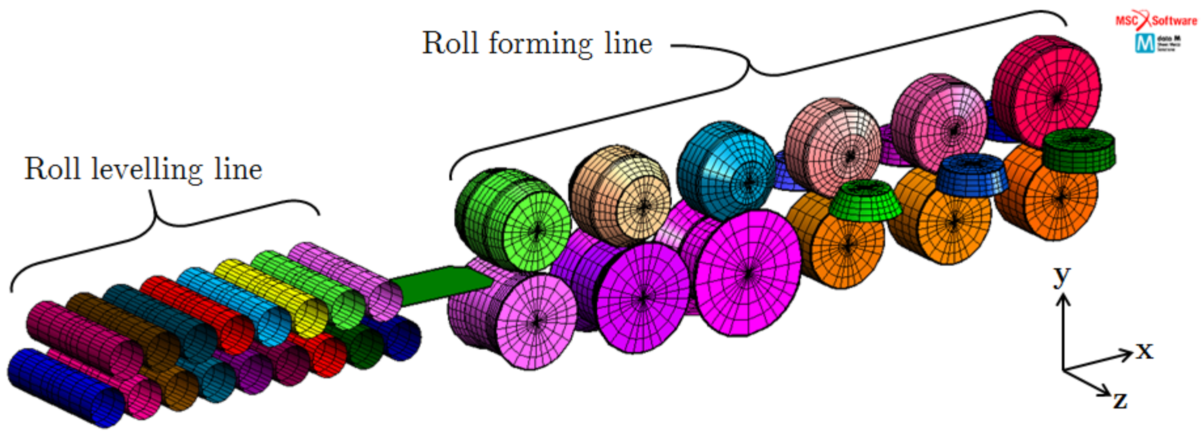

Figure 6.1 – Combined roll levelling and roll forming FE model.

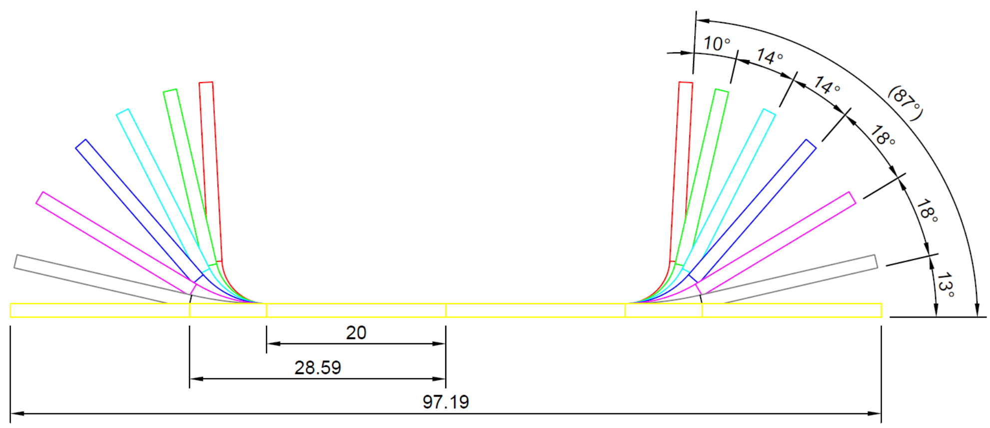

Figure 6.2 – Roll forming flower (dimensions in mm).

6.3 Mesh

In this chapter, a locally refined mesh with 1-to-3 elements through thickness is applied, in order to fit both roll levelling and roll forming process simulations.

From the thickness distribution of residual stress and accumulated plastic strain, observed during the 2D analyses and as proceeded in Chapter 5, the fine area has 3 elements across the thickness which have different thicknesses. The middle element is 0.3 mm thick and the outer elements 0.6 mm.

Knowing that a "U" profile is roll formed, the discretisation should also be designed in width direction by taking into account the position of the bending zone. From the forming flower (Figure 6.2), one knows that the before mentioned zone extends from 20.00 mm to 28.59 mm from the centre of the strip and, therefore, the mesh is adjusted to these locations. Another requirement for roll forming FEA is that a chamfer should be assigned to the front end of the strip.

As consequence, the strip is locally refined in width direction (section A) in order to fulfil the width discretisation requirements for the roll forming analysis. Also a chamfer is incorporated in the front end of this section. Within section A, another local refinement takes place. This last mesh (Section B) has 3 elements through thickness and a length of 165 mm, as suggested by Figure 6.4. The length of Section B was designed to be approximately 1.4× the distance between roll forming stations (120mm), in order to provide a smooth transition between consecutive stations and according to dataM's expertise. Figure 6.3 illustrates the top view of the strip analysed during different simulation stages, as both ends of the strip are neglected after each process.

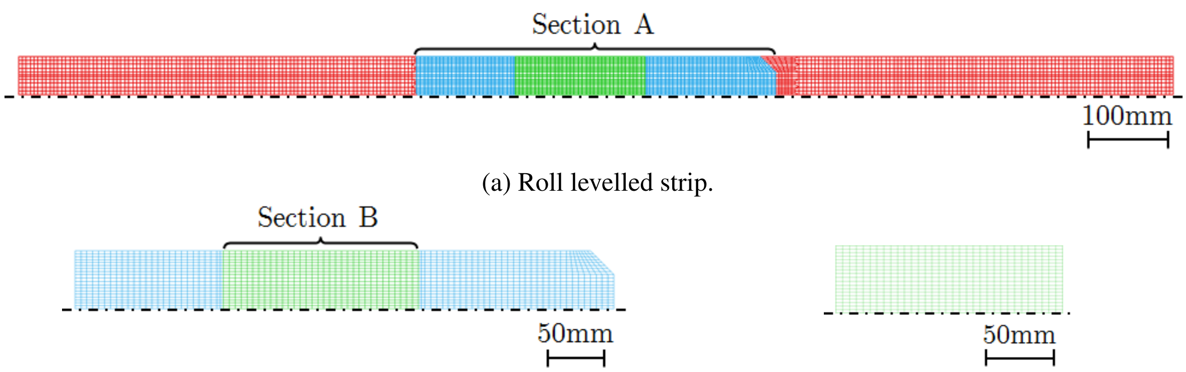

(a) Roll levelled strip.

(b) Roll formed strip (section B).

(c) Final strip (section A).

Figure 6.3 – Strip at different analysis stages (top view).

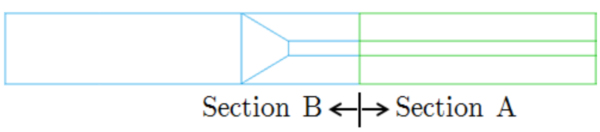

Figure 6.4 – Mesh transition from 1-to-3 elements (side view).

6.4 Results under scope

Considering that roll levelling pre-process is applied in real production lines to minimise unexpected shape defects after forming due to a poor consistency of the incoming material, shape defects such as springback, end-flare, transverse bow, longitudinal bow and twisting are analysed in this chapter. Some of these defects are mentioned in Section 2.1.

The most common shape defect is springback. It is the elastic recovery of the material and is associated with every forming process. Particularly for the "U"-profile under scope, the springback is assessed as the variation of the angle between the web and leg of the profile when it exits the last set of rolls, as illustrated in Figure 6.5a

If the springback is assessed before and after the front and rear ends of the strip are cut, an insight on the end-flare effect (Figure 6.5b) is possible. This phenomena is expected to be reflected in a springback reduction in the front end and a springback increase in the rear end of the strip.

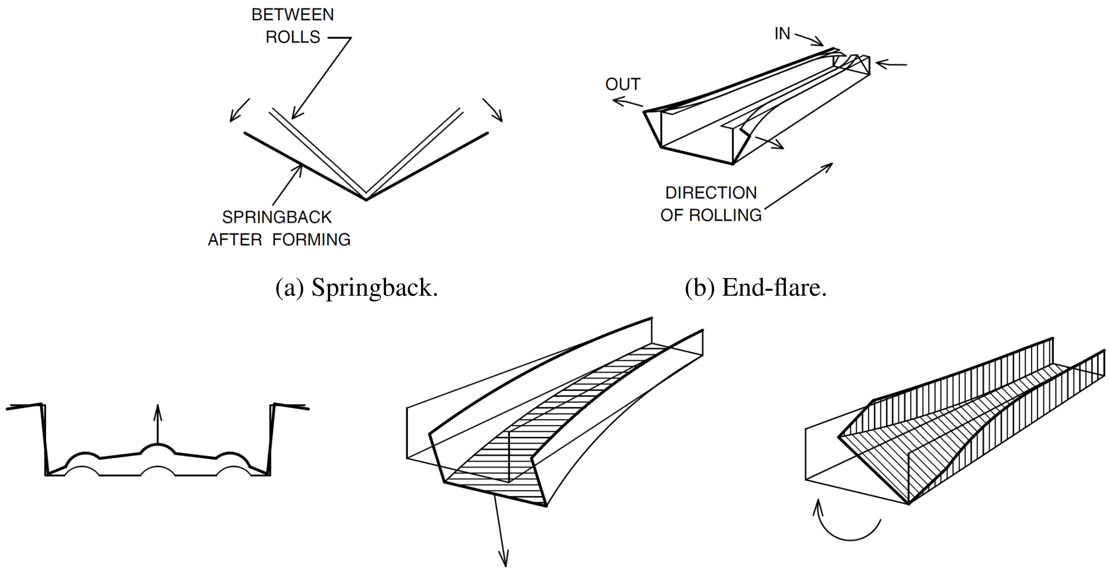

(a) Springback. (b) End-flare.

(c) Transverse bow. (d) Longitudinal bow. (e) Twisting.

Figure 6.5 – Illustration of multiple shape defects (Halmos, 2005).

Also the transverse and longitudinal bows (Figures 6.5c and 6.5d, respectively) are evaluated. The bows consist on the curvature of profile's web and are quantified as the relative vertical displacement of each node across the width (or length) of the strip.

The last shape defect under scope is twisting (Figure 6.5e). It is the relative rotation of the profile in rolling direction and is analysed by comparing the angle between the web and the reference coordinate system of multiple cross-sections of the profile.

Additionally to the geometrical analysis, a search for the impact of roll levelling pre-process in the distributions of residual stress and accumulated plastic strain in the final profile is performed.

6.5 Results analysis

In this section, the integrated finite element analysis of roll levelling (RL) and roll forming (RF) is compared with a standard roll forming FEA. Table 6.1 resumes the computation time of the before mentioned simulations, in which all process and simulation variable are used consistently.

In addition to the CPU time, Table 6.1 also resumes the average springback before and after cutting the ends of the profile, the maximum longitudinal and transverse bow and the maximum twist angle.

Table 6.1 – Simulations proceeded during the study of integrated roll levelling and roll forming FEA.

RL	RF	CPU time (h)	Springback before cutting (°)	Springback after cutting (°)	Longitudinal bow (mm)	Transverse bow (mm)	Twisting (°)
Yes	Yes	13.3	3.37[a]	3.82[a]	0.06[b]	0.10[b]	0.20[b]
No	Yes	1.8	3.85[a]	4.31[a]	0.08[b]	0.02[b]	0.25[b]

[a] Average springback value throughout the full length of the profile.
[b] Maximum value after cutting in the profile.

From the previous table, two immediate observations are possible: implementing roll levelling in a roll forming simulation leads to a significant increase of the computation time (by a factor of ≈7.5) and a reduction of ≈0.5° on the average springback. However, if the geometrical results are analysed on detail, further observations are possible.

From the analysis of the bent angle in multiple cross-sections along the profile length (Figure 6.6), it is observable that the springback varies significantly at the ends of the profile when the ends are cutted. Before cutting, the springback in the rear end of the profile (length of 0 mm) is below the average and increases up to a maximum value in the front end (length of 165 mm). However, when both ends are cutted, the springback increases significantly in the rear end of the profile (4-5 mm), remains approximately constant in the middle of the profile and reduces in the front end. This phenomena is known as end-flare and is induced by the release of residual stresses in the free-ends.

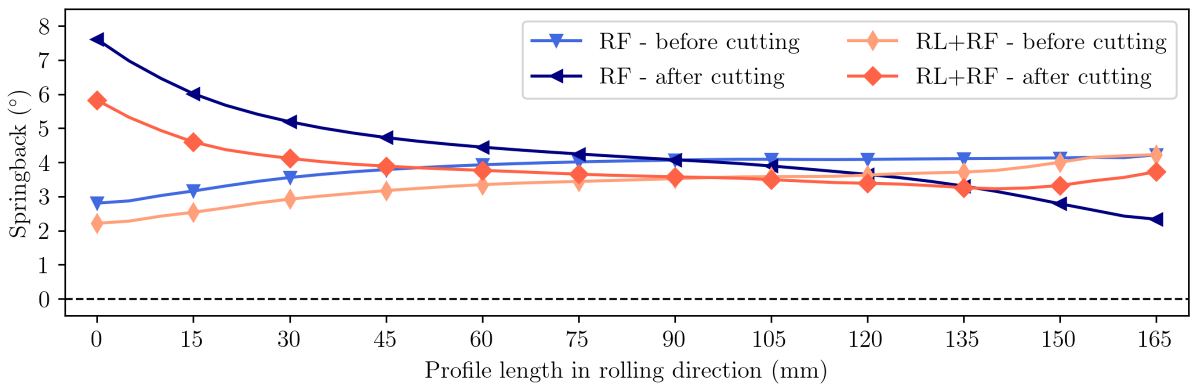

Figure 6.6 – Profile geometry after roll forming (springback).[1]

[1] More data points are analysed than those signed with markers.

Therefore, it is possible to conclude that both the springback and end-flare are relevant in this roll forming process, however the roll levelling pre-process enables the reduction of ≈0.5° on the average springback and soften the end-flare effect.

At the end, roll levelling contributes to an improvement of ≈1.8° on the maximum angular deviation of the bend angle, as can be observed in Figure 6.7 where multiple cross-sections of the profile are displayed and both models are compared. This figure also corroborates that the springback is maximum in the rear end of the profile and reduces up to a minimum value in the front end of the profile, whether roll levelling is considered or not.

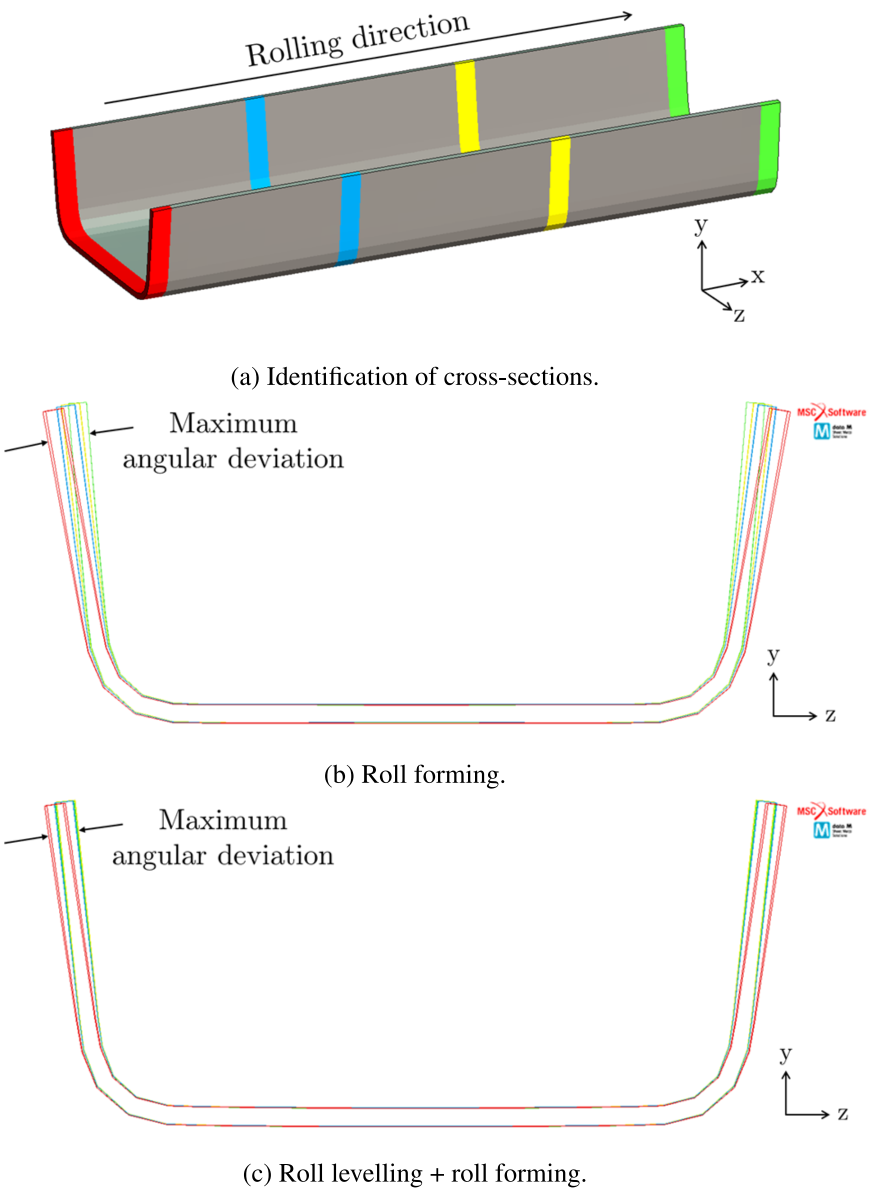

(a) Identification of cross-sections.

(b) Roll forming.

(c) Roll levelling + roll forming.

Figure 6.7 – Profile geometry in different cross-sections after cutting (front view).

Finally, considering the springback, end-flare and twisting reductions enabled by the roll levelling pre-process, the edge wave effect is also expected to be attenuated during the combined FEA.

Regarding the longitudinal bow in the web of the profile (Figure 6.8a), no explicit impact of roll levelling is observed. Also, the longitudinal bow is so small ($\leq$0.01% of the profile length) that can be neglected.

On the contrary, a significant impact on the transverse bow (Figure 6.8b) is noticed when a combined roll levelling and roll forming FEA is performed, as the bow increases by a factor of 5. Nonetheless, the maximum transverse bow corresponds to 0.25% of the width of the web and 6.67% of strip's thickness. Thus, depending on the tolerances required, roll levelling negative impact on the transverse bow may be irrelevant for the roll forming analysis.

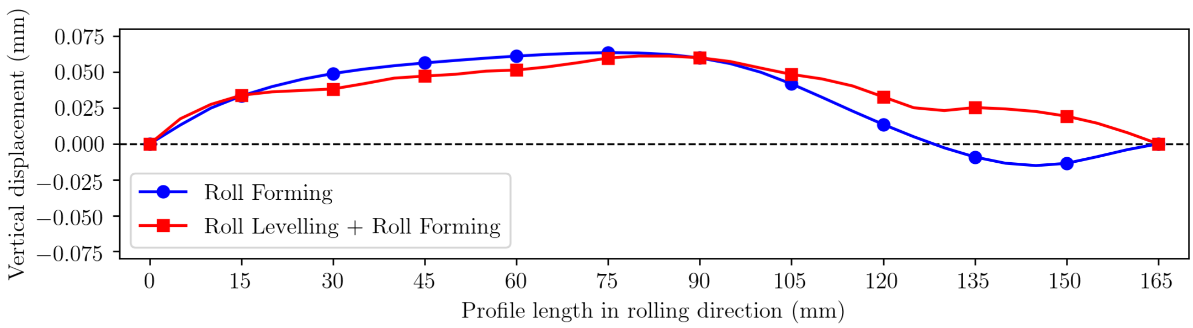

(a) Longitudinal bow.[2]

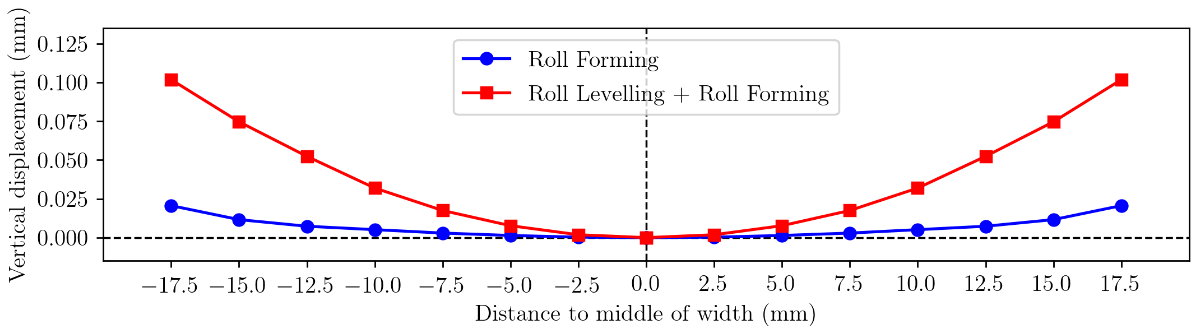

(b) Transverse bow.

Figure 6.8 – Profile geometry after roll forming (bow in the web).

In order to search for any other effect roll levelling may have in the roll formed profile, hereinafter the analysis focus goes to the stress and strain state before, during and after roll forming.

Following the same procedure as in the 2D and 3D roll levelling analyses, Figures 6.9 and 6.10 represent the average distribution across thickness of residual stress and accumulated plastic strain distributions, respectively. Partial average results are also displayed, in order to enable a better insight on the thickness distribution of results in the leg, bend and web areas of the "U"-profile. Considering that the resolution through thickness is very limited, the results are evaluated in the integration points.

[2]More data points are analysed than those signed with markers.

As one might expect, the highest stress levels are longitudinal and in the bend area. The shear components of stress are not displayed, since their magnitude is irrelevant when compared to the normal components (component 11 (longitudinal), component 22 (transverse in thickness direction) and component 33 (transverse in width direction)). These observations are valid whether a roll levelling pre-process FEA is performed or not (Figures 6.9a and 6.9b, respectively). The only difference observed is a small increase in stress magnitude when a combined analysis is executed, due to the pre-stress induced during roll levelling.

Therefore, according to the average thickness results, roll levelling has a small impact on the residual stress distribution of a roll formed profile, when compared to a standard roll forming FEA. However, it is important to mention that roll levelling pre-process is expected to have a significant impact in reducing the magnitude of residual stress in a roll formed profile, when initial defects are present in the strip.

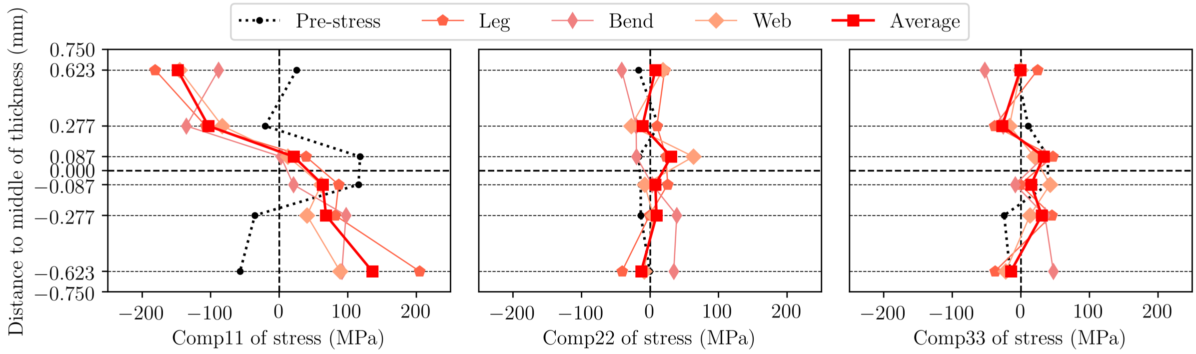

(a) Roll levelling and roll forming.

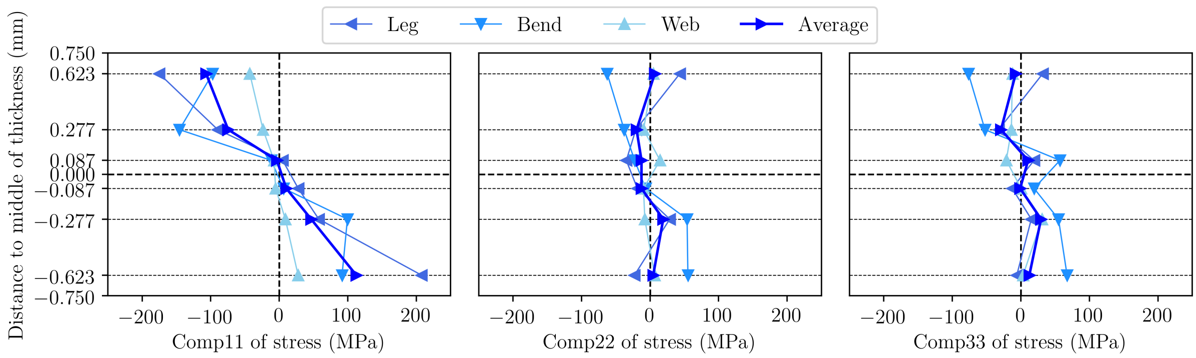

(b) Roll forming.

Figure 6.9 – Residual stress distribution through thickness in the roll formed profile.[3]

On the contrary to what is observed in the stress distribution analysis, roll levelling plays a important role in the final distribution of accumulated plastic strain across thickness (Figure 6.10). When the strip is levelled, it reaches a maximum plastification of $\geq 25\%$ in the superficial fibres. Despite this pre-strain, the plastic strain accumulated during the roll forming process is similar between both simulations, displaying a maximum value in the bend area.

[3]Results evaluated in the integration points.

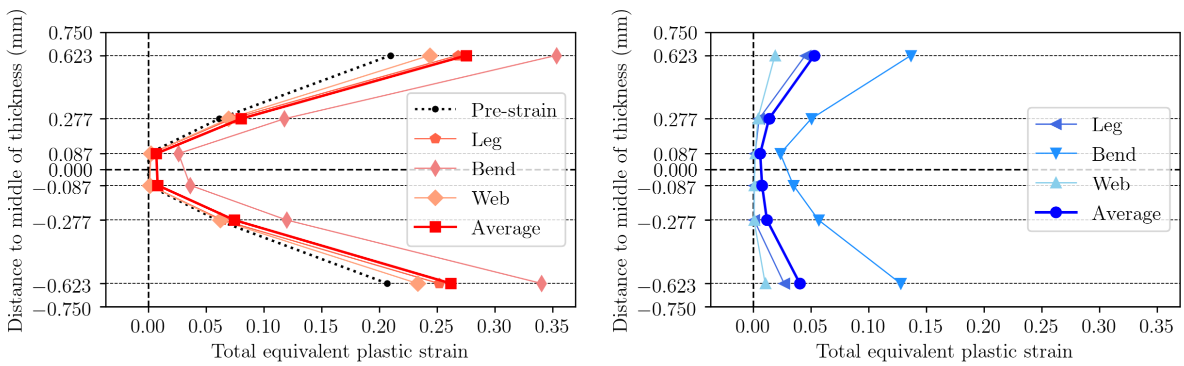

(a) Roll levelling and roll forming.

(b) Roll forming.

Figure 6.10 – Accumulated plastic strain distribution through thickness in the roll formed profile.[4]

If an exterior node from each area of the profile (edge, leg, bend and web) is selected and its total equivalent plastic strain evaluated throughout the roll forming process, it is possible to corroborate some previously stated remarks. From 6.11 it is easily noticeable that a plastification offset is induced during roll levelling, the accumulation of plastic strain during roll forming is consistent between both models, and that the bending area is the most plasticised.

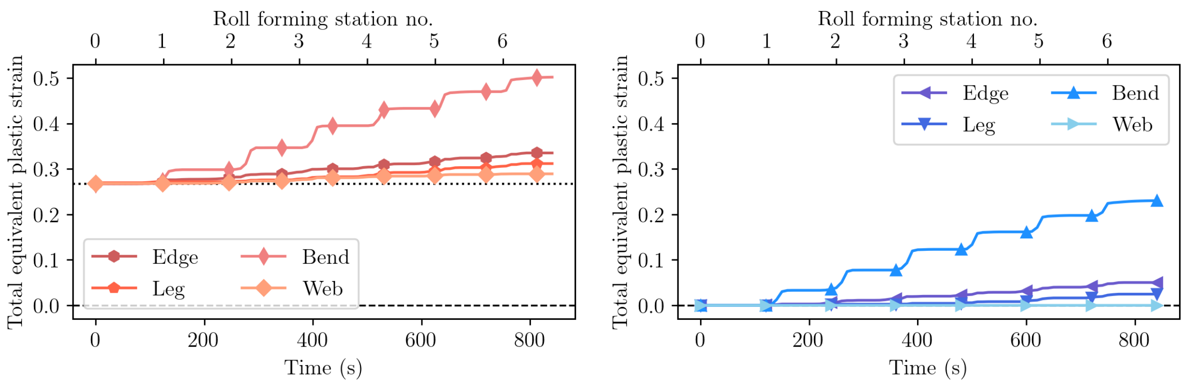

(a) Roll levelling and roll forming.

(b) Roll forming.

Figure 6.11 – Plastic strain accumulation throughout the roll forming process.[5]

Instead of assessing the average residual stress and accumulated plastic strain, if one focus on a general analysis of the roll formed profile it is possible to have a different perspective on the impact roll levelling pre-process has on a roll forming FEA.

Figures 6.12a and 6.12b display the longitudinal component of residual stress in the "U"-profile after a roll forming simulation with and without roll levelling pre-process, respectively. Despite both simulations leading similar average thickness distributions of residual stress, overall roll levelling is observed to have a positive impact in reducing the stress magnitude and homogenise its distribution. This effect is mostly noticeable in the exterior surface of the leg of the profile.

[4]Results evaluated in the integration points.

[5]More data points are analysed than those signed with markers.

This study complements the analysis of the average thickness distribution of residual stress (illustrated in Figure 6.9), since it enables the expected conclusion that roll levelling reduces and homogenises the thickness distribution of residual stress.

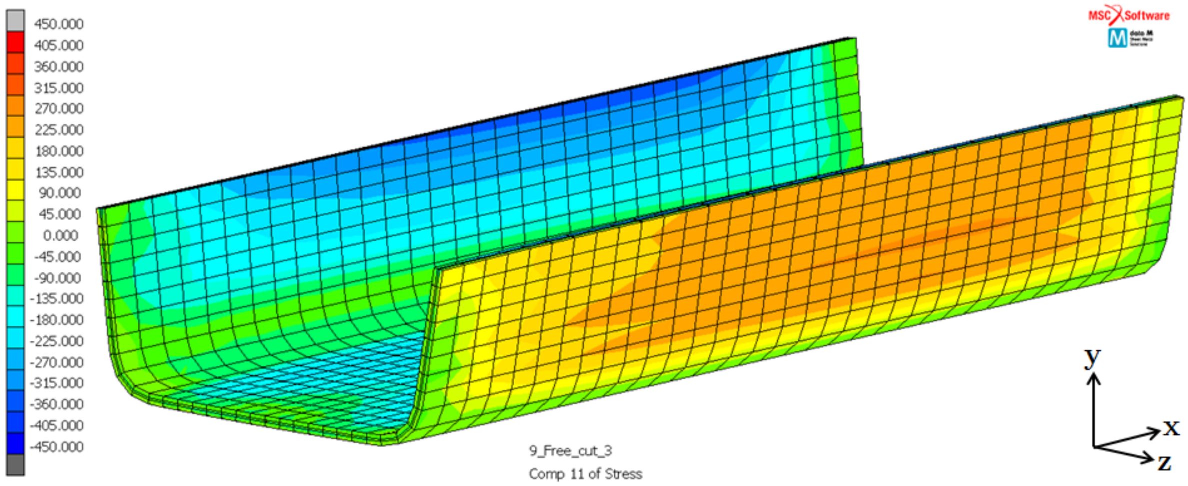

(a) Roll levelling and roll forming.

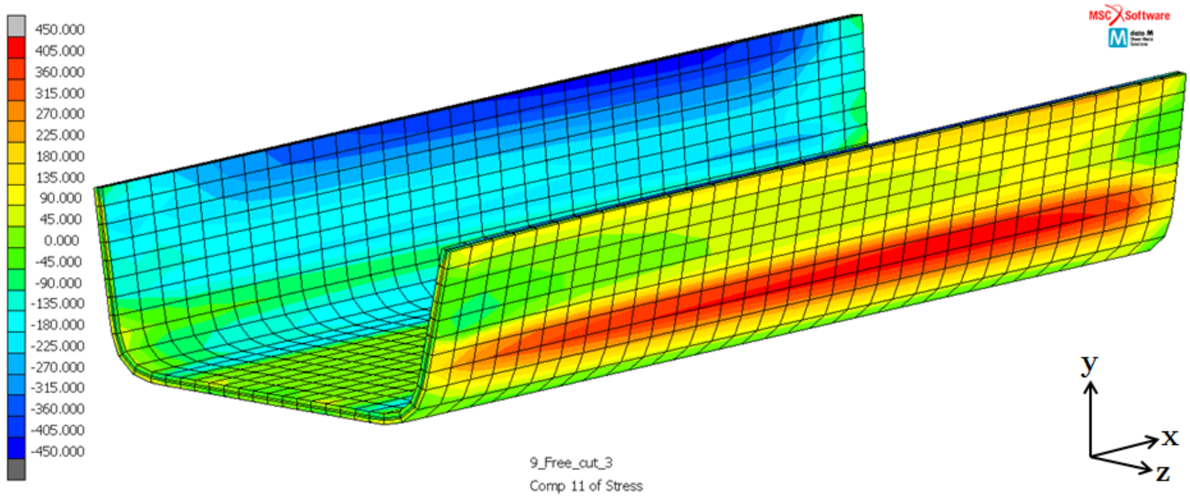

(b) Roll forming.

Figure 6.12 – Residual stress in the roll formed profile (values in MPa).

When the accumulated plastic strain is analysed throughout the roll formed profile (Figure 6.13), it is observed that it is consistent not only throughout the length of the profile but also throughout its width, except in the bending area where more plastic strain is accumulated. Roll levelling pre-process is found to lead to the increase of the amount of plastic strain accumulated close to the inner and outer surfaces of the strip. Regardless of considering roll levelling or not, the centre of the strip is never plasticised.

All this observations corroborate what was stated previously when the average thickness distribution of accumulated plastic strain was analysed in Figure 6.10.

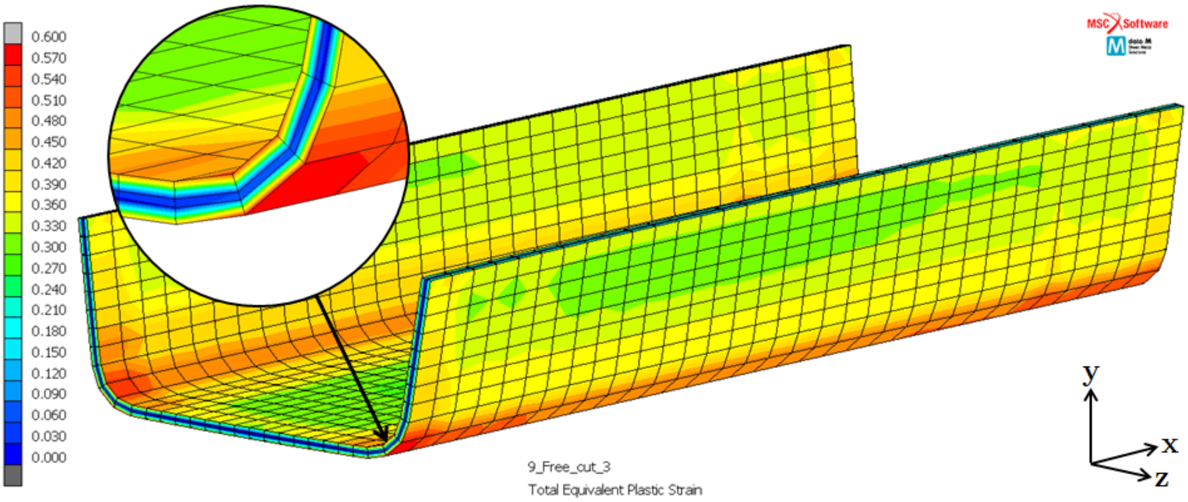

(a) Roll levelling and roll forming.

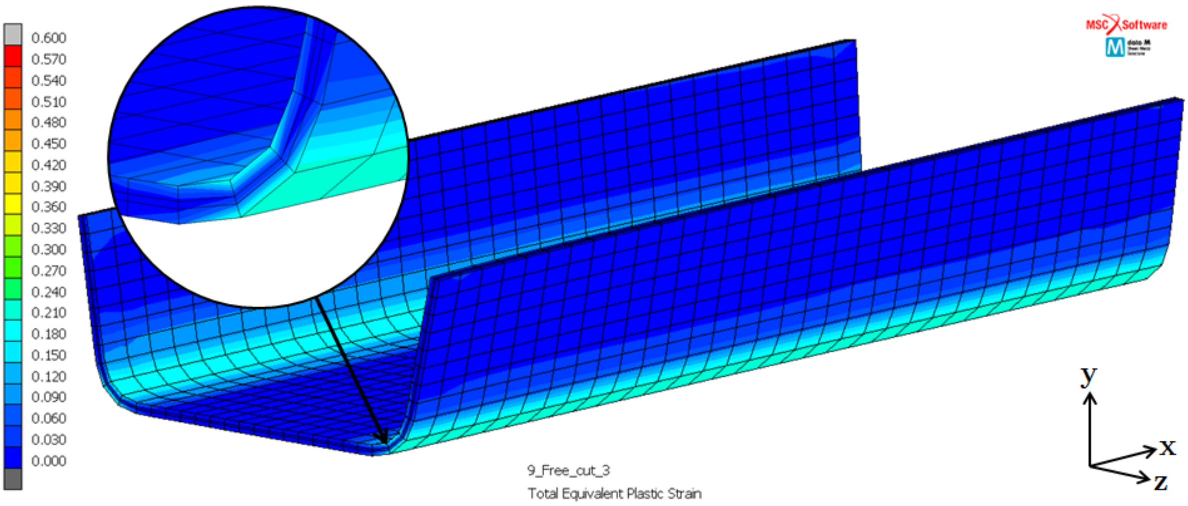

(b) Roll forming.

Figure 6.13 – Accumulated plastic strain in the roll formed profile.

6.6 Alternative approach (2D-to-3D)

Since the standard roll forming FEA are executed in three dimensions, the integration of the roll levelling pre-process is first suggested to be performed in a single 3D analysis. However, as mentioned before, such combined study is very time costly and, therefore, is unfeasible for most applications.

A possible compromise solution between computation time and results quality can be achieved by a 2D-to-3D approach, where the pre-process is analysed in two dimensions and its results mapped into a three dimensional mesh, which is later submitted into a roll forming FEA.

Table 6.2 resumes the computation times from two roll levelling simulations, in 2D and 3D, with the discretisation and properties considered in the previous integrated analysis. The results suggest that a saving of 97.3% on the pre-process computation time is achieved when roll levelling is analysed in a 2D plane-strain simulation. The CPU time reduction is expected to increase even further, when a wider strip is under scope.

Table 6.2 – Simulations proceeded during the 2D *vs* 3D roll levelling FEA study.

Analysis dimension	**Computation time** (h)	(%)
3D	11.1	100
2D	0.3	3

In order to assess if such approach is feasible, one should compare the distributions of results after levelling, both from the 2D and 3D analysis. From the distribution of residual stress and accumulated plastic strain across thickness, it is possible to conclude that the 2D model provides a very good approach of the average 3D results. It is important to mention that the residual stress distributions are different from those observed in Chapters 4 and 5 due to boundary conditions which simulate the subsequent roll forming process.

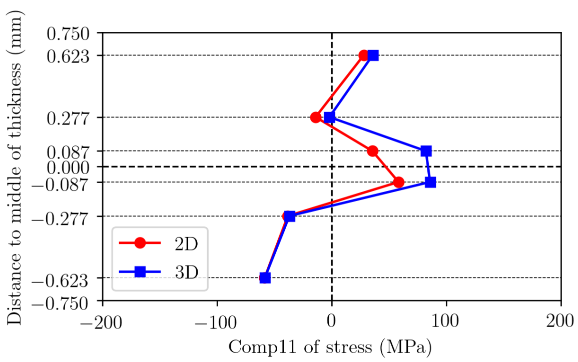

(a) Residual stress.

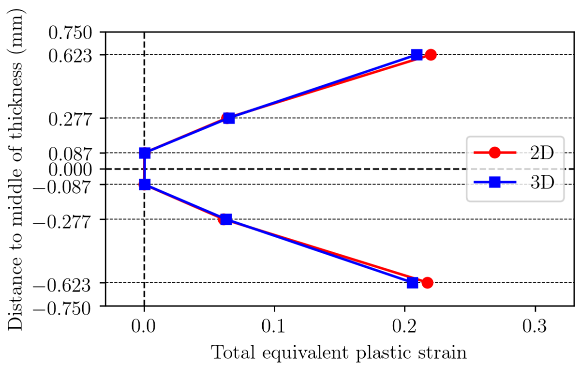

(b) Accumulated plastic strain.

Figure 6.14 – Results' thickness distribution after levelling (2D *vs* 3D analysis).[6]

[6]Results evaluated in the integration points.

Despite being acceptably represented by the 2D analysis, the 3D results displayed in Figure 6.14 are the average thickness distributions across the full width of the strip. Thus, also a study on results' consistency across width is required.

Figure 6.15 displays the residual stress and accumulated plastic strain of each integration point at different width positions. It is possible to observe that the results are very consistent throughout the whole width, except for the residual stresses at the edge of the strip (≈1/5$^{\text{th}}$ of width, highlighted in blue) which display a significant drop due to the discontinuity of material.

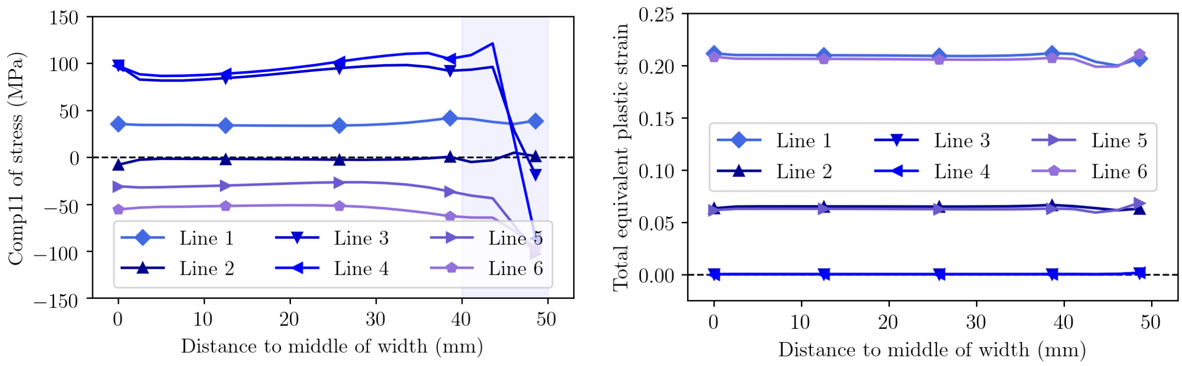

(a) Residual stress.

(b) Accumulated plastic strain.

Figure 6.15 – Results' width distribution after levelling (3D analysis).[7][8]

Considering that the 2D roll levelling analysis enables acceptable results with a much smaller computation effort, integrating a 2D roll levelling FEA in a standard 3D roll forming FEA by means of a mapping procedure is expected to be a feasible alternative to the time costly exclusively 3D roll levelling and roll forming integrated simulation.

Knowing that the exclusively 3D integrated analysis requires a computation time of 13.3 h (from Table 6.1), from which 11.1 h correspond to the roll levelling analysis and 2.2 h to the roll forming FEA, the before mentioned 2D-to-3D integrated analysis is estimated to require as much as 2.5 h.

Table 6.3 – Computation time of integrated roll levelling and roll forming FEA (different approaches).

Roll levelling	**Roll forming**	**Computation time** (h)	(%)
-	3D	1.8	100
2D	3D	2.5[a]	139[a]
3D	3D	13.3	739

[a] Estimated values.

Therefore, performing a 2D roll levelling FEA and integrating its results in a standard 3D roll forming simulation only leads to a penalty of 39% on the CPU time. Despite some additional caution is required

[7] Results evaluated in the integration points.
[8] More data points are analysed than those signed with markers.

when performing the 2D-to-3D mapping, due to the chosen hardening model, the approach suggestes in this section unquestionably stands out as a promising modelling solution.

6.7 Conclusions

From the study of an integrated roll levelling and roll forming finite element analysis performed in this chapter, the following conclusions are made.

The first conclusion regards the computation time required to perform a 3D combined analysis. As expected, considering the roll levelling pre-process leads to a severe penalty on the computation time require to simulate the roll forming process. In this study, the penalty corresponded to more than seven times the computation time required during a standard roll forming FEA.

During this chapter, only one discretisation with a local refinement through thickness is analysed. Despite only having a maximum of three elements over the thickness (0.6/0.3/0.6 mm), this mesh strategy it is found to be a feasible solution to take into account the most important properties of a roll levelled strip - thickness distribution of accumulated plastic strain - into the roll forming FEA and enables good insight on the final geometry of the profile.

A higher resolution over the thickness is possible by adding more layers of elements, as proceeded in the 2D roll levelling analysis. Despite possibly leading to some improvement on the results, implementing a finer mesh is associated with extra penalty time. Also, considering that standard roll forming FEA are often performed with only one element over strip's thickness and that mostly geometrical results are evaluated, the discretisation used in this chapter is suggested.

When the roll formed profile is analysed, the first results under scope are geometrical results. As expected, a significant springback and end-flare are observed, mainly in the front and rear end of the profile, whether roll levelling is considered or not. However, roll levelling is concluded to have a positive impact in both the springback and end-flare of a roll formed profile, namely a reduction of 0.5° on the average springback and 1.2° on the end-flare are observed. Overall, roll levelling contributes to the reduction of 1.8° on the maximum angular deviation.

On the other hand, it is found that a pronounced transverse bow is induced in the web when the roll levelling pre-process is simulated. This bow corresponds to 6.67% of strip's thickness and may be considered relevant, depending on the tolerance requirements. The longitudinal bow on the web of the profile is found to be neglectable and is not influenced by roll levelling.

Concerning the evaluation of residual stress distribution on the roll formed profile, it is possible to conclude that the distribution through thickness is close to point symmetric, with the majority of the interior half of the strip under compression and the exterior half under tension. The main component of residual stress is in rolling direction (component 11) and it is close to the bending area where the highest stress magnitude is found.

When roll levelling is considered, a positive impact on the distribution of residual stress is observed throughout the full profile, particularly in the edges and legs of the profile.

Regarding the distribution of accumulated plastic strain, it is significantly affected by roll levelling pre-process. It is mostly affected by the addition of a accumulated plastic strain offset before roll forming (pre-strain) which corresponds to the plastic strain accumulated during the roll levelling process. It is also in the bending area where the largest plastification is found, as expected.

Despite having very different initial strain states and, consequently, different initial yield stress values, both finite element models (with and without roll levelling) result in a similar plastification during roll forming. This leads to the conclusion that the Chaboche-Lemaitre hardening model achieves the saturated yield stress within the first load cycles and corroborates the similarity between the residual stress distributions.

Overall, combining roll levelling pre-process and roll forming in a single FEA contributes to lower geometrical variations. The only exception is found to be the transverse bow, which is negatively impacted. The downside of performing such analysis is the enormous increase on the computation time, even when a thickness discretisation of 3 elements is considered. Such restriction may rule the pre-process simulation as unfeasible for many applications.

Alternatively to the first suggested approach of integrating both processes in a single 3D finite element analysis, a 2D-to-3D mapping where the results from a 2D roll levelling analysis are assigned as an initial condition to the workpiece of a standard 3D roll forming simulation is also proposed. By performing the pre-process analysis in two dimensions, the computation time related with the roll levelling simulation is expected to reduce by 97.3% and, thus, integrating roll levelling in standard roll forming finite element analyses becomes feasible.

Chapter 7

Conclusions and discussion

The ultimate objective of this dissertation is to study the finite element modelling of roll levelling as a roll forming pre-process. To that extent, a continuous study on roll levelling modelling is performed in which the meshing strategy, contact algorithm, material constitutive model, machine deformation and analysis dimension are under scope. The integration of roll levelling and roll forming processes in a single finite element model, in which a DP1000 advanced high strength steel strip is formed, is also performed in order to assess the impact roll levelling has in a standard roll forming FEA.

Initially, a literature review on roll levelling is performed with the purpose of gathering knowledge on the process and its finite element modelling. It is observed that roll levelling submits the material to cyclic tension-compression loads in order to minimise unexpected shape defects after forming due to a poor consistency of results in the incoming material. Regarding the finite element modelling of the process, several authors have experimented different meshing strategies, material models and induced initial shape defects on the strip. On the other hand, topics such as machine deformation and analysis dimension stand as interesting research topics since they are still to be developed.

Later a two dimensional roll levelling study is performed. It is first observed that the pre-process finite element analysis requires a considerable computation time and, therefore, a locally refined discretisation is suggested. It is also confirmed that the process submits the material to large tension-compression cycles. Therefore, when the DP1000 steel (which exhibits a strong Bauschinger effect) is roll levelled, its hardening behaviour is better described by a combined isotropic-kinematic hardening model (Chaboche-Lemaitre was chosen) than by a pure isotropic alternative. On the contrary, Young's modulus degradation is neglected. Regarding the contact modelling and taking into account that in roll levelling simulations contact is very important, a research on the adequate contact algorithm is performed. The node-to-segment contact algorithm is chosen, since no advantage is found in considering neither the segment-to-segment alternative nor segments' analytical description. Concerning the process effectiveness, the machine settings under scope enable the complete correction of coil set defects, as no impact is observed in the levelled strip when multiple coil set radius are induced before levelling. It is also concluded that gravity can be neglected in the roll levelling FEA.

Two other topics have been studied within the two dimensional analysis, however a complete conclusion is not possible. Regarding the machine settings study, it is observed that the more severe the entry gap is, the highest is the plastic rate (PR) achieved. By analysing the results in the integration points and performing a simple data analysis it is possible to achieve a relation between entry gap and PR. Nonetheless, the number of elements through thickness limits the quality of the analysis and, therefore, analytical and semi-analytical models may be preferable to design the machine settings. During the machine deformation study, the working rolls are considered to be position controlled in their ends and at the location of every backup roll, therefore, only deformations directly associated with the levelling rolls (deflection and flattening) are relevant. Since in the 2D finite element analyses a plane-strain condition is assumed, deflection is not possible to model. An alternative is first proposed in this work to approximate working rolls' deflection in a 2D finite element analysis, in which working rolls' vertical position is defined by a grounded spring which stiffness is equivalent to the combined stiffness of both working and intermediate rolls. This simplification suggests that the deflection is very small and has no significant impact on 2D roll levelling analyses' results. Also rolls' flattening is studied and only a small elastic cross-section variation is observed. Hence, rolls' cross-section is assumed to be perfectly circular in both 2D and 3D analyses.

When a novel three dimensional roll levelling finite element modelled is developed and executed, an enormous increase of the computation time is observed (approximately $\times 10$), even when discretisations with only two and three elements over the thickness are analysed. This penalty is mostly due to the fact that a wide strip is being levelled (1500 mm in width direction). The decision of analysing a wide strip was made considering that the 3D roll levelling analyses serve as a complement to the 2D analyses, in which no plane-strain condition is assumed. Thus, the formation of shape defects in width direction and rolls' deflection are the main topics under scope. Concerning the shape defects, it becomes clear that a centre buckle is formed even when no rolls' deflection is modelled. This phenomenon is due to a stress release at the edges of the strip, where a discontinuity of material takes place. If rolls are modelled as deflectable bodies, by means of beam elements, several transverse buckles are formed. In this scenario, a high number of backup rolls leads to more buckles (one between two consecutive backup rolls) of smaller amplitude and *vice versa*. Finally, for the machine settings under scope, rolls' deflection is considered to be small and have an insignificant impact on the roll levelled strip. Also, modelling the rolls with beam elements motivated severe modelling instabilities and required an unfeasible computation time, as smaller step sizes and segment-to-segment contact algorithm (S2S) are required to establish beam-to-solid contact (rolls-to-strip).

Considering the accumulated knowledge on roll levelling finite element modelling and data M's expertise on roll forming, a three dimensional roll levelling and roll forming model is developed. A study on levelling and forming of a "U"-profile with an approximate width of 100 mm is performed and the results are compared to those from a standard roll forming FEA. During this analysis, a locally refined discretisation with a maximum of three elements across thickness is considered, the contact and material modelling suggested in the 2D study are used and only rigid working rolls are modelled. After each process, the front and rear ends of the strip/profile are neglected and a chamfer is created in the levelled strip. When the final geometry of the roll formed profile is evaluated, roll levelling reveals to significantly contribute for springback and end-flare reduction, enabling an improvement of 0.5° on the average springback and 1.8° on the maximum angular deviation. On the other hand, the transverse bow is observed to increase when the pre-process is simulated. Regarding the residual stress distribution, roll levelling significantly contributes homogenise the distribution of residual stress throughout the full strip. On the contrary, the levelling pre-process contributes to a significant offset of accumulated plastic strain when compared to a standard roll forming FEA. Such offset suggests that material hardening occurs in the pre-process.

In a final remark, it is possible to conclude that roll levelling pre-process has a meaningful impact in the finite element analysis of a roll forming process, namely in the geometrical properties of the roll formed profile and residual stress homogenisation. As expected, the process contributes to the reduction of springback and end-flare. Nevertheless, a severe penalty on the computation time ($\approx$750%) is observed when a combined analysis is executed. Therefore, performing an integrated 3D analysis of both processes is found to be unfeasible for most applications. Alternatively to the exclusively 3D integrated analysis, a 2D-to-3D mapping approach is suggested as a compromise solution, where the pre-process is studied in 2D and its results assigned to a the workpiece of a standard 3D roll forming FEA. With this last approach, the computation time of the integrated analysis is expected to reduce by 97.3%.

7.1 Future work

The work developed in this work enabled an insight on the impact roll levelling pre-process has in a standard roll forming FEA and on several particularities of the pre-process finite element modelling. However, some initial questions and other arisen during this work are still to be answered.

Considering that the work developed in this dissertation is exclusively numerical, a comparison between the results from both the 2D and 3D roll levelling analyses and experimental data is required to validate the models. Particularly, it would be interesting to evaluate real rolls' deflection, the geometry of the levelled strip and corroborate the material hardening and Young's modulus models by means of a mechanical characterisation of the material, before and after levelling.

Regarding the combined roll levelling and roll forming finite element analysis, there are several future perspectives. An extensive mesh sensitivity study should be performed in order to find the most appropriate discretisation required to provide an acceptable prediction of the final properties of the profile. Also, a search for the effect of levelling rolls' deflection in the final roll formed profile is suggested, since it would be interesting to quantify the impact deflection has in the final roll formed profile. Finally, an investigation on how common coil set defects impact standard roll forming FEA and comparison with a combined roll levelling and roll forming simulation is required to highlight the advantages of implementing roll levelling pre-process to its full extent.

Considering that a 2D-to-3D combined analysis is suggested as the best approach to take into account the levelling pre-process during a standard roll forming FEA, a mapping strategy study is required. The mapping procedure aims to assign the strip properties from a 2D roll levelling analysis to the initial state of a 3D roll forming finite element model. Later, both approaches of performing the combined analysis (exclusively 3D and 2D-to-3D) should be compared and validated with experimental data.

Another future perspective and one of the main topics to be developed is related with beam elements' modelling. The need for further study on this topic was noticed when severe instabilities were faced when modelling levelling rolls with beam elements, namely when contact was established. Therefore, a detail study to determine the best contact settings for an efficient simulation with beam-to-solid and beam-to-beam contact is required.

Finally, the development of a simple 2D roll levelling model based in a three-point bending, similarly to the model illustrated in Figure 4.48, is suggested. It is expected that, if the punch movement drives the strip to consecutive reverse bendings with the same amplitude observed in the real roll levelling process, an acceptable approach of the stress-strain state of a roll levelled strip is possible within a short computation time.

References

A.P. DESIGN (2009). *Levelling in detail*. Accessed: 2019-03-07. URL: http://apdesign.co.za/levelling.html.

ABVABI, A. et al. (2015). "The influence of residual stress on a roll forming process". In: *International Journal of Mechanical Sciences* 101-102, pp. 124–136. DOI: https://doi.org/10.1016/j.ijmecsci.2015.08.004.

ADEEB, S. (2019). *One and Two Dimensional Isoparametric Elements and Gauss Integration*. Accessed: 2019-06-14. URL: https://sameradeeb-new.srv.ualberta.ca/finite-element-analysis/one-and-two-dimensional-isoparametric-elements-and-gauss-integration.

ARCELORMITTAL (2018). *Automotive steels catalogue*. URL: https://automotive.arcelormittal.com/saturnus/sheets/ArcelorMittal%20Automotive%20product%20offer%20EN.pdf.

ASTM A1030 (2011). *Standard Practice for Measuring Flatness Characteristics of Steel Sheet Products*. Standard. Pensilvania, US: American Society for Testing and Materials. DOI: https://doi.org/10.0.5.240/10.1520/A1030_A1030M-11.

BECKER, S. (2007). *New generation of levelers tames high-strength steels*. Accessed: 2019-03-26. URL: https://www.thefabricator.com/article/stamping/new-generation-of-levelers-tames-high-strength-steels.

BLACK, J. T. and R. A. KOHSER (2012). *DeGarmo's materials and processes in manufacturing*. John Wiley & Sons. ISBN: 978-0-470-92467-9.

BSSA, B. (2019). *Tolerances to ISO 9445 for cold rolled narrow and wide strip, plate/sheet and cut lengths*. Accessed: 2019-03-21. URL: https://www.bssa.org.uk/topics.php?article=312.

DATA M SMS (2012). *History of data M*. Accessed: 2019-06-19. URL: http://www.datam.de/en/about-data-m/history-of-data-m.

DATA M SMS (2013). *Software para conformação por laminagem a frio (rolos)*. Accessed: 2019-06-19. URL: https://datambrasil.wordpress.com/home/software.

DATA M SMS (2019a). *3D Roll Forming Center*. Accessed: 2019-06-21. URL: https://www.copra.info/en/lp/3d-roll-forming-center.

DATA M SMS (2019b). *COPRA ProfileScan*. Accessed: 2019-06-21. URL: https://www.copra.info/en/cps.

DINGS, J. (2007). *Reducing CO2 Emissions from New Cars: A Study of Major Car Manufacturers' Progress in 2006*. European Federation for Transport and Environment.

FERREIRA, P. (2016). "Roll Forming - a study on machine deflection by means of experimental analysis and numerical developments". MA thesis. Faculty of Engineering of the University of Porto.

GALDOS, L. and E. SILVESTRE (2018). "Roll Levelling". In: *CIRP Encyclopedia of Production Engineering*. Springer Berlin Heidelberg, pp. 1–7. ISBN: 978-3-642-35950-7. DOI: 10.1007/978-3-642-35950-7_16844-1.

GALDOS, L., E. ARGANDOÑA, et al. (2017). "Numerical simulation of the roll levelling of third generation fortiform 1050 steel using a nonlinear combined hardening material model". In: *Journal of Physics: Conference Series* 896, p. 012122. DOI: 10.1088/1742-6596/896/1/012122.

GIL, I. et al. (2014). "Influence of material's hardening law in the simulation of DP1000 deep drawing and subsequent springback". In: *International Deep Drawing Research Group 2014 conference*.

GINZBURG, V. (2009). *Flat-rolled steel processes: Advanced technologies*, pp. 1–367. ISBN: 978-1-420-07292-1.

GOVIK, A. et al. (2014). "A study of the unloading behaviour of dual phase steel". In: *Materials Science and Engineering: A* 602, pp. 119–126. DOI: https://doi.org/10.1016/j.msea.2014.02.069.

GRÜBER, M. and G. HIRT (2017). "A strategy for the controlled setting of flatness and residual stress distribution in sheet metals via roller levelling". In: *Procedia Engineering*. DOI: https://doi.org/10.1016/j.proeng.2017.10.892.

GRÜBER, M. and G. HIRT (2018). "Investigation of correlation between material properties, process parameters and residual stresses in roller levelling". In: *Procedia Manufacturing* 15, pp. 844–851. DOI: https://doi.org/10.1016/j.promfg.2018.07.180.

GRÜBER, M. et al. (2015). "The Effect of the Initial Stress and Strain State in Sheet Metals on the Roller Levelling Process". In: Key Engineering Materials 651, pp. 1023–1028. DOI: 10.4028/www.scientific.net/KEM.651-653.1023.

HALMOS, G. (2005). *Roll Forming Handbook*. Manufacturing Engineering and Materials Processing. CRC Press. ISBN: 0-8247-9563-6.

JUNG, J. et al. (2017). "Anisotropic Hardening Behaviour and Springback of Advanced High-Strength Steels". In: *Metals* 7.11, p. 480. DOI: 10.3390/met7110480.

KELLY, J. C. et al. (2015). "Impacts of Vehicle Weight Reduction via Material Substitution on Life-Cycle Greenhouse Gas Emissions". In: *Environmental Science & Technology* 49.20. PMID: 26393414, pp. 12535–12542. DOI: 10.1021/acs.est.5b03192.

LEMAITRE, J. and J.-L. CHABOCHE (1990). *Mechanics of Solid Materials*. Cambridge University Press. DOI: 10.1017/CBO9781139167970.

LEVELTEK PROCESSING (2016). *What Is It - Stretch Leveling*. Accessed: 2019-03-26. URL: http://leveltek.com/stretcher-leveling/what-is-it/.

LIU, X. et al. (2017). "Investigation of forming parameters on springback for ultra high strength steel considering Young's modulus variation in cold roll forming". In: *Journal of Manufacturing Processes* 29, pp. 289–297. DOI: https://doi.org/10.1016/j.jmapro.2017.08.001.

MALIK, A. S. and R. V. GRANDHI (2008). "A computational method to predict strip profile in rolling mills". In: *Journal of Materials Processing Technology* 206.1, pp. 263–274. DOI: https://doi.org/10.1016/j.jmatprotec.2007.12.026.

MATHIEU, N. et al. (2013). “Flatness defects after bridle rolls: a numerical analysis of leveling”. In: *International Journal of Material Forming* 6.2, pp. 255–266. DOI: https://doi.org/10.1007/s12289-011-1083-2.

MENDIGUREN, J. et al. (2015). “Elastic behaviour characterisation of TRIP 700 steel by means of loading–unloading tests”. In: *Materials Science and Engineering: A* 634, pp. 147–152. DOI: https://doi.org/10.1016/j.msea.2015.03.050.

MSC SOFTWARE CORPORATION (2018). *Marc® 2018.0 User Manual. Volume B: Element Library*. Manual. MSC Software Corporation.

PAAS, L. (2016). *Action for Climate Empowerment: Guidelines for accelerating solutions through education, training and public awareness*. UNESCO Publishing.

PARK, K.-c. and S.-M. HWANG (2002). “Development of a Finite Element Analysis Program for Roller Leveling and Application for Removing Blanking Bow Defects of Thin Steel Sheet”. In: *ISIJ International* 42.9, pp. 990–999. DOI: 10.2355/isijinternational.42.990.

PERELOMA, E. and I. TIMOKHINA (2017). “9 - Bake hardening of automotive steels”. In: ed. by R. RANA and S. B. SINGH, pp. 259–288. DOI: https://doi.org/10.1016/B978-0-08-100638-2.00009-2.

QUACH, W. et al. (2004). “Residual stresses in steel sheets due to coiling and uncoiling: a closed-form analytical solution”. In: *Engineering Structures* 26.9, pp. 1249–1259. DOI: https://doi.org/10.1016/j.engstruct.2004.04.005.

SATYENDRA (2016). *Metallurgical Processes and Defects in Steel Products*. Accessed: 2019-03-20. URL: http://ispatguru.com/metallurgical-processes-and-defects-in-steel-products/.

SEDLMAIER, A. and T. DIETL (2018). “3D roll forming center for automotive applications”. In: *Procedia Manufacturing* 15. Proceedings of the 17th International Conference on Metal Forming METAL FORMING 2018 September 16 – 19, 2018, Loisir Hotel Toyohashi, Toyohashi, Japan, pp. 767–774. DOI: https://doi.org/10.1016/j.promfg.2018.07.319.

SEO, J. H. et al. (2016). “Effect of Roll Configuration on the Leveling Effectiveness of Tail-Up Bent Plate Using Finite-Element Analysis”. In: *J. Manuf. Sci. Eng.* 138.7, p. 071004. DOI: 10.1115/1.4032392.

SHIGLEY, J. E. (1972). *Mechanical engineering design*. McGraw-Hill. ISBN: 0-390-76487-6.

SILVESTRE, E., J. MENDIGUREN, L. GALDOS, et al. (2015). “Comparison of the hardening behaviour of different steel families: From mild and stainless steel to advanced high strength steels”. In: *International Journal of Mechanical Sciences* 101-102, pp. 10–20. DOI: https://doi.org/10.1016/j.ijmecsci.2015.07.013.

SILVESTRE, E., E. ARGANDOÑA, et al. (2014). “Testing and Modeling of Roll Levelling Process”. In: *Key Engineering Materials* 611, pp. 1753–1762. DOI: 10.4028/www.scientific.net/KEM.611-612.1753.

SILVESTRE, E., E. ARGANDOÑA, et al. (July 2015). “Comparison of Three Methods for Material Hardening Parameter Identification under Cyclic Tension-Compression Loadings: Roll Levelling Case Study”. In: *Key Engineering Materials* 651-653, pp. 957–962. DOI: 10.4028/www.scientific.net/KEM.651-653.957.

SILVESTRE, E., L. GALDOS, et al. (2014). “Analysis of plastic behavior under cyclic loadings of advanced materials”. In: *IDDRG 2014 Conference*.

SILVESTRE, E., D. GARCIA, et al. (2016). "Roll levelling semi-analytical model for process optimization". In: *Journal of Physics: Conference Series* 734, p. 032034. DOI: 10.1088/1742-6596/734/3/032034.

SILVESTRE, E., J. MENDIGUREN, E. ARGANDOÑA, et al. (2012). "Roll levelling numerical simulation using a nonlinear mixed hardening material model". In: *Steel Research International*, pp. 1295–1298.

SILVESTRE, E., J. MENDIGUREN, E. ARGANDOÑA, et al. (2013). "Influence of number of backstresses on the mixed hardening Chaboche-Lemaitre model for modelling roll levelling processes". In:

SILVESTRE, E., J. MENDIGUREN, L. GALDOS, et al. (2013). "Influence of the Number of Tensile/Compression Cycles on the Fitting of a Mixed Hardening Material Model: Roll Levelling Process Case Study". In: *Key Engineering Materials* 554, pp. 2375–2387. DOI: 10.4028/www.scientific.net/KEM.554-557.2375.

SOSZYŃSKI, and A. STUDNICKA (2012). "A review of contemporary solutions for cold rolling that allow quality improvement". In: *Journal of Achievements in Materials and Manufacturing Engineering* Vol. 55.nr 2. ISSN: 1734-8412.

SUN, L. and R. WAGONER (2011). "Complex unloading behavior: Nature of the deformation and its consistent constitutive representation". In: *International Journal of Plasticity* 27.7, pp. 1126–1144. DOI: https://doi.org/10.1016/j.ijplas.2010.12.003.

THEIS, E. (2001). *Flatness in coil processing operations: New turns in the leveling process*. Accessed: 2019-03-22. URL: https://www.thefabricator.com/article/stamping/flatness-in-coil-processing-operations-new-turns-in-the-leveling-process.

THEIS, E. (2002a). *Everything you need to know about flatteners and levelers for coil processing - Part 2*. Accessed: 2019-03-21. URL: https://www.thefabricator.com/article/stamping/everything-you-need-to-know-about-flatteners-and-levelers-for-coil-processing-part-2.

THEIS, E. (2002b). *Everything you need to know about flatteners and levelers for coil processing - Part 3*. Accessed: 2019-03-21. URL: https://www.thefabricator.com/article/stamping/everything-you-need-to-know-about-flatteners-and-levelers-for-coil-processing-part-3.

THEIS, E. (2002c). *Everything you need to know about flatteners and levelers for coil processing - Part 4*. Accessed: 2019-03-21. URL: https://www.thefabricator.com/article/stamping/everything-you-need-to-know-about-flatteners-and-levelers-for-coil-processing-part-4.

ULIBARRI, U. et al. (2016). "Friction characterisation in levelling processes". In: *Advances in Materials and Processing Technologies*, pp. 1–11. DOI: 10.1080/2374068X.2016.1247230.

YAN, L. and B. SNIDER (2008). *Reducing setup time in strip leveling - Equations minimize trial and error in strip or coil processing*. Accessed: 2019-03-29. URL: https://www.thefabricator.com/article/stamping/reducing-setup-time-in-strip-leveling.

YOSHIDA, F. et al. (2002). "Elastic–plastic behavior of steel sheets under in-plane cyclic tension–compression at large strain". In: *International Journal of Plasticity* 18.5, pp. 633–659. DOI: https://doi.org/10.1016/S0749-6419(01)00049-3.

Appendix A

Residual stress evaluation

The evaluation of residual stress distribution through thickness after levelling, explained in several chapters and applied on Chapter 4.2, is one of the most important result analysis to be executed in this work. Due to its high importance, this appendix has the purpose to explain how the FEA results are assessed.

After levelling, the stress measurement is proceeded in a cross section on the refined part of the strip (or in an equivalent position if the mesh is continuous). This refined part passes through the hole levelling process during the simulation and its location (view Figure 3.14) are intended to ensure that the simulation results are a valid representation of a continuous process.

The residual stress state is equivalent to the final stress state of the strip. Therefore, in order to quantify its distribution through thickness, all final stress components should be considered. These components are: normal stress in rolling direction (Comp11), normal stress in the vertical direction (Comp22), normal stress in the plane direction (Comp33) and shear stress in the plane (Comp12).

In Figure A.1, the stress results of a simulation with a regular mesh of 16 elements through thickness (also mentioned in Table 4.1) is under scope. It is possible to observe that the stress component in rolling direction (Comp11) has the highest magnitude through the majority of the thickness and, therefore, residual stress distribution through thickness will be assessed by measuring the Comp11 of stress distribution through thickness.

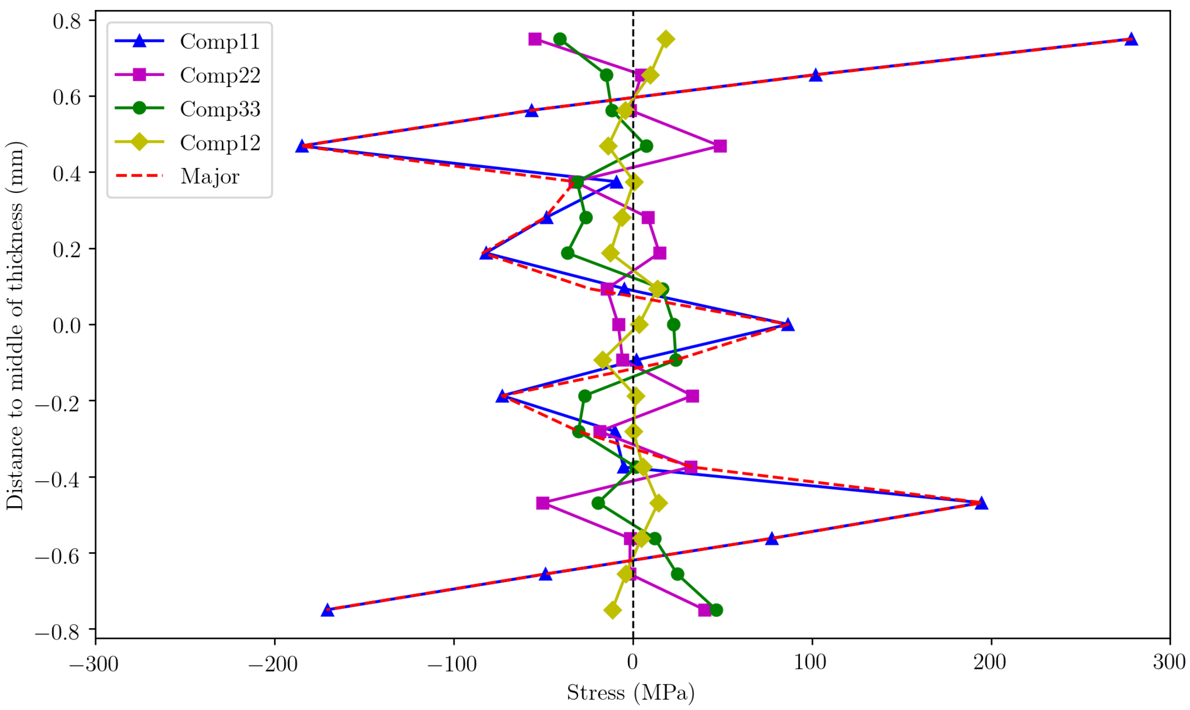

Figure A.1 – Example of different stress components distribution through thickness.

A.1 Evolution of the distribution through thickness

In order to understand how does the distribution of residual stress through thickness achieves the shape observed in Figure A.1, the longitudinal component of stress is analysed through thickness in multiple stages of the levelling process. Figure A.2 resumes the before mentioned results, which are assessed before levelling, when in contact with the 3rd, 8th, 13th and 16th working roll and after levelling.

If the stress magnitude is under scope, it is observable that the largest magnitude is mostly observed close to the surfaces of the strip (most distanced from the middle of the strip) and that the stress magnitude decreases from the first to last working rolls. Particularly close to the middle of the thickness, the stress level is decreases significantly during levelling.

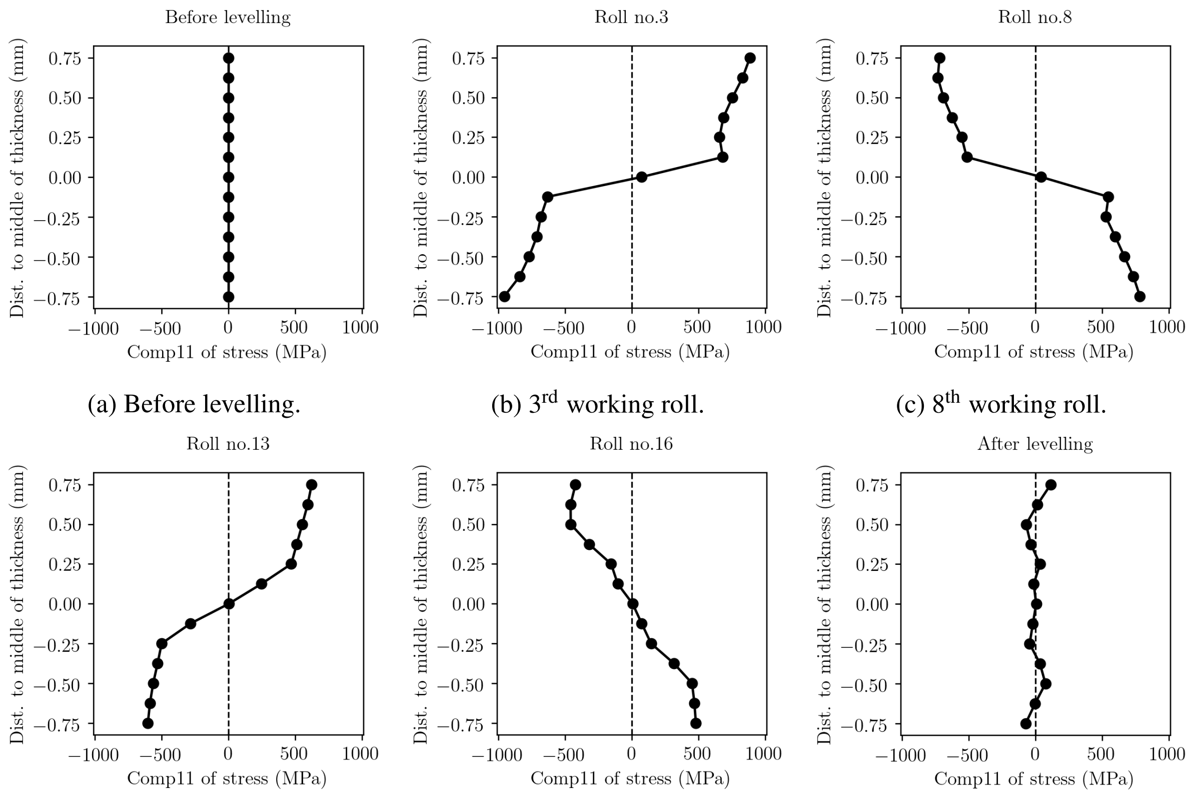

(a) Before levelling. (b) 3rd working roll. (c) 8th working roll.

(d) 13th working roll. (e) 16th working roll. (f) After levelling.

Figure A.2 – Evolution throughout levelling of the thickness distribution of stress (longitudinal component).

In Figures A.2b, A.2c and A.2d two different regions are visible on the stress distribution: an elastic and a plastic region. In the elastic region, which is located close to the middle of the thickness, the stress distribution is linear and has a steep slope. In the plastic region, which is corresponds to the remaining thickness, the distribution is non-linear (due to work hardening) and only a small variation of stress magnitude is noticed.

The final stress distribution (residual stress) exhibits a very small maximum magnitude when compared to those induced during levelling. This means that the levelling process is able to correct pre-existent geometrical defects and homogenise residual stresses by overcoming the yield stress of the material across the majority of the thickness and later reduce the induced stresses to a smaller magnitude. Considering that the process consists on a cyclic bending with decreasing curvature, it results in a residual stress distribution through thickness which varies repeatedly from positive to negative, and *vice versa*.

Appendix B

Stiffness of the working rolls

In order to create a realistic deformable model with an acceptable computation time, deflectable rolls are modelled through different strategies, both in 2D and 3D.

In the next section, the moment of inertia of a new beam (combined working and intermediate rolls) is calculated. The following sections explain how simple models only with working rolls are modelled, so that the structural effect of both backup and intermediate rolls is taken into account.

B.1 Moment of inertia

Since both working and intermediate rolls have the same length (2200 mm) and a small deflection is expected, one can assume that the rolls behave as a single beam. Figure B.1a illustrates the before mentioned assumption, where roll no.1 is a working roll and rolls no.2 and no.3 are intermediate ones.

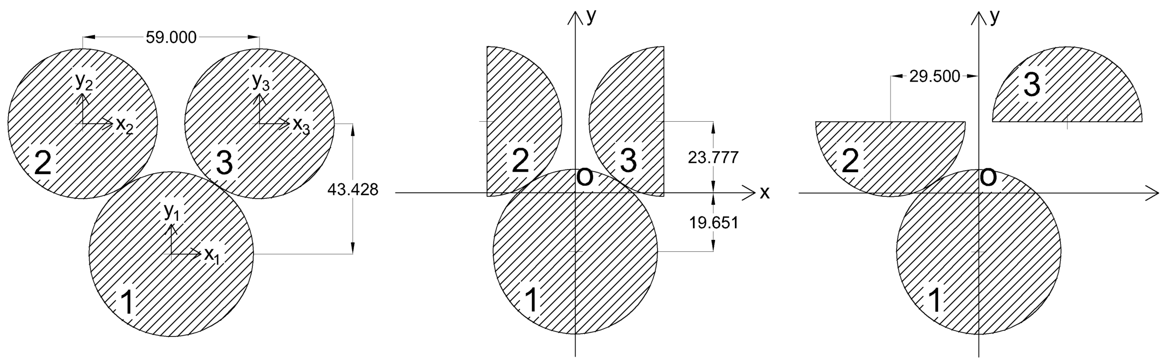

(a) Combined beam. (b) Moment of inertia, I_{xx}. (c) Moment of inertia, I_{yy}.

Figure B.1 – Combined working and intermediate rolls' illustration (dimensions in mm).

Considering that every intermediate roll supports two working rolls, except for the first and last one, it is assumed that each intermediate roll contributes with 50% of its stiffness to each working roll.

Knowing the diameter of both working and intermediate rolls (D_w and D_i, respectively), it is possible to calculate the moment of inertia of each roll. When calculated at the centre of a circular section, the moment of inertia is constant in all directions of a local coordinate system.

Therefore $I_{j,x_jx_j} = I_{j,y_jy_j} = I_j$, $\forall j \in \{1,2,3\}$, and:

$$\begin{cases} I_1 = \dfrac{\pi \cdot D_w}{64} & , D_w\text{=55 mm} \\ I_2 = I_3 = \dfrac{\pi \cdot D_i}{64} & , D_i\text{=50 mm} \end{cases} \Rightarrow \begin{cases} I_1 = 449180.25\,\text{mm}^4 \\ I_2 = I_3 = 306796.16\,\text{mm}^4 \end{cases} \tag{B.1}$$

In order to calculate a total moment of inertia, the position of the centre of area (O) needs to be calculated. The coordinates are computed relatively to the coordinate system of the working roll, (x_1, y_1).

$$\begin{cases} x_o = \dfrac{\Delta x_1 \cdot A_1 + \Delta x_2 \cdot A_2/2 + \Delta x_3 \cdot A_3/2}{A_1 + A_2/2 + A_3/2} \\ y_o = \dfrac{y_1 \cdot A_1 + y_2 \cdot A_2/2 + y_3 \cdot A_3/2}{A_1 + A_2/2 + A_3/2} \end{cases} \Rightarrow \begin{cases} x_o = 0.00\,\text{mm} \\ y_o = 19.65\,\text{mm} \end{cases} \tag{B.2}$$

where Δx_1=0 mm, Δx_3=$-\Delta x_2$=29.50 mm, Δy_1=0.00 mm, Δy_2=Δy_3=43.428 mm, A_1=2375.83 mm^2 and A_2=A_3=1963.50 mm^2.

From Steiner's theorem and Equation B.1, it is possible to calculate the moment of inertia of each roll at the centre of area, relatively to (x, y) coordinate system, as illustrated in Figures B.1b and B.1c.

$$\begin{cases} I_{1,xx} = I_1 + A_1 \cdot {d_{y,1}}^2 & , d_{y,1} = -19.651\text{ mm}^4 \\ I_{1,yy} = I_1 + A_1 \cdot {d_{x,1}}^2 & , d_{x,1} = 0\text{ mm}^4 \\ I_{2,xx} = I_{3,xx} = I_2 + A_2 \cdot {d_{y,2}}^2 & , d_{y,2} = d_{y,3} = 23.777\text{ mm}^4 \\ I_{2,yy} = I_{3,yy} = I_2 + A_2 \cdot {d_{x,2}}^2 & , -d_{x,2} = d_{x,3} = 29.500\text{ mm}^4 \end{cases} \tag{B.3}$$

$$\Rightarrow \begin{cases} I_{1,xx} = 1366606.82\,\text{mm}^4 \\ I_{1,yy} = I_1 = 449180.25\,\text{mm}^4 \\ I_{2,xx} = I_{3,xx} = 1416885.38\,\text{mm}^4 \\ I_{2,yy} = I_{3,yy} = 2015528.04\,\text{mm}^4 \end{cases} \tag{B.4}$$

Consequently, the total moment of inertia in the centre of area (O) is:

$$\begin{cases} I_{total,xx} = I_{1,xx} + \dfrac{I_{2,xx}}{2} + \dfrac{I_{3,xx}}{2} \\ I_{total,yy} = I_{1,yy} + \dfrac{I_{2,yy}}{2} + \dfrac{I_{3,yy}}{2} \end{cases} \Rightarrow \begin{cases} I_{total,xx} = 2783492.20\,\text{mm}^4 \\ I_{total,yy} = 2464708.29\,\text{mm}^4 \end{cases} \tag{B.5}$$

Since in the finite element model only the working rolls are modelled, Steiner's theorem is applied again to obtain the total moment of inertia in the centre of the working roll ((x_1, y_1) coordinate system).

$$\begin{cases} I_{total,xx} = I_{total,x_1x_1} + (A_1 + A_2/2 + A_3/2) \cdot {d_{y,1}}^2 \\ I_{total,yy} = I_{total,y_1y_1} + (A_1 + A_2/2 + A_3/2) \cdot {d_{x,1}}^2 \end{cases} \tag{B.6}$$

$$\Rightarrow \begin{cases} I_{total,x_1x_1} = 1107861.86\,\text{mm}^4 \\ I_{total,y_1y_1} = 2464708.29\,\text{mm}^4 \end{cases} \tag{B.7}$$

Considering that the loads on the working rolls are expected to be mostly in vertical direction, the highest bending occurs over the x_1x_1 axis, which is also the weakest bending direction of the machine. Therefore, I_{total,x_1x_1} is the appropriate moment of inertia to be assigned to each working roll.

B.2 2D modelling

In order to model rolls' deflection during the roll levelling process, a 3D model with deformable rolls is modelled. However, it is also interesting to see how accurately can a 2D model represent the same deflection phenomena and its impact on the strip properties.

Modelling rolls' deflection in 2D is not possible, taking into account that a plane-strain condition is considered. Therefore, the most accurate 2D representation is achieved by assigning the stiffness of the combined working and intermediate rolls to a spring, which controls the vertical position of the 2D roll in function of the load. Backup rolls' effect is considered by assuming a beam length equal to the distance between two consecutive backup rolls. This simplification reduces the deflection to an equivalent vertical displacement, meaning that in 2D the results are constant through the width of the strip. Figure B.3 clarifies the before mentioned concept.

In Figure B.2, one can find an illustrative diagram of the problem, where F is the distributed load, L the distance between two consecutive backup rolls, and D_w the diameter of the working roll. The goal is to find the displacement, $y(x)$, in function of the transverse position, x ($0<x<L$). A maximum value of deflection is expected at the middle of the width ($x = L/2$).

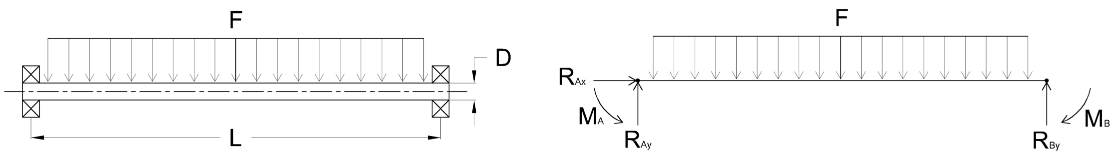

(a) Mechanical diagram. (b) Forces diagram.

Figure B.2 – Diagram of a working roll with no backup rolls.

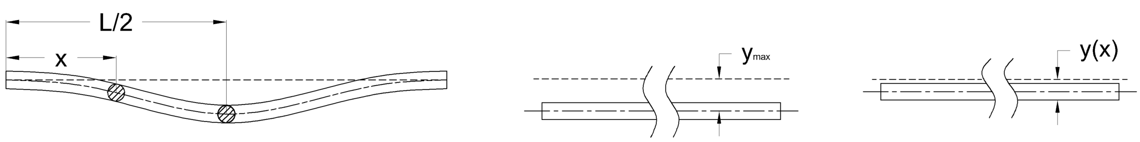

(a) Deflection. (b) Displacement ($x = \frac{L}{2}$). (c) Displacement ($x \neq \frac{L}{2}$).

Figure B.3 – Deflection representation in 2D models.

Since this is a hyperstatic problem of second order (as can be seen in Figure B.2b), the force method is used. The real distributed load (F), an virtual point load (X_1) and an virtual torque (X_2) are applied individually as illustrated in the following figures, leading to the isolated displacement ($y_1(x)$, $y_2(x)$ and $y_3(x)$, respectively).

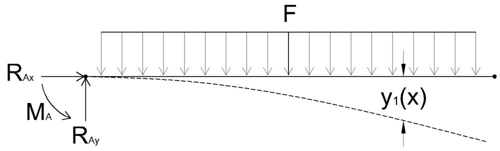

(a) Real loads.

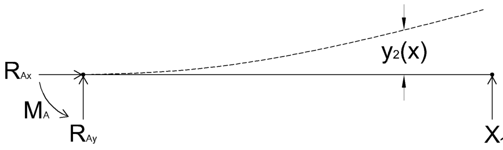

(b) Virtual load, X_1.

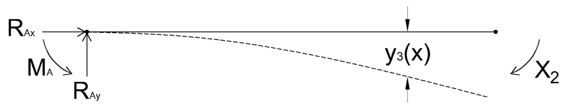

(c) Virtual torque, X_2.

Figure B.4 – Effects of individual loads.

According to Shigley (1972), the deflection and slope of an isostatic cantilever beam are calculated as indicated in Table B.1, where E is the material Young's modulus and I the inertia moment of the beam.

Table B.1 – Deflection and slope at free end of a cantilever beam.

Load type	**Deflection**	**Slope at free end**
Uniformly distributed load (F) Figure B.4a	$y(x) = -\dfrac{F \cdot x^2}{24 \cdot E \cdot I} \cdot \left(x^2 + 6 \cdot L^2 - 4 \cdot L \cdot x\right)$	$\left.\dfrac{\delta y}{\delta x}\right\|_{x=L} = \dfrac{F \cdot L^3}{6 \cdot E \cdot I}$
Load at the free end (X_1) Figure B.4b	$y(x) = \dfrac{X_1 \cdot x^2}{6 \cdot E \cdot I} \cdot (3 \cdot L - x)$	$\left.\dfrac{\delta y}{\delta x}\right\|_{x=L} = -\dfrac{X_1 \cdot L^3}{2 \cdot E \cdot I}$
Torque at the free end (X_2) Figure B.4c	$y(x) = -\dfrac{X_2 \cdot x^2}{2 \cdot E \cdot I}$	$\left.\dfrac{\delta y}{\delta x}\right\|_{x=L} = \dfrac{X_2 \cdot L}{E \cdot I}$

Considering that the superposition theorem is applied together with the force method, the total deflection and slope can be written as:

$$\begin{cases} y(x) = y_1(x) + y_2(x) + y_3(x) \\ \dfrac{\delta y}{\delta x}(x) = \dfrac{\delta y_1}{\delta x}(x) + \dfrac{\delta y_2}{\delta x}(x) + \dfrac{\delta y_3}{\delta x}(x) \end{cases} \tag{B.8}$$

Knowing that the deflection and slope at $x = L$ are zero $\left(y\big|_{x=L} = \frac{\delta y}{\delta x}\big|_{x=L} = 0\right)$,

$$\begin{cases} y_1\big|_{x=L} + y_2\big|_{x=L} + y_3\big|_{x=L} = 0 \\ \left.\dfrac{\delta y_1}{\delta x}\right|_{x=L} + \left.\dfrac{\delta y_2}{\delta x}\right|_{x=L} + \left.\dfrac{\delta y_3}{\delta x}\right|_{x=L} = 0 \end{cases} \tag{B.9}$$

$$\Leftrightarrow \begin{cases} -\frac{F \cdot L^4}{4} + \frac{2 \cdot X_1 \cdot L^3}{3} - X_2 \cdot L^2 = 0 \\ \frac{F \cdot L^2}{6} - \frac{X_1 \cdot L}{2} + X_2 = 0 \end{cases} \quad \Leftrightarrow \quad \begin{cases} X_1 = \frac{F \cdot L}{2} \\ X_2 = \frac{F \cdot L^2}{12} \end{cases} \tag{B.10}$$

Therefore, from Equations B.8 and B.10, the general deflection equation is calculated.

$$\Rightarrow y(x) = -\frac{F \cdot x^2}{24 \cdot E \cdot I} \cdot \left(x^2 + 6 \cdot L^2 - 4 \cdot L \cdot x\right) + \frac{F \cdot L \cdot x^2}{12 \cdot E \cdot I} \cdot (3 \cdot L - x) - \frac{F \cdot L^2 \cdot x^2}{24 \cdot E \cdot I} \tag{B.11}$$

$$\Leftrightarrow y(x) = -\frac{F \cdot x^2 \cdot (l - x)^2}{24 \cdot E \cdot I} \tag{B.12}$$

Having determined the deflection equation, the equivalent stiffness can be calculated for any transversal position.

$$K_{eq} = \frac{F \cdot L}{|y(x)|} = \frac{24 \cdot E \cdot I \cdot L}{x^2 \cdot (L - x)^2} \tag{B.13}$$

Considering that the roll levelling equipment modelled in this work has steel rolls, with a diameter of 55 mm, combined moment of inertia from the working and intermediate rolls and a distance between two consecutive backup rolls of 440 mm, the required variables to calculate the K_{eq} are set as follows:

$$\begin{cases} E = 210\,\text{GPa} \\ I = I_{total,x_1x_1} = 1107861.86\,\text{mm}^4 \\ L = 440\,\text{mm} \end{cases} \tag{B.14}$$

Therefore, the K_{eq} for this work can be calculated for multiple transverse positions, as illustrated in Figure B.3a. The equivalent stiffness values are resumed in Table B.2.

Table B.2 – Equivalent stiffness in function of the transverse position.

Transverse position x/L (%)	**Equivalent stiffness** K_{eq} (N/mm)
0	$+\infty$
5	29051656
10	8092320
15	4032159
20	2560460
25	1864470
30	1486344
35	1266471
40	1137982
45	1070058
50	1048764

B.3 3D modelling

In order to create a realistic three dimensional model with an acceptable computation time, deflectable rolls are modelled with beam elements. Ideally, a simple model with only one layer of rolls (working rolls) would be designed, however the structural effect of both intermediate and backup rolls also has to be taken into account.

The backup rolls' effect is easily modelled by means of translation boundary conditions, directly applied on the working rolls in both transverse (x) and vertical (y) directions, as explained in Section 5.2.

Also a last modelling artifice is performed, in order to create working rolls with their real geometry ($D_{w,real} = 55$ mm) and take into account the structural effect of the intermediate rolls. Knowing that the rolls are made of steel ($E_{steel} = 210$ GPa) and should provide a moment of inertia equal to I_{total,x_1x_1}, it is possible to calculate a new Young's modulus value (E_{eq}) which provides the required stiffness.

$$I_{total,x_1x_1} \cdot E_{steel} = I_{1,x_1x_1} \cdot E_{eq} \tag{B.15}$$

$$\Leftrightarrow \quad E_{eq} = \frac{I_{total,x_1x_1}}{I_{1,x_1x_1}} \cdot E_{steel} \tag{B.16}$$

$$\Leftrightarrow \quad E_{eq} = 517.95\,\text{GPa} \tag{B.17}$$

By modelling the working rolls as beam elements with a diameter of 55 mm and a Young' modulus of 517.95 GPa, it is possible to create a simple 3D model with deflectable rolls which takes into account an approximation of intermediate rolls' structural effect without modelling them.